Mohamed Boudiaf University - M'sila

FACULTY OF SCIENCES

PHYSICS DEPARTEMENT

Serial number……..…

Registration number……..……

Thesis

Presented for graduation from

DOCTORATE 3rd cycle

Field: Physics

Option: Theoretical Physics

THEME

Quantum Oscillations in Confined Degenerate Fermi Gases

Presented by:

BERKANE Amina

Defended on: 19/02/2025

In front of the jury composed of :

Last Name&First Name	Grade	Etablishement	Quality
MAIRECHE Abdelmadjid	Professor	Med Boudiaf University- M'sila	President
MENOUAR Salah	Professor	Ferhat Abbas University- Setif-1	Examiner
BAADJI Nadjib	Professor	Med Boudiaf University- M'sila	Examiner
KASRI Yazid	Professor	Med Boudiaf University- M'sila	Examiner
BENCHEIKH Kamel	Professor	Ferhat Abbas University- Setif-1	Invited
MEDJEDEL Soheyb	Senior Lecturer	Med Boudiaf University- M'sila	Supervisor

Academic year: 2024/2025

Abstract

This thesis conducts a comprehensive analysis of some important fundamental equilibrium properties of a harmonically confined two-dimensional electron gas subjected to a uniform perpendicular magnetic field. Using single-particle wave functions and Bloch density matrix method, we obtain exact analytical expressions for various local and integral properties, including particle density, current distribution, microscopic magnetization, total magnetic moment, and the integrated persistent current. We provide a direct deduction of the total persistent current from the orbital microscopic magnetization, emphasizing their inherent connection. Numerical investigation, concentrating on strong magnetic field regimes, uncovers well-defined compressible and incompressible regions within the particle density profile. We unravel the underlying structure of the counter-propagating equilibrium currents in high-field regimes, induced by the oscillatory behavior of microscopic magnetization, which we derive in exact analytical form in real physical space. Moreover, an examination of changes in the energy spectrum reveals intricate influences on these properties, resulting in quantum oscillation patterns at high magnetic fields.

Keywords: Orbital microscopic magnetization, Persistent electric current, Orbital magnetism Particle density, Two-dimensional electron gas, Quantum oscillation

Dedication

I dedicate this work of all these years

To my deceased father

To my mother

To all my family

Acknowledgements

Above all, I thank Almighty God for having given me health, patience, willpower and help throughout my life. First and foremost,

I would like to express my deep gratitude to Mr MEDJEDEL Soheyb, professor at the University of M'sila, my supervisor, who assumed the direction of this work. I would like to thank him for his dedication, patience, availability, advice and kindness.

We would like to thank Mr MAIRECHE Abdelmadjid professor at the University of M'sila, for agreeing to judge and review our work.

I would also like to thank all the members of the jury Mr MENOUAR Salah professor at the University of Ferhat Abbas University- Setif-1, Mr BAADJI Nadjib professor at the University of M'sila, Mr KASRI Yazid professor at the University of M'sila, and BENCHEIKH Kamel professor at the University of Ferhat Abbas University- Setif-1, who agreed to examine my doctoral thesis.

I will not forget to thank all the teachers who, through their teaching, their encouragement and their help, have contributed to my training during all the years of my studies from primary school to university.

Table of contents

Abstract …… I

Dedication……... II

Acknowledgements…… III

Table of contents…… IV

Abbreviations and notations……. VI

Introduction ……. 1

Chapter 1: An Overview of 2DEGs: Concepts, Experimental Realization, and Applications……..... 7

1. Introduction ……... **7**
2. Experimental realization of 2DEG……..... **8**
3. Parabolic confinement of the 2DEG……... **9**
4. Quantum dots ……..... **9**
5. Free charged particle in a normal magnetic field ……..... **10**

5.1. Gauge Fields……. **10**

5.2. Landau Levels……... **12**

6. The Quantum Hall Effect……... **14**
7. Quantum oscillations as function of magnetic field ……. **15**

7.1. Quantum oscillations in the specific heat……. **15**

7.2. Quantum oscillations in magnetization…… **16**

Chapter 2: Harmonically Confined 2DEG Under a Normal Magnetic Field: Description and Theoretical Frameworks……..... 18

1. Introduction……..... **18**
2. System description……. **19**
3. Stationary solutions of the Schrodinger equation ……. **20**
4. Energy spectrum……. **22**
5. Theoretical Frameworks ……... **24**

5.1. Single-particle wave-function-based approach…… **24**

5.2. Bloch density matrix formalism …….. **25**

5.2.1. Definition of the Bloch Density Matrix $C(\mathbf{r}, \mathbf{r}'; \xi)$……... **25**

5.2.2. Relationship between BDM and some important physical quantities…… **27**

6. Analytical expression of $C(\mathbf{r}, \mathbf{r}'; \xi)$ for the system under study……. **30**
7. Derivation of the energy spectrum from the Bloch density matrix…… **31**
Chapter 3: Exact Analytical Expressions for Key Equilibrium Orbital Properties… **33**
1. Introduction…… **33**
2. Exact quantum mechanical expressions for particle and current densities…… **34**
2.1. The first-order density matrix $\rho(\mathbf{r}, \mathbf{r}'; \mu)$ …… **34**
2.2. The particle density $\rho(\mathbf{r})$……. **36**
2.3. The orbital electric current density $\mathbf{J}(\mathbf{r})$…… **36**
3. The total orbital magnetic moment $\mathbf{M}$…… **38**
4. The microscopic magnetization $\boldsymbol{\mathcal{M}}(\mathbf{r})$……... **40**
5. The total azimuthal persistent current…… **41**
Chapter 4: Results and Discussion…… 44
1. Introduction…… **44**
2. Evolution of the energy spectrum……... **45**
2.1. Evolution of the energy spectrum with magnetic field ……... **45**
2.2. Evolution of the energy spectrum with radial distance …….. **48**
3. Spatial distribution of particle, current and magnetization densities ……. **51**
3.1. The particle density profile ……..... **51**
3.2. The equilibrium orbital current distribution ……..... **53**
3.3. Oscillations of the orbital microscopic magnetization…….…. **58**
4. Quantum oscillations of total magnetic moment and integrated current…… **60**
4.1. Oscillations of total magnetic moment……. **60**
4.2. Oscillations of the integrated current…… **63**
General conclusion…… 65
References……... 67

Abbreviations and notations

2DEG	Two-dimensional electron gas.
BDM	Bloch Density matrix.
$C(\mathbf{r},\mathbf{r}';\xi)$	Bloch density matrix elements.
N	Number of electrons.
m^*	Effective mass of electron.
$q=-e\ (e>0)$	Electron charge.
$V(\mathbf{r})$	Confining potentiel.
$\mathbf{L}=\mathbf{r}\times\mathbf{p}$	Orbital angular momentum.
$\mathbf{r}=(x,y)$	Position vector operator.
$\mathbf{p}$	Canonical momentum.
$\mathbf{B}$	Magnetic Field.
$\mathbf{A}$	Vector potential.
$\Omega=\sqrt{\omega_0^2+\omega_L^2}$	The magnetic-field-shifted frequency.
$\Omega_\pm=\Omega\pm\omega_L$	Hybrid frequencies.
ω_0	The harmonic oscillator frequency.
$\omega_L=\dfrac{eB}{2m^*}$	The Larmor frequency.
$\alpha=\frac{\omega_L}{\Omega}$	The magnetic field parameter
$\ell=\sqrt{\hbar/m^*\Omega}$	The effective magnetic length.
$\psi_{nm}(r,\varphi),\psi_{n_rm}(r,\varphi)$	The single-particle wave functions
E_{nm},E_{n_rm}	Energy levels.
$(n_rm),(n,m)$	Quantum numbers.
$\mathbf{R}=(\mathbf{r}+\mathbf{r}')/2$	Center of mass coordinate.
$\mathbf{S}=\mathbf{r}-\mathbf{r}'$	Relative coordinate.
L_k^d	Generalized Laguerre polynomials of order d and degree k
$\Theta(x)$	The step function.
μ	The Fermi energy
$\rho(\mathbf{r})$	The local particle density

$\mathbf{J}(\mathbf{r})$	The physical orbital current density
$\mathbf{J}_p(\mathbf{r})$	The paramagnetic orbital current density
$\boldsymbol{\mathcal{M}}(\mathbf{r})$	The microscopic magnetization
$\mathbf{M}$	The total orbital magnetic moment
I	The total azimuthal persistent current

Introduction

Introduction

In the presence of strong magnetic fields, electrons in metals experience quantum oscillations in their equilibrium and transport properties as a function of magnetic field intensity, usually observed at extremely low temperatures. The oscillations originate from the quantization of the electron energy spectrum, resulting in discrete energy levels referred to as Landau levels. Oscillations in the electron density of states at the Fermi level are caused by variable magnetic field intensities. As a result, various properties such as magnetization, conductivity, magnetoresistance, thermal and optical characteristics display oscillatory behavior. The intriguing phenomena, de Haas-van Alphen (magnetization) and Shubnikov–de Haas (magnetoresistance) oscillations, are essential tools for investigating the fundamental physical properties of metals. They offer insights into Fermi surface shape, effective electron mass, ect …,. Comprehensive experimental observations and theoretical analyses have been performed to clarify the complex nature of these oscillations, examining their dependencies on factors such as temperature, magnetic field intensity, and carrier density [1-8]

The study of quantum oscillations in metals has found a distinctive and powerful platform in two-dimensional electron gases (2DEGs). Emerging alongside semiconductor breakthroughs in the late 1960s, 2DEGs have become a cornerstone of modern condensed matter physics. Although the fast-growing field of newer low-dimensional materials, such as graphene, offers intriguing properties and functionalities, 2DEGs still attract considerable attention. While these novel quantum materials exhibit capabilities surpassing those of traditional 2DEGs, the latter have revolutionized areas like semiconductor physics and device engineering. As a versatile platform for investigating exotic quantum phenomena, including those resembling quantum oscillations in metals, 2DEGs have applications ranging from high-mobility transistors to potential components for quantum computers. Today, 2DEGs continue to be fertile ground for both fundamental research and future technological innovation [8-18].

Persistent currents in a non-uniform electron gas flow without energy dissipation even in thermal equilibrium when time-reversal symmetry is broken, for instance, by an external magnetic field. Orbital magnetism, such as Landau diamagnetism, arises from these nonvanishing equilibrium currents, which reveal their fascinating quantum mechanical origin. To understand the microscopic nature of current flow phenomena, such as the quantum Hall effect, it is essential to analyze the equilibrium and non-equilibrium current distributions in confined electron gases.

Furthermore, this comprehension sheds light on mesoscopic transport phenomena in general and the electrical characteristics of low-dimensional semiconductor nanostructures, including quantum dots and wires, when subjected to magnetic fields. In addition, the orbital magnetic characteristics of the confined electron system can be calculated by analyzing the current distribution [19-31].

The study of orbital magnetism originates from Landau's influential paper on diamagnetism in the 1930s [32]. This groundbreaking research presented fundamental quantum mechanical concepts such as Landau levels, which delineate the quantization of electron energy levels in a magnetic field, establishing essential foundations for comprehending the impact of electron orbital motion on their magnetic properties. This foundational framework has since underpinned investigations into a broad range of remarkable phenomena in condensed matter physics. Notably, it has been indispensable in exploring orbital magnetism and its quantum oscillations in various contexts, particularly in systems of reduced dimensionality such as 2DEGs.

Landau's theory, while innovative, mostly focused on extensive systems without explicitly accounting for boundary effects. Subsequent research has investigated orbital magnetism in systems characterized by finite sizes or particular geometries (reduced dimensionality). Diverse confining potentials, simulating boundary effects, have been utilized to investigate the thermodynamic features of electron gases under these constraints. This research has been crucial for comprehending phenomena such as the quantum Hall effect, electric current distribution, Landau diamagnetism with size corrections, and quantum oscillations of magnetization, particularly in mesoscopic and nanometer-scale systems [34-41].

The parabolic confinement has been studied extensively, especially in relation to 2DEG-based quantum dots, among other confining potentials. Its importance is largely due to the precise analytical solutions it provides, which allow for in-depth examination of the thermodynamic properties, such as specific heat, orbital magnetic moment, and other important features of confined electron gases, as well as their behavior in response to external electric or magnetic fields. A non-interacting electron system's one-particle Hamiltonian, the Fock-Darwin Hamiltonian [33,36], reduces to a quadratic form under parabolic confinement. The exact single-particle energy spectrum can be found using different algebraic methods [41-43], in addition to solutions obtained directly from the Schrödinger equation. This provides valuable insights into its behaviour under combined confinement and magnetic field. In addition, the harmonic oscillator confinement

potential provides the basis for more sophisticated many-body calculations when interactions between particles are taken into account [44].

Several theoretical approaches have been used to examine the thermodynamic equilibrium characteristics of the Fock-Darwin model, particularly its total orbital magnetic moment **M**. These frameworks encompass investigations utilizing single-particle wave functions [27,36-38], coherent states [46], Bloch density matrix technique [39-41], and exact trace formulas [46]. Moreover, researchers have investigated the model in the framework of non-commutative quantum mechanics[47] and examined the impact of minimal lengths[48]. Nevertheless, despite comprehensive research focused on the total orbital magnetic moment of this system, a significant gap remains. The spatial distribution of the magnetic moment **M** in real physical space is yet to be investigated. The microscopic orbital magnetization, denoted as $\boldsymbol{\mathcal{M}}(\mathbf{r})$, is given linked to the magnetic field-induced orbital persistent current density $\mathbf{J}(\mathbf{r})$, as given by the standard relation $\mathbf{J}(\mathbf{r}) = \boldsymbol{\nabla} \times \boldsymbol{\mathcal{M}}(\mathbf{r})$. The theory set out in Refs. [24, 26] proposes that, at low temperatures and high magnetic fields, the persistent current distribution in a confined quantum Hall fluid manifests an alternating pattern of counter-propagating currents when transitioning from an incompressible region to an adjacent compressible one within the particle density profile. The underlying reason for this outstanding behavior of counter-flowing currents is believed to be the oscillatory response of the equilibrium orbital magnetization of the 2DEG to variations in particle density under a fixed magnetic field.

Innovations in nanoscale magnetic field imaging techniques have revolutionized the examination of characteristics in quantum materials, particularly in two-dimensional systems and thin-film devices. These advanced techniques provide high-resolution imaging of magnetization patterns and current distributions, among others (see Ref. [49]). A notable breakthrough has recently occurred with direct nanoscale imaging of the counter-flowing persistent currents pattern, a phenomena theoretically predicted in Ref. [24] and long eluded conventional transport measurements. This milestone was achieved in graphene within quantum Hall edge states, thanks to scanning SQUID-on-tip microscopy [50]. Moreover, this experimental investigation has demonstrated that these currents can propagate throughout the entire sample, rather than being restricted solely to the sample boundaries.

Inspired by the new experimental results in Ref. [50], this study examines in detail important equilibrium properties of a completely degenerate harmonically confined two-dimensional

spinless electron gas under a normal magnetic field. There are two major reasons for using the idealized Fock-Darwin model, even if it might not completely represent the intricacies of the real world. First, because it is analytically tractable and useful for establishing basic ideas and understanding experimental results in many different kinds of physical systems (e.g., quantum dots). Also, Landau condensation with infinitely degenerate levels does not actually happen in a parabolic confining potential. A nondegenerate energy spectrum, with the exception of incidental degeneracies, is the consequence of quantum states continually experiencing the effects of the oscillator potential. As a result, our quantum eigenstates are considered to be edge states, making them susceptible to carrying currents throughout the entire system and thereby influencing the electronic properties of the 2DEG. In situations when sharp boundary wall potentials are involved, the bulk levels remain degenerate because the lifting of degeneracy mainly impacts a small number of states at the physical .

Our main objective is to explore and enhance comprehension of local orbital properties, specifically spatial matter distribution, current flow, and microscopic magnetization, alongside global properties like total magnetic moment and integrated persistent current, including their evolution in response to magnetic fields and their remarkable interplay. Furthermore, we intend to investigate how changes in the system's energy spectrum influence their behavior. we derive exact closed-form analytical formulations for all previously described properties., using two distinct methods: based on single-particle wave functions and the other on the Bloch matrix approach. Although these two approaches may initially yield seemingly different expressions, rigorous mathematical analysis or numerical computation reveals their equivalence, underscoring the reliability and consistency of the derived expressions and ensuring a comprehensive grasp of the system’s quantum behavior.

Some previously obtained analytical results are rederived here to achieve more concise, simpler, and efficient expressions than before, rendering them suitable for numerical computations. This facilitates deeper exploration of these properties. The analytical expression of the microscopic magnetization $\boldsymbol{\mathcal{M}}(\mathbf{r})$ enables deduction of the system’s total persistent electric current I without requiring a full derivation. [25,14]. This deduction is made possible by acknowledging that the integrated persistent current is equivalent to the microscopic magnetization at the center of the electron system, $I = \mathcal{M}(0)$.

The emergence of compressible and incompressible areas within the particle density profile is one of the intriguing phenomena that appear at strong magnetic fields. Therefore, we focus on presenting, analyzing, and discussing our numerical results within these quantizing magnetic field regimes, where Landau levels form and quantum oscillations become prominent. Specifically, we unravel the underlying structure of the counter-propagating equilibrium currents observed in these high regimes, driven by the oscillatory behavior of the microscopic magnetization, which we derive for the first time in exact analytical form in the real physical space.

This thesis is structured into four chapters, each addressing distinct aspects of our investigation into the equilibrium orbital properties of a completely degenerate, harmonically confined two-dimensional electron gas (2DEG) subjected to a perpendicular magnetic field. Through this work, we provide both theoretical insights and numerical results, offering a comprehensive understanding of the system's quantum behavior

Chapter 1 introduces the two-dimensional electron gas (2DEG), a cornerstone of modern condensed matter physics. We outline its fundamental characteristics, physical significance, and the experimental conditions under which it is typically realized in semiconductor heterostructures. This chapter underscores the pivotal role of 2DEGs as a platform for exploring quantum phenomena, setting the stage for the subsequent theoretical and numerical analysis.

Chapter 2 explores the behavior of a harmonically confined 2DEG in the presence of a perpendicular magnetic field. We begin by describing the physical system and introduce two complementary theoretical frameworks: the single-particle wave function approach and the Bloch density matrix formalism. These frameworks provide a robust foundation for investigating the system's orbital properties. Within the single-particle approach, we derive the stationary solutions of the Schrödinger equation and the corresponding energy spectrum. Simultaneously, we highlight the advantages of the Bloch density matrix formalism, particularly its efficacy in deriving key physical quantities such as the particle density and current distribution. This chapter lays the groundwork for the analytical derivations presented in Chapter 3.

Chapter 3 is dedicated to the derivation of exact analytical expressions for several equilibrium orbital properties of the system. Using the two frameworks introduced in Chapter 2, we obtain expressions for the particle density, current distribution, microscopic magnetization $\boldsymbol{\mathcal{M}}(\mathbf{r})$, total magnetic moment, and integrated persistent electric current I. Although the two approaches initially yield seemingly distinct results, we demonstrate their equivalence through numerical

verification. This consistency not only validates our derivations but also deepens the understanding of the system's quantum behavior. A key finding of this chapter is the relationship between the microscopic magnetization $\boldsymbol{\mathcal{M}}(\mathbf{r})$ and the total persistent electric current I. We show that I can be deduced directly from the value of $\boldsymbol{\mathcal{M}}(\mathbf{r})$ at the center of the electron system, bypassing the need for a full derivation of the current. This result highlights the elegance and efficiency of our analytical approach.

Chapter 4 presents and analyzes our numerical results, focusing on regimes dominated by high magnetic fields. In these regimes, the system exhibits striking features, such as the formation of compressible and incompressible regions within the particle density profile. We examine the behavior of Landau levels and quantum oscillations, which become prominent under strong magnetic fields. A particular emphasis is placed on the counter-propagating equilibrium currents observed in these regimes, which arise from the oscillatory behavior of the microscopic magnetization. By deriving the microscopic magnetization in exact analytical form in real physical space and numerically studying its behavior, we provide new insights into the spatial structure of these currents. This chapter not only validates our theoretical predictions but also reveals the intricate interplay between magnetic fields and quantum effects in confined 2DEGs.

A **general conclusion** terminates the thesis, summarizing the key findings, their implications, and potential directions for future research. This final section consolidates the theoretical and numerical insights gained throughout the work, emphasizing their significance for the study of quantum phenomena in confined 2DEGs and their broader relevance to condensed matter physics

Chapter 1

An Overview of 2DEGs: Concepts, Experimental Realization, and Applications

Chapter 1

An Overview of 2DEGs: Concepts, Experimental Realization, and Applications

1. Introduction

A two-dimensional electron gas (2DEG) is a model in solid-state physics that describes a system of electrons confined to move in two dimensions while being tightly restricted in the third dimension. This confinement results in quantized energy levels along the third axis, allowing for simplified analysis of the system as effectively two-dimensional [9].

The confinement of electrons in (2DEG) leads to discrete energy levels, meaning that at low temperatures, only specific energy states are occupied. This quantization is crucial for studying phenomena like the quantum Hall effect and other quantum transport properties [51]. 2DEGs are primarily realized in semiconductor structures, such as Metal-Oxide-Semiconductor Field-Effect Transistors (MOSFETs), where electrons accumulate at the semiconductor-oxide interface, and in High-Electron-Mobility Transistors (HEMTs), which use heterojunctions to achieve superior electron mobility. Additionally, quantum wells, which confine electrons in stacked semiconductor layers, and advanced materials like graphene and transition-metal oxides, have expanded the applications of 2DEGs to next-generation electronic devices and quantum computing.

In this chapter, we will explore fundamental concepts essential for understanding the physics of two-dimensional electron gases (2DEGs) and their behavior under external magnetic fields. We begin by discussing the experimental realization of 2DEGs, which serve as a cornerstone in the study of quantum systems in reduced dimensions. Next, we examine the effects of harmonic (parabolic) confinement, which significantly influences the electronic properties of 2DEGs by restricting the motion of electrons within a well-defined potential landscape.

Quantum dots, often referred to as artificial atoms, will also be addressed in the context of 2DEGs, highlighting their relevance to quantum computing and nanotechnology. These quantum dots, which can be fabricated within 2DEG systems, benefit from the unique confinement and quantum effects of the underlying 2DEG structure, thereby playing a significant role in both experimental and applied quantum physics.

We will then focus on the study of a free charged particle in a perpendicular magnetic field, with an emphasis on the influence of different gauge choices and the formation of Landau levels.

The chapter will also cover the Quantum Hall Effect, a groundbreaking phenomenon that has provided profound insights into the nature of topological phases of matter. Finally, we will explore quantum oscillations in various physical properties, such as specific heat and magnetization, which serve as experimental probes into the quantum states of the system.

2. Experimental realization of 2DEG

The experimental realization of a two-dimensional electron gas (2DEG) in both metal-oxide-semiconductor field-effect transistors (MOSFETs) and high-electron-mobility transistors (HEMTs) has been pivotal in advancing semiconductor technology. These structures exploit the unique properties of 2DEGs to enhance device performance, particularly in high-speed applications.

In MOSFETs, a 2DEG is formed at the semiconductor-oxide interface when a voltage is applied to the gate. This voltage induces an inversion layer, allowing electrons to accumulate beneath the gate oxide. The resulting 2DEG is characterized by high electron mobility and density, which can be tuned through gate voltage[52].

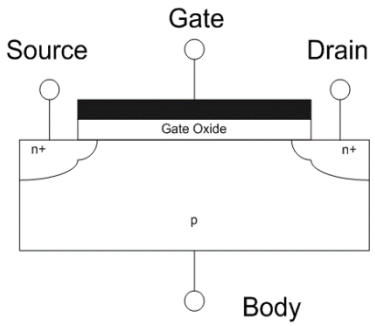

Fig 1 : In MOSFETs ,the 2DEG is only present when the transistor is in inverion mode, and is found directly beneath the gate oxide

HEMTs utilize heterojunctions between different semiconductor materials, such as AlGaN/GaN or InGaN/InN, to create a 2DEG. The design allows for an undoped channel that minimizes ionized impurity scattering, resulting in higher electron mobilities compared to traditional MOSFETs.

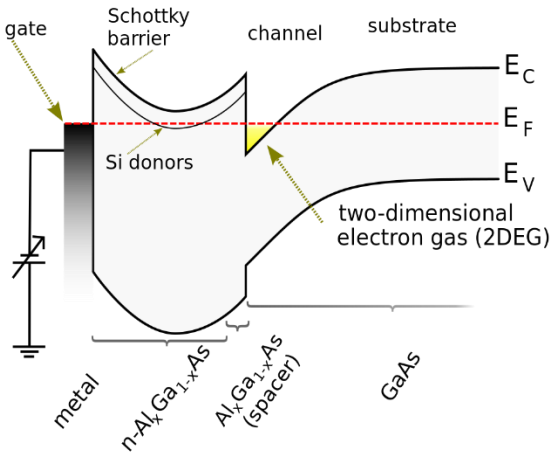

Fig 2 : Band edge diagram of a basic HEMT. Conduction band edge $\boldsymbol{E_C}$ and Fermi level $\boldsymbol{E_F}$ determine the electron density in the 2DEG. Quantized levels form in the triangular well (yellow region) and optimally only one of them lies below $\boldsymbol{E_F}$ [53].

3. Parabolic confinement of the 2DEG:

We employ a harmonic confining potential to laterally restrict electrons to a two-dimensional plane, specifically within a semiconductor heterostructure that hosts a two-dimensional electron gas (2DEG). This parabolic confinement provides a well-defined framework for studying the quantum mechanical properties of the system under an applied magnetic field.

The harmonic potential in polar coordinates (r, θ) is given by:

$$V(r) = \frac{1}{2} m^* \omega_0 r^2 \tag{1.1}$$

where:

m^* is the effective mass of the electron,

ω_0 is the angular frequency of the harmonic potential,

r is the radial distance from the center of the trapping potential.

This potential leads to quantized energy levels. The interplay between this confining potential and an applied magnetic field significantly influences the physical properties of the 2DEG.

4. Quantum dots

Quantum dots are a significant area of research in semiconductor physics, particularly for their applications in quantum information processing and nanoelectronics. The formation and behavior of quantum dots in 2DEGs are influenced by the unique properties of these systems, which allow for precise control over electron confinement and manipulation.

Quantum dots can spontaneously form within 2DEGs due to potential fluctuations caused by impurities or defects in the semiconductor material. In devices like GaN/AlGaN field-effect transistors (FETs), quantum dots have been observed near the depletion region of the 2DEG, where electrons become trapped in potential minima. This trapping leads to quantization effects, such as single-electron charging and size quantization, which are essential for the operation of quantum bits [54].

5. Free charged particle under a normal magnetic field

In this section, we will attempt to get an understanding of how quantum particles respond to magnetic fields. Before we get to the description of quantum effects, we need to emphasize a few of the more subtle elements that come up when talking about classical physics in the presence of a magnetic field.

5.1. Gauge Fields

The electric field $\mathbf{E}(\mathbf{r},t)$ and magnetic field $\mathbf{B}(\mathbf{r},t)$ may be expressed using a scalar and a vector potential ϕ and $\mathbf{A}$, respectively.

$$\mathbf{E} = -\nabla\phi - \frac{\partial \mathbf{A}}{\partial t} \ , \mathbf{B} = \nabla \times \mathbf{A} \tag{1.2}$$

$\mathbf{A}$ and ϕ are called gauge fields.

When a particle with mass m and charge q moves in an electromagnetic field with background, its Lagrangian is

$$L = \frac{1}{2}m\dot{\mathbf{r}}^2 + q\dot{\mathbf{r}} \cdot \mathbf{A} - q\phi \tag{1.3}$$

From this Lagrangian, the classical equation of motion that is produced is

$$m\ddot{\mathbf{r}} = q(\mathbf{E} + \dot{\mathbf{r}} \times \mathbf{B}) \tag{1.4}$$

This is the Lorentz force law

5.2. Motion in a Constant Magnetic Field

We will assume that $\mathbf{B} = (0, 0, B)$ is a constant magnetic field oriented in the z-direction. Let's assume $\mathbf{E} = \mathbf{0}$. The particle's equation of motion $m\ddot{z} = 0$, indicates that it is free in the z-direction.

The (x, y)-plane, where the equations of motion are located, is where the most fascinating dynamics occur [55].

$$m\ddot{x} = qB\dot{y},\ m\ddot{y} = -qB\dot{x} \tag{1.5}$$

The general solution is:

$$x(t) = X + R\,sin(\omega_B(t - t_0))\,, y(t) = Y + R\,cos(\omega_B(t - t_0)) \tag{1.6}$$

It is evident that the particle travels in in the opposite direction within a circle if $B > 0$ and $q > 0$ (Fig(3))

The definition of the cyclotron frequency is

$$\omega_c = \frac{qB}{m} \tag{1.7}$$

The circle's centre (X, Y), its radius (R), and its phase (t_0) are all random

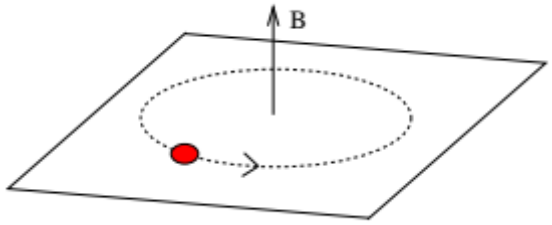

Fig 3 : the motion of a particle for $\mathbf{B} > \mathbf{0}$ and $\boldsymbol{q} > \mathbf{0}$

5.2.1. The Hamiltonian

The canonical momentum in the presence of gauge fields is

$$\mathbf{p} = \frac{\partial L}{\partial \dot{\mathbf{r}}} = m\dot{\mathbf{r}} + q\mathbf{A} \tag{1.8}$$

This is obviously not the same as $m\dot{\mathbf{r}}$, which is what we refer to as kenitic momentum.

The Hamiltonian is given by

$$H = \dot{\mathbf{r}}\,.\,\mathbf{p} - L = \frac{1}{2m}(\mathbf{p} - q\mathbf{A})^2 + q\phi \tag{1.9}$$

5.2.2. Gauge Transformations

The gauge fields **A** and ϕ are not unique. We can change them as

$$\phi \to \phi - \frac{\partial \alpha}{\partial t}\ ;\quad \mathbf{A} \to \mathbf{A} + \boldsymbol{\nabla}\alpha \tag{1.10}$$

Where $\alpha = \alpha(\mathbf{r}, t)$ is an arbitrary function. Under these transformations, the electric and magnetic fields (1.2) remain unchanged. The Lagrangian (1.3) changes by a total derivative, but this is sufficient to ensure that the resulting equations of motion (1.5) are unchanged. Different choices of α are said to be different choices of gauge.

According to equation (1.6), the canonical momentum $\mathbf{p}$ is not gauge invariant; rather, it undergoes a transformation as $\mathbf{p} \to \mathbf{p} + q\boldsymbol{\nabla}\alpha$. This indicates that the numerical value of $\mathbf{p}$ cannot possibly have any physical significance since it is dependent on the gauge that we take into consideration. In contrast, the particle's velocity is more important. Both the Hamiltonian H and the gauge invariant $\dot{\mathbf{r}}$ are physical in nature since they are gauge invariant.

The Schrodinger Equation

Following the standard process for quantization, we substitute the canonical momentum with an operator as following

$$\mathbf{p} \to -i\hbar\boldsymbol{\nabla}$$

For a charged particle, such an electron, moving in a magnetic field, the time-independent Schrödinger equation takes the form:

$$\left[\frac{1}{2m}(-i\hbar\boldsymbol{\nabla} - q\mathbf{A})^2 + V(\mathbf{r})\right]\psi(\mathbf{r}) = E\psi(\mathbf{r}) \tag{1.11}$$

5.3. Landau Levels

We need to determine the spectrum and wavefunctions of the Schrödinger equation. We are interested in the scenario when the electric field vanishes ($\mathbf{E} = \mathbf{0}$) and the magnetic field remains constant. The quantum Hamiltonian is

$$H = \frac{1}{2m}(\mathbf{p} - q\mathbf{A})^2 \tag{1.12}$$

We take the magnetic field to lie in the $z-$direction, so that $\mathbf{B} = (0, 0, B)$. To proceed, we need to find a gauge potential $\mathbf{A}$ which obeys $\nabla \times \mathbf{A} = \mathbf{B}$. There is, of course, no unique choice. Here we pick

$$\mathbf{A} = (0, xB, 0) \tag{1.13}$$

We refer to this choice as the Landau gauge. It should be noted that in the $(x, y)-$plane, the magnetic field $\mathbf{B} = (0, 0, B)$ is invariant under both translational and rotational symmetry, but the choice $\mathbf{A}$ is not; it breaks both rotational and translational symmetry in the x direction (but not in the y direction). This implies that the intermediate computations will not be obviously invariant, even if the physics will be invariant under all symmetries. This kind of compromise is common in magnetic field applications.

The Hamiltonian (1.12) becomes :

$$H = \frac{1}{2m}\left(p_x^2 + \left(\mathrm{p_y} - qBx\right)^2\right) \tag{1.14}$$

We may search for energy eigenstates that are also eigenstate of p_y because we have $[p_y, H] = 0$ due to our evident translational invariance in the y direction. This is what spurs the idea.

$$\psi(\mathbf{r}) = e^{ik_y y}\chi(x) \tag{1.15}$$

Applying momentum operators to this wavefunction $p_y = -\mathrm{i}\hbar\partial_y$, we have

$$p_y\psi(\mathbf{r}) = \hbar k_y\psi(\mathbf{r}) \tag{1.16}$$

Substituting (1.15) in the stationary Schrodinger equation $H\psi(\mathbf{r}) = E\psi(\mathbf{r})$, simply replaces p_y with its eigenvalues, and we have:

$$H\psi(\mathbf{r}) = \frac{1}{2m}\left(p_x^2 + \left(\hbar k_y - q\mathrm{Bx}\right)^2 + \hbar^2 {k_z}^2\right)\psi(\mathbf{r}) = E\psi(\mathbf{r}) \tag{1.17}$$

which can be written as an eigenvalue equation for $\chi(x)$. We have

$$\breve{H}\chi(x) = E\chi(x) \tag{1.18}$$

Where $\breve{H}$ is the Hamiltonian for a harmonic oscillator in the x direction, with the centre displaced from the origin

$$\breve{H} = \frac{1}{2m}p_x^2 + \frac{m\omega_c^2}{2}\left(x - k_y l_B^2\right)^2 \tag{1.19}$$

The harmonic oscillator has the cyloctron frequency defined by $\omega_c = qB/m$ .The characteristic length scale l_B, which governs the quantum phenomena in a magnetic field, is called the magnetic length and is given by

$$l_B = \sqrt{\frac{\hbar}{qB}} \tag{1.20}$$

In the Hamiltonian (1.19) the momentum in the y direction, $\hbar k_y$, has turned into the position of the harmonic oscillator in the x direction, which is now centred at $x = k_y l_B^2$.

We can immediately write the energy eigenvalues of (1.19), they are simply those of the harmonic oscillator

$$E = \hbar\omega_c\left(n + \tfrac{1}{2}\right), \; n=0,1,2,..... \tag{1.21}$$

Each Landau level has a high degree of degeneracy, meaning that many quantum states correspond to the same energy. This degeneracy is related to the area of the two-dimensional system and the strength of the magnetic field. The number of available quantum states in each Landau level is proportional to the total magnetic flux through the system.

5.3.1. Symmetric Gauge

It seems sense to carry out the aforementioned computations again with a different gauge selection. This will provide us with a slightly perspective on the physics. The obvious option is symmetric gauge.

$$\mathbf{A} = -\frac{1}{2}\mathbf{r} \,.\, \mathbf{B} = \frac{B}{2}(-y, x, 0) \tag{1.22}$$

Translational symmetry is broken by this gauge selection in both the x and y axes. On the other hand, rotational symmetry around the origin is preserved. This indicates that angular momentum is now a useful quantum number for state labelling.

In this gauge, the Hamiltonian is given by

$$H = \frac{1}{2m}\left[\left(p_x + \frac{qBy}{2}\right)^{\mathbf{2}} + \left(p_y - \frac{qBx}{2}\right)^2\right] \tag{1.23}$$

$$= \frac{-\hbar^2}{2m}\boldsymbol{\nabla}^2 + \frac{q^2B^2}{8m}(x^2 + y^2) - \frac{qB}{2m}L_z$$

Where

$$L_z = xp_y - yp_x \tag{1.24}$$

6. The Quantum Hall Effect

Electrons in the system are limited to motion within the (x, y) −plane. $q = -e$ represents an electron's charge. When a magnetic field is present, they will initially occupy the $N = eBA/2\pi\hbar$ states in the $n = 0$ lowest Landau level. The $n = 1$ Landau level will be filled with any remaining particles, and so forth.

Increasing the magnetic field B depletes higher Landau levels as the quantity of states N contained within them increases.

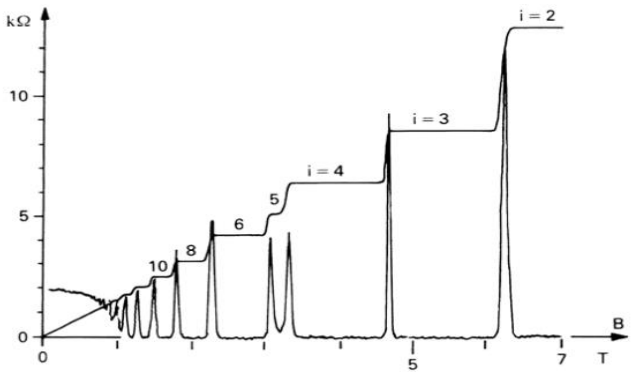

Fig 4 :The integer quantum Hall effect[56].

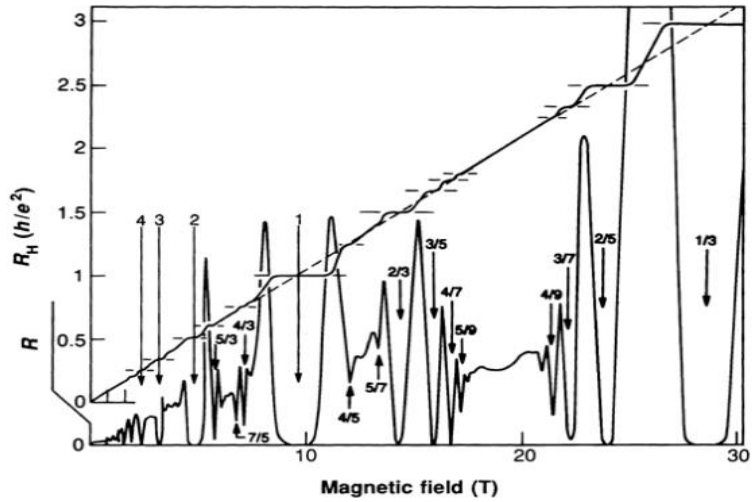

Fig 5 :The fractional quantum Hall effect[56]

As illustrated in Figures 4 and 5, the behaviour of the resistivity as a function of the applied magnetic field is demonstrated. It turns out that the integer quantum Hall effect is a direct consequence of theexistence of discrete Landau levels.

7. Quantum oscillations as function of magnetic field

Quantum oscillations are a phenomenon observed in various materials when subjected to strong magnetic fields, leading to quantized energy levels known as Landau levels. These oscillations are closely related to the properties of the Fermi surface and are crucial for understanding electronic behavior in metals and insulators.

The De Haas-Van Alphen effect (dHvA) arises from the quantization of energy levels (Landau levels) in a magnetic field, leading to periodic oscillations specific heat and magnetization.

7.1. Quantum oscillations in the specific heat

In specific heat measurements, quantum oscillations can be observed as the magnetic field strength increases. These oscillations are closely linked to the density of states at the Fermi level, which varies with the magnetic field due to the Landau level structure.

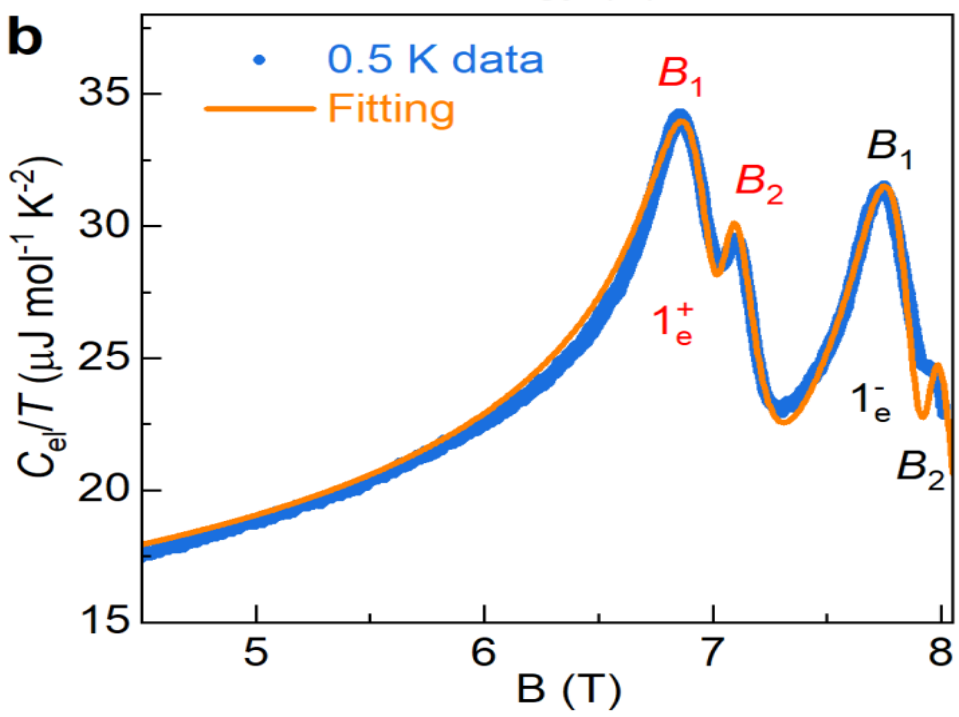

Fig 6 : Electronic specific heat divided by temperature C_{el}/T in graphite as a function of magnetic field at $T = 0.5\ K$[57]

7.2. Quantum oscillations in magnetization

Quantum oscillations in magnetization, known as the (dHvA) effect, are a significant phenomenon observed in both metals and insulators under strong magnetic fields.The oscillations in magnetization arise from the periodic filling of these levels as the magnetic field varies.

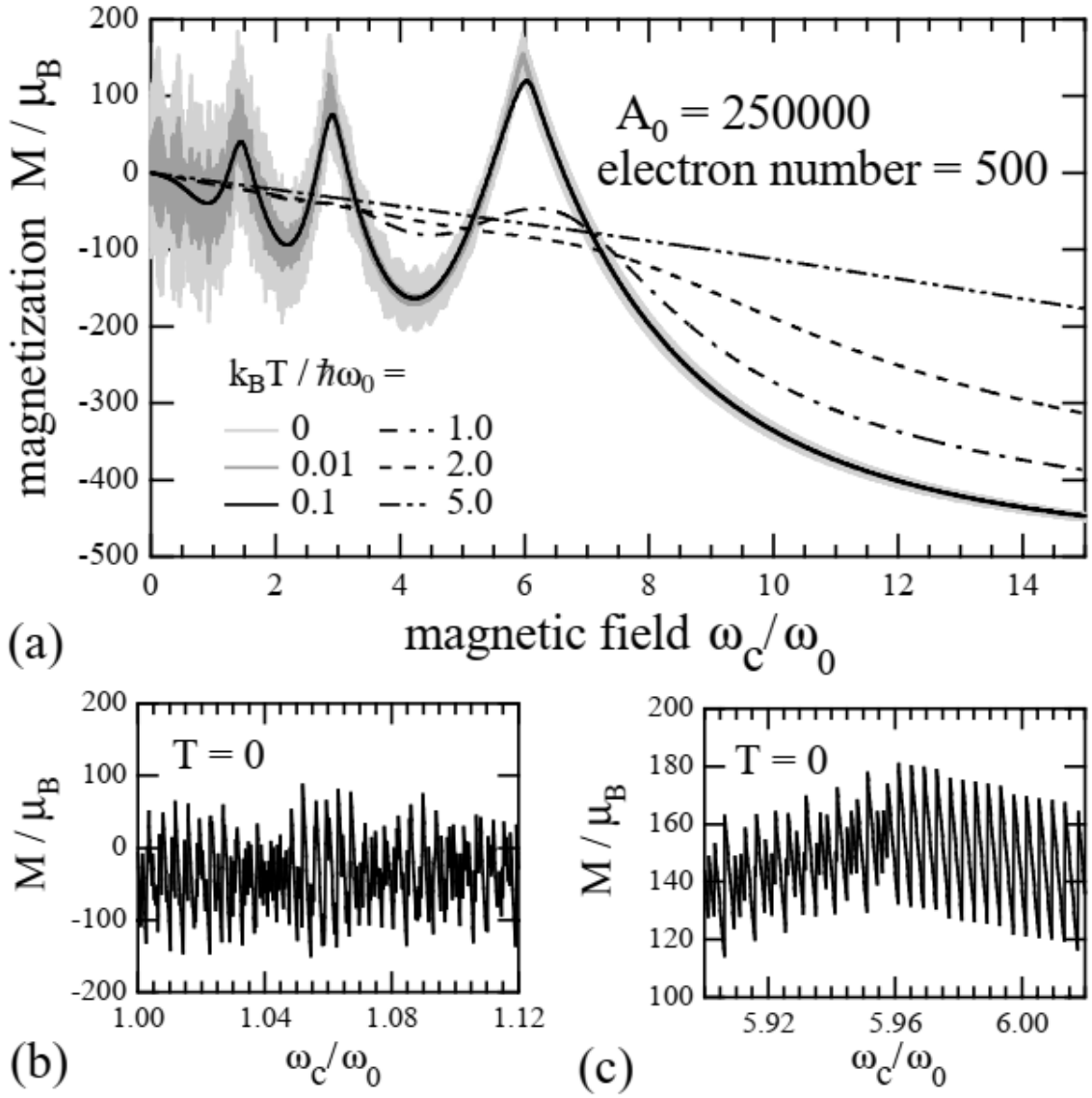

Figure 7 : Example of the magnetic field dependence of the magnetization of a ring with electron number = 500 and several choices of temperatures [58].

Chapter 2

Harmonically Confined 2DEG Under a Normal Magnetic Field: Description and Theoretical Frameworks

Chapter 2

Harmonically Confined 2DEG Under a Normal Magnetic Field: Description and Theoretical Frameworks

1. Introduction

In quantum mechanics, the behavior of electrons is characterized by wavefunctions, which encapsulate all the information about a particle's position, momentum, and energy. The stationary Schrödinger equation formalizes the relationship between the Hamiltonian operator, which represents the total energy of the system, and the wavefunction of the electron. By solving this equation, one can derive the possible energy states that the electron can occupy under the influence of a magnetic field.

Another approach which will be used in this work is based on the use of what is known as the Bloch density matrix [59], abbreviated as BDM and denoted by $C(\mathbf{r},\mathbf{r}';\xi) = \langle\mathbf{r}|\exp(-\xi H)|\mathbf{r}'\rangle$, where "$\xi$" is a general complex mathematical parameter with positive real part, possessing the dimension of an inverse energy This density matrix represents the Bloch propagator $\exp(-\xi H)$ in the position representation $\{|\mathbf{r}\rangle\}$.

Two key reasons typically support the use of the Bloch density matrix approach. Firstly, $C(\mathbf{r},\mathbf{r}';\xi)$ provides direct access to $\rho(\mathbf{r},\mathbf{r}')$, crucial for deriving thermodynamic and magnetic properties of quantum gases. Secondly, explicit knowledge of single-particle wave functions and energies of the confining potential is not required. Additionally, by replacing ξ with an imaginary time interval $i(t-t')/\hbar$, it allows defining the single-particle propagator. Moreover, the use of the Bloch density matrix approach in the investigation of our system enables the derivation of an analytical expression for the microscopic magnetization, as will be discussed in the chapter 3.

In this work, we explore the fascinating behavior of a harmonically confined (2DEG) subjected to a perpendicular magnetic field. This system serves as a crucial model for understanding the interplay between quantum confinement and magnetic effects, offering insights into various quantum phenomena.

A central focus of this chapter is solving the Schrödinger equation for our harmonically confined 2DEG in the presence of a magnetic field. We will derive the stationary solutions, which reveal how the magnetic field modifies the electron wavefunctions and energy levels, offering insights into the quantum behavior of the system.

In the next step, we will introduce the Bloch density matrix formalism, and we will show how it connects to various physical quantities of interest.

2. System description

When electrons are confined to move in a plane and subjected to a perpendicular magnetic field, their motion becomes quantized due to the interaction with the magnetic field. This quantization leads to the formation of Landau levels, which are discrete energy levels that electrons can occupy.

We consider a completely degenerate two-dimensional electron gas, made up of N non-interacting spinless electrons of charge $-e$ $(e > 0)$ and effective mass m^*. The system is confined, in the $xy-$plane, by a radially symmetric harmonic potential $V(r) = m^*\omega_0^2\, r^2$ frequency ω_0, and subjected to a uniform perpendicular magnetic field $\mathbf{B} = B\mathbf{e_z}$ along the z axis of unit vector $\mathbf{e_z}$, where $\mathbf{B}$ is a positive constant. The quantum one-body Hamiltonian H governing the non-relativistic motion of the electron reads

$$H = \frac{1}{2m^*}(\mathbf{p} + e\mathbf{A})^2 + \frac{1}{2}m^*\omega_0^2\, r^2 \tag{2.1}$$

where $\mathbf{p}$ is the canonical momentum of the electron, and $r = |\mathbf{r}| = \sqrt{x^2 + y^2}$. The vector potential $\mathbf{A}$ *i*s associated with the external magnetic field $\mathbf{B}$ by the relation

$$\mathbf{B} = \boldsymbol{\nabla} \times \mathbf{A} \tag{2.2}$$

Knowing that this magnetic field is constant, we can then choose the following symmetrical gauge (the Coulomb gauge).

$$\mathbf{A} = \frac{1}{2}(\mathbf{B} \times \mathbf{r}) = \frac{1}{2}\mathbf{B}\,(-y\mathbf{e_x} + x\mathbf{e_y}) \tag{2.3}$$

for which the two operators $\mathbf{A}$ and $\mathbf{p}$ commute ($\mathbf{Ap} = \mathbf{pA}$). this allows the one-particle Hamiltonian (2.1) expansion to be written as

$$H = \frac{1}{2m^*}\mathbf{p}^2 + \frac{1}{2}m^*{\omega_0}^2 r^2 + \frac{e}{m^*}\mathbf{A}\cdot\mathbf{p} + \frac{e^2}{2m^*}\mathbf{A}^2 \tag{2.4}$$

We have according to (2.3)

$$\mathbf{Ap} = \frac{1}{2}(\mathbf{B} \times \mathbf{r})\,\mathbf{p} = \frac{1}{2}\mathbf{B}(\mathbf{r} \times \mathbf{p}) = \frac{1}{2}\mathbf{B}.\mathbf{L} = \frac{1}{2}B.L_Z \tag{2.5}$$

where **L** is the orbital angular momentum of the electron and L_z is its projection on the axis (Oz). also, we have

$$\mathbf{A}^2 = \frac{1}{4}B^2\,(x^2 + y^2) = \frac{1}{4}B^2r^2 \tag{2.6}$$

Inserting (2.5) and (2.6) into the expression of the Hamiltonian (2.4) gives

$$H = \frac{1}{2m^*}\mathbf{p}^2 + \frac{1}{2}m^*\omega_0^2r^2 + \omega_L L_z + \frac{1}{2}\omega_L^2r^2 \tag{2.7}$$

where ω_L is the Larmor frequency with

$$\omega_L = \frac{eB}{2m^*} \tag{2.8}$$

By putting

$$\Omega = \sqrt{\omega_0^2 + \omega_L^2} \tag{2.9}$$

we can rewrite the Hamiltonian (2.7) as follows

$$H = \frac{1}{2m^*}\mathbf{p}^2 + \frac{1}{2}m^*\Omega^2\mathbf{r}^2 + \omega_L L_z \tag{2.10}$$

3. Stationary solutions of Schrodinger equation

The Schrödinger equation corresponding to the Hamiltonian H, given by (2.10), in polar coordinates (r, φ) takes the form:

$$\left[\frac{-\hbar^2}{2m^*}\left(\frac{\partial^2}{\partial r^2} + \frac{1}{r}\frac{\partial}{\partial r} + \frac{1}{r^2}\frac{\partial^2}{\partial \varphi^2}\right) + \frac{m^*\Omega^2}{2}r^2 + \omega_L L_z\right]\psi(r,\varphi) = E\psi(r,\varphi) \tag{2.11}$$

Where E are the energies associated with the Hamilton H. This differential equation makes it possible to factorize $\psi(r,\varphi)$ into two radial and angular functions:

$$\psi(r,\varphi) = \chi(r)\phi(\varphi) \tag{2.12}$$

The determination of the angular part $\phi(\varphi)$ is made directly by taking into account the fact that $\psi(r,\varphi)$ is an eigenfunction of L_z. We have:

$$L_z\psi(r,\varphi) = m\hbar\psi(r,\varphi) \Rightarrow -i\hbar\frac{\partial}{\partial\varphi}\chi(r)\phi(\varphi) = m\hbar\chi(r)\phi(\varphi) \tag{2.13}$$

Where ($m = 0, \pm 1, \pm 2, \ldots$) indicates the possible values of the projection of L_z on the Oz axis. Not to be confused with the mass of the particle. The solution of the equation (2.14) is thus:

$$\phi(\varphi) = \exp(im\varphi) \tag{2.14}$$

For the radial part, the Schrödinger equation (2.11) can be put in the following form:

$$\left[\frac{\partial^2}{\partial r^2} + \frac{1}{r}\frac{\partial}{\partial r} - \frac{m^2}{r^2} - \frac{1}{\ell^4}r^2 + k^2\right]\chi(r) = 0 \tag{2.15}$$

Where we put:

$$\ell = \sqrt{\hbar/m^*\Omega} \tag{2.16}$$

Is the effective magnetic length, and

$$k^2 = \frac{2m^*E}{\hbar^2} - 2\alpha\frac{m}{\ell^2} \tag{2.17}$$

Where $\alpha = \frac{\omega_L}{\Omega}$ is a dimensionless magnetic field parameter, which encodes the magnetic field strength. Therefore, $0 \leq \alpha \leq 1$. The zero and one limiting values correspond to cases of vanishing magnetic field and switched off confining potential, respectively.

The equation (2.15) is a second-order differential equation whose solutions are given by [60]:

$$\chi(r) = r^{|m|}\exp\left(-\frac{r^2}{2\ell^2}\right)\ {}_1F_1\left(\lambda, |m|+1, \frac{r^2}{\ell^2}\right) \tag{2.18}$$

With

$$\lambda = \frac{1}{2}(|m|+1) - \frac{1}{4}\ell^2k^2 \tag{2.19}$$

is the argument of the hypergeometric confluent series ${}_1F_1$. Indeed, these solutions in the form of a confluent hypergeometric series are divergent solutions, except if the argument λ is a negative integer.

$$\lambda = -n_r \quad , n_r = 0,1,2, \ldots \ldots \ldots \ldots \tag{2.20}$$

Thus, the wave functions would be normalizable, with this condition on the value of λ, we can obtain the corresponding eigenenergies E. According to (2.16), (2.17), (2.19), and (2.20), we find:

$$E_{n_r,m} = (2n_r + |m| + 1)\hbar\Omega + m\hbar\omega_L \tag{2.21}$$

In this case, the confluent hypergeometric series is related to generalized Laguerre polynomial as [61]

$$ {}_1F_1\left(-n_r, |m|+1, \frac{r^2}{\ell^2}\right) = \frac{n_r!\,|m|!}{(n_r+|m|)!} L_{n_r}^{|m|}\left(\frac{r^2}{\ell^2}\right) \tag{2.22} $$

We inject this relation into (2.18), and by using the two equations (2.12) and (2.14), we get the wave functions of the Hamiltonian (2.10) with the energy spectrum (2.21):

$$ \psi_{n_r,m}(r,\varphi) = C\,\frac{n_r!\,|m|!}{(n_r+|m|)!} r^{|m|} e^{\left(-\frac{r^2}{2\ell^2}\right)} L_{n_r}^{|m|}\left(\frac{r^2}{\ell^2}\right) e^{im\varphi} \tag{2.23} $$

Where C is the normalization constant, which follows from the condition:

$$ \int_0^{\infty}\int_0^{2\pi} {\psi^*}_{n_r,m}(r,\varphi)\psi_{n_r,m}(r,\varphi) r\,dr\,d\varphi = 1 \tag{2.24} $$

And using the relationship [61]:

$$ \int_0^{\infty} x^p \exp(-x)\left[L_n^p(x)\right]^2 dx = \frac{(n+p)!}{n!} \tag{2.25} $$

We find the value of the constant C which after insertion in (2.23) gives the explicit form of the eigenfunctions of the Hamiltonian (2.10).

$$ \psi_{n_r,m}(r,\varphi) = \frac{1}{\ell}\sqrt{\frac{n_r!}{\pi(n_r+|m|)!}}\left(\frac{r}{\ell}\right)^{|m|} \exp\left(-\frac{r^2}{2\ell^2}\right) L_{n_r}^{|m|}\left(\frac{r^2}{\ell^2}\right) e^{im\varphi} \tag{2.26} $$

We can write Eq (2.26) in this form

$$ \psi_{n_r,m}(r,\varphi) = \mathcal{R}_{n_r m}(r) e^{im\varphi} \tag{2.27} $$

where the radial function $\mathcal{R}_{n_r m}(r)$ reads

$$ \mathcal{R}_{n_r m}(r) = \frac{1}{\ell}\sqrt{\frac{n_r!}{\pi(n_r+|m|)!}}\left(\frac{r}{\ell}\right)^{|m|} \exp\left(-\frac{r^2}{2\ell^2}\right) L_{n_r}^{|m|}\left(\frac{r^2}{\ell^2}\right) \tag{2.28} $$

4. Energy spectrum

At high magnetic field regimes, quantum effects become increasingly significant, profoundly influencing the behavior of various thermodynamic quantities. In our numerical investigation, we will observe that distinct regularities in the studied physical properties emerge as the ratio α approaches 0.99 and beyond. This behavior can be attributed to the well-known phenomenon where increasing the magnetic field clusters the energy spectrum into highly degenerate Landau

levels.These discrete levels exert a unique influence on each equilibrium property, underscoring the intricate interplay between quantum mechanics and macroscopic observables.

The single-particle energies, given by (2.21) and commonly referred to as the Fock-Darwin spectrum [33,36], can be expressed as:

$$E_{n_r,m} = (2n_r + |m| + 1)\hbar\Omega + m\hbar\omega_L = (\mathcal{N} + 1)\hbar\Omega + m\hbar\omega_L \qquad (2.29)$$

Where $\mathcal{N} = 2n_r + |m| = 0,1,2$ ... is the principal quantum number indicating the harmonic oscillator shells in the absence of magnetic field.

It's worth noting that the energy spectrum of the considered system can also be expressed as the sum of the spectra of two independent harmonic oscillators with different frequencies, $\Omega_\pm = \Omega \pm \omega_L$. This can be achieved using only purely algebraic methods based either on the rotating creation and annihilation operator approach [42]. or the canonical transformation technique [43], both leading to the following alternative expression for the eigenenergies

$$E_{nm} = (n + 1/2)\hbar\Omega_+ + (m + 1/2)\hbar\Omega_- = (n + m + 1)\hbar\Omega + (n - m)\hbar\omega_L \qquad (2.30)$$

Here n and m are non-negative integer quantum numbers representing the number of right and left circularly polarized quanta, respectively. To gain further interpretation of this new set of quantum numbers (n, m), let's examine their relationship with the previously defined numbers, namely $\mathcal{N}$, n_r and m. By comparing the two Eqs (2.29) and (2.30), we find the following relationships

$$\begin{cases} n + m = 2n_r + |m| = \mathcal{N} \\ n - m = m \end{cases} \qquad (2.31)$$

Thus, the sum $(n + m)$ corresponds to the index of the harmonic oscillator shells, while the difference $(n - m)$ represents the angular momentum magnetic quantum number. Furthermore, the number n uniquely identifies each Landau level in the case of unconfined electrons as we will discuss later on. Conversely, we get for the radial number n_r the following relation

$$n_r = \min\{n, m\} \qquad (2.32)$$

The single-particle wave functions $\psi_{nm}(r, \varphi)$ corresponding to the new set of quantum numbers (n, m) take the following form

$$\psi_{nm}(r,\varphi) = \frac{1}{\sqrt{\pi}\ell} e^{\left(-\frac{r^2}{2\ell^2}\right)} e^{i(n-m)\varphi} \times \begin{cases} \sqrt{\frac{m!}{n!}} \left(\frac{r}{\ell}\right)^{n-m} L_m^{n-m}\left(\frac{r^2}{\ell^2}\right) & \text{for} \quad n > m \\ \sqrt{\frac{n!}{m!}} \left(\frac{r}{\ell}\right)^{m-n} L_n^{m-n}\left(\frac{r^2}{\ell^2}\right) & \text{for} \quad n < m \end{cases} \tag{2.33}$$

In the case where $n = m$, the two expressions in Eq (2.33) are equivalent. It is important to note that the authors of [38], after scaling all lengths by ℓ, provided only the expression in the first line of (2.33), implicitly assuming $n > m$. However, for strong magnetic fields, the majority of quantum states exhibit negative orbital magnetic quantum numbers m, which, according to Eq (2.31), result in $n < m$.

Each pair of quantum numbers, (n_r, m) and (n, m), along with their corresponding wave functions $\psi_{n_r m}$ and ψ_{nm}, respectively, offer distinct advantages. These will be utilized in their respective approaches.

5. Theoretical Frameworks

5.1. Single-particle wave-function-based approach

5.1.1. The first-order density matrix $\rho(\mathbf{r}, \mathbf{r}')$

The first-order density matrix $\rho(\mathbf{r}, \mathbf{r}')$ of independent fermionic particles at zero temperature is given by:

$$\rho(\mathbf{r}, \mathbf{r}'; \mu) = \sum_i \varphi_i(\mathbf{r}) \varphi_i^*(\mathbf{r}') \theta(\mu - E_i) \tag{2.34}$$

where the index $\{i\}$ represents all the quantum numbers involved in the complete determination of the stationary states $|\varphi_i\rangle$ associated with the eigenenergies E_i of the Hamiltonian H. Using the set of quantum numbers (n_r, m), the first-order density matrix can be expressed as follows

$$\rho(\mathbf{r}, \mathbf{r}'; \mu) = \sum_{n_r=0}^{\infty} \sum_{m=-\infty}^{\infty} \psi_{n_r m}^*(\mathbf{r}') \psi_{n_r m}(\mathbf{r}) \Theta\left(\mu - E_{n_r m}\right) \tag{2.35}$$

Where $\Theta(\mathrm{x})$ is the unit step function and μ is the Fermi energy.

For a given number N of particles, μ can be determined through the relation $N = \sum_{n_r} \sum_m \Theta\left(\mu - E_{n_r m}\right)$, which stems from the normalization condition of the local particle

density, $\int \rho(\mathbf{r})d\mathbf{r} = N$. At zero temperature, the Fermi energy μ then depends on the magnetic field strength B and the number of electrons N.

5.1.2.The particle density $\rho(\mathbf{r})$

The particle density $\rho(\mathbf{r})$ is simply the local part of the density matrix $\rho(\mathbf{r}, \mathbf{r}')$, i.e.

$$\rho(\mathbf{r}) = \sum_{n_r=0}^{\infty} \sum_{m=-\infty}^{\infty} \left|\psi_{n_r m}(\mathbf{r})\right|^2 \Theta\left(\mu - E_{n_r m}\right) \tag{2.36}$$

This expression sums the contributions of all occupied states, weighted by their probability densities, to determine the spatial distribution of particles in the system. The Heaviside function, appearing in both Eqs. (2.35) and (2.36) as well as in subsequent sums throughout our analysis, plays a crucial role by ensuring that only states below the Fermi energy contribute to the particle density. This reflects the Pauli exclusion principle and the system's quantum statistics, which govern the occupation of energy levels. By linking the microscopic wave functions to the macroscopic particle density, this formulation provides a powerful framework for analyzing the system's spatial structure and its response to external parameters, such as magnetic fields.

5.1.3. The orbital electric current density $\mathbf{J}(\mathbf{r})$

The paramagnetic orbital current density $\mathbf{J}_p(\mathbf{r})$ is derived from the first-order density matrix $\rho(\mathbf{r}, \mathbf{r}')$ using the standard quantum mechanical definition:

$$\mathbf{J}_p(\mathbf{r}) = \frac{\hbar}{2m^* i}\left[(\boldsymbol{\nabla}_{\mathbf{r}} - \boldsymbol{\nabla}_{\mathbf{r}'})\rho(\mathbf{r}, \mathbf{r}')\right]_{\mathbf{r}=\mathbf{r}'} \tag{2.37}$$

Here, the subscript p in $\mathbf{J}_p(\mathbf{r})$ denotes the paramagnetic or "canonical" current, which describes the current density in the absence of an external magnetic field ($\mathbf{B} = \mathbf{0}$). This expression captures the intrinsic current flow arising from the quantum mechanical motion of particles, independent of any magnetic field effects.

When an external magnetic field is introduced, it alters the spatial distribution of the current within the system. To ensure gauge invariance and satisfy the continuity equation $\boldsymbol{\nabla} \cdot \mathbf{J}(\mathbf{r}) = 0$, a diamagnetic contribution term must be added to Eq. (2.37). This term, proportional to the vector potential $\mathbf{A}$, is given by $(e\rho(\mathbf{r})/m^*)\mathbf{A}$. Working in the symmetric gauge, which in polar coordinates is expressed as $\mathbf{A} = (Br/2)\mathbf{e}_{\varphi}$, the total physical current density $\mathbf{J}(\mathbf{r})$ in the presence of the magnetic field $\mathbf{B}$ becomes:

$$\mathbf{J}(\mathbf{r}) = \mathbf{J}_p(\mathbf{r}) + \omega_L r\rho(\mathbf{r})\mathbf{e}_\varphi \tag{2.38}$$

Where $\mathbf{e}_\varphi = \mathbf{e}_Z \times \mathbf{e}_\varphi$ is the azimuthal unit vector.

By substituting Eqs (2.35) and (2.36) into Eq (2.38), one obtains the following expression for the total orbital current density

$$\mathbf{J}(\mathbf{r}) = \frac{\hbar}{m^*}\sum_{n_r=0}^{\infty}\sum_{m=-\infty}^{\infty}\left\{\mathrm{Im}\left[\psi^*_{n_r m}(\mathbf{r})\nabla_{\mathbf{r}}\psi_{n_r m}(\mathbf{r})\right] + \alpha\frac{r}{\ell^2}\left|\psi_{n_r m}(\mathbf{r})\right|^2\mathbf{e}_\varphi\right\}\Theta\left(\mu - E_{n_r m}\right) \tag{2.39}$$

In above, $\mathrm{Im}\{z\}$ denotes the imaginary part of the complex number z.

5.2. Bloch density matrix formalism

5.2.1. Definition of the Bloch Density Matrix $C(\mathbf{r}, \mathbf{r}'; \xi)$

The central theoretical tool that we will use to study the physical properties of our system is the so-called Bloch density matrix, denoted by $C(\mathbf{r}, \mathbf{r}'; \xi)$ and defined as:

$$C(\mathbf{r}, \mathbf{r}'; \xi) = \langle \mathbf{r}|\exp(-\xi H)|\mathbf{r}'\rangle \tag{2.40}$$

in $\{|\mathbf{r}\rangle\}$ representation. For some physical systems, where the analytical expression of $C(\mathbf{r}, \mathbf{r}'; \xi)$ is known, the use of this formalism allows us to bypass the need to search for the system's wave functions, solutions of the Schrödinger equation. The power of this formalism lies in its ability to link the various physical quantities characterizing the system's behavior to the matrix elements $C(\mathbf{r}, \mathbf{r}'; \xi)$, as we will see in the next paragraph.

For the system studied in this work, it was the authors of [62] were the first to derive an exact expression for $C(\mathbf{r}, \mathbf{r}'; \xi)$ using a simple ansatz inspired by the work of the authors of [63].

In order to demonstrate how $C(\mathbf{r}, \mathbf{r}'; \xi)$ can be related to certain physical quantities, it is necessary to introduce the $\{|\varphi_i\rangle\}$ basis constructed by the eigenstates $|\varphi_i\rangle$ of the system's Hamiltonian H, which satisfy the following eigenvalue equation

$$H|\varphi_i\rangle = E_i|\varphi_i\rangle \tag{2.41}$$

In (2.41), we twice insert the closure relation

$$\sum_i |\varphi_i\rangle\langle\varphi_i| = \mathbb{I} \tag{2.42}$$

where $\mathbb{I}$ is the identity operator. We then find that

$$C(\mathbf{r}, \mathbf{r}'; \xi) = \sum_{i,j}\langle \mathbf{r}|\varphi_i\rangle\langle\varphi_i|\exp(-\xi H)|\varphi_j\rangle\langle\varphi_j|\mathbf{r}'\rangle \tag{2.43}$$

The equation (2.41) of the eigenvalues of the Hamiltonian H indicates that

$$\exp(-\xi H)|\varphi_j\rangle = \exp(-\xi E_j)|\varphi_j\rangle \tag{2.44}$$

which, together with the orthonormalization relation for the state vectors $|\varphi_j\rangle$

$$\langle\varphi_i|\varphi_j\rangle = \int \varphi_i^*(\mathbf{r})\varphi_i(\mathbf{r}) = \delta_{ij} \tag{2.45}$$

lead to

$$C(\mathbf{r},\mathbf{r}';\xi) = \sum_i \varphi_i(\mathbf{r})\varphi_i^*(\mathbf{r}')\exp(-\xi E_i) \tag{2.46}$$

From this last relationship, we can establish the link between $C(\mathbf{r},\mathbf{r}';\xi)$ and some interesting physical quantities we have chosen. The diagonal elements of the Bloch matrix are obtained by setting $\mathbf{r} = \mathbf{r}'$ in (2.46). We then have

$$C(\mathbf{r};\xi) = \sum_i \varphi_i(\mathbf{r})\varphi_i^*(\mathbf{r})\exp(-\xi E_i) \tag{2.47}$$

Using (2.45), we can easily demonstrate that

$$\int C(\mathbf{r};\xi)d\mathbf{r} = \sum_i \exp(-\xi E_i) \tag{2.48}$$

An expression that is useful for determining the energy spectrum using the Bloch density matrix, thereby eliminating the need to resort to solving the Schrödinger equation

5.2.2. Relationship between BDM and some important physical quantities:

Before looking for the relations between the elements of the Bloch density matrix and certain quantities of the system, we prefer to give a brief presentation of the Laplace transformation and its inverse transformation so that the derivation of the relations which will follow be evident.

5.2.2.1.The Laplace transformation $\mathcal{L}$ and its inverse $\mathcal{L}_\mu^{-1}$

The Laplace transform of a function $f(\mu)$, which we denote by $\mathcal{L}\{f(\mu)\}$ is given by the following integral

$$\mathcal{L}\{f(\mu)\} = F(\xi) = \int_0^\infty \exp(-\xi\mu)f(\mu)d\mu\,, \qquad Re(\xi) > 0 \tag{2.49}$$

while the inverse Laplace transform is

$$\mathcal{L}_\mu^{-1}\{F(\xi)\} = f(\mu) = \frac{1}{2\pi i}\int_{c-i\infty}^{c+i\infty} F(\xi)\exp(\xi\mu)\,d\xi \tag{2.50}$$

Where c is a real number greater than the real part of all singularities of $F(\xi)$.

Example: The Heaviside step function $\theta(\mu)$ is defined by

$$\theta(x) = \begin{cases} 0 & , x \leq 0 \\ 1 & , \ x > 0 \end{cases} \tag{2.51}$$

This function can be obtained by an inverse laplace transform of the function $F\ (\xi)\ =\ \xi^{-1}$.

$$\theta(\mu\ ) = \frac{1}{2\pi i}\int_{c-i\infty}^{c+i\infty} \frac{\exp\ (\xi\mu)}{\xi}\, d\xi \tag{2.52}$$

For the form that interests us subsequently, it is a function of type $\theta(\mu - E_i)$ that we can write according to (2.52) as follows:

$$\theta(\mu\ - E_i) = \frac{1}{2\pi i}\int_{c-i\infty}^{c+i\infty} \frac{\exp\ (\xi(\mu\ - E_i))}{\xi}\, d\xi = \mathcal{L}_{\mu}^{-1}\left\{\frac{\exp\ (-\xi E_i)}{\xi}\right\} \tag{2.53}$$

Where μ is the Fermi energy, which is the energy of the last level occupied by the particles in the system.

5.2.2.2. Relationship between BDM and the first-order density matrix $\boldsymbol{\rho(\mathbf{r},\mathbf{r}';\mu\ )}$

The first-order density matrix $\rho(\mathbf{r},\mathbf{r}';\mu\ )$ associated with a system consisting of N independent fermions is given, at zero temperature, by the expression

$$\rho(\mathbf{r},\mathbf{r}';\mu\ ) = \sum_i \varphi_i(\mathbf{r})\varphi_i^*(\mathbf{r}')\theta(\mu - E_i) \tag{2.54}$$

where μ is the chemical potential of the system, which becomes, for $T\ =\ 0K$, the energy of the Fermi level. The sign $\sum_i$ indicates that the summation in (2.54) is made over the whole set of quantum numbers $\{i\}$ characterising the quantum states $\varphi_i\ (\mathbf{r})$ associated with the spectrum E_i. If we replace the Heaviside function $\theta(\mu - E_i)$ in (2.54) by its expression (2.53), we obtain

$$\rho(\mathbf{r},\mathbf{r}';\mu\ ) = \mathcal{L}_{\mu}^{-1}\left[\frac{1}{\xi}\left(\overbrace{\sum_i \varphi_i\ (\mathbf{r})\varphi_i^*(\mathbf{r}')\exp\ (-\xi E_i)}^{\boldsymbol{C}\ (\mathbf{r},\mathbf{r}';\xi\ )}\right)\right] \tag{2.55}$$

We therefore obtain the following relation between the Bloch density matrix $C\ (\mathbf{r},\mathbf{r}';\xi\ )$ and the first-order density matrix $\rho(\mathbf{r},\mathbf{r}';\mu\ )$.

$$\rho(\mathbf{r},\mathbf{r}';\mu\ ) = \mathcal{L}_{\mu}^{-1}\left[\frac{1}{\xi}C\ (\mathbf{r},\mathbf{r}';\xi\ )\right] \tag{2.56}$$

Then the knowledge of $C\ (\mathbf{r},\mathbf{r}';\xi\ )$ makes it possible to derive the expression of $\rho(\mathbf{r},\mathbf{r}';\mu\ )$ without looking for the solutions $\varphi_i\ (\mathbf{r})$

5.2.2.3. Relationship between $C(\mathbf{r},\xi)$ and the particle density $\rho(\mathbf{r})$

The expression of the particle density $\rho(\mathbf{r})$ as a function of the wave functions $\varphi_i(\mathbf{r})$ is obtained from the expression (2.54) of the density matrix $\rho(\mathbf{r},\mathbf{r}';\mu)$ by setting $\mathbf{r}=\mathbf{r}'$. It is the local part of the matrix $\rho(\mathbf{r},\mathbf{r}';\mu)$. We have

$$\rho(\mathbf{r})=\sum_i \varphi_i(\mathbf{r})\varphi_i^*(\mathbf{r})\theta(\mu-E_i) \tag{2.57}$$

This local density is related to the total number N of particles of the system by the normalization relation

$$\int \rho(\mathbf{r})\,d\mathbf{r}=N \tag{2.58}$$

Where the integral is extended over the whole space of the system. This normalization relation gives according to (2.57) and (2.58) the following relation

$$N=\sum_i \theta(\mu-E_i) \tag{2.59}$$

which will allow us to calculate the Fermi energy level as a function of the number of particles in the system. As far as the derivation of the relationship between the particle density $\rho(\mathbf{r})$ and the diagonal elements of the Bloch density matrix $C(\mathbf{r};\xi)$, is concerned, we can derive it directly from (2.56) by setting $\mathbf{r}=\mathbf{r}'$, we thus find

$$\rho(\mathbf{r})=\mathcal{L}_\mu^{-1}\left[\frac{1}{\xi}C(\mathbf{r};\xi)\right] \tag{2.60}$$

This is another relationship we will use in the next chapter.

5.2.2.4. Relationship between BDM and the current density J (r)

The current density $\mathbf{J}(\mathbf{r})$ can be derived from the particle density matrix $\rho(\mathbf{r},\mathbf{r}';\boldsymbol{\mu})$ through the relation

$$\mathbf{J}_{\boldsymbol{p}}(\mathbf{r})=\frac{\hbar}{2m^*i}[(\boldsymbol{\nabla}_{\mathbf{r}}-\boldsymbol{\nabla}_{\mathbf{r}'})\rho(\mathbf{r},\mathbf{r}';\boldsymbol{\mu})]_{\boldsymbol{r}=\boldsymbol{r}'} \tag{2.61}$$

By injecting the relation (2.56) directly into (2.61) we obtain the relation between $\mathbf{J}_{\boldsymbol{p}}(\mathbf{r})$ and the Bloch density matrix $C(\mathbf{r},\mathbf{r}';\xi)$

$$\mathbf{J}_{\boldsymbol{p}}(\mathbf{r})=\frac{\hbar}{2m^*i}\mathcal{L}_\mu^{-1}\left\{\frac{1}{\xi}\left[(\boldsymbol{\nabla}_{\mathbf{r}}-\boldsymbol{\nabla}_{\mathbf{r}'})C(\mathbf{r},\mathbf{r}';\xi)\right]_{\boldsymbol{r}=\boldsymbol{r}'}\right\} \tag{2.62}$$

Which can be rewritten also as

$$\mathbf{J_p}(\mathbf{r}) = \frac{\hbar}{im^*}\mathcal{L}_\mu^{-1}\left\{\frac{1}{\xi}[\boldsymbol{\nabla}_\mathbf{S} C(\mathbf{R},\mathbf{S};\xi)]_{\mathbf{S}=\mathbf{0}}\right\} \tag{2.63}$$

where $\mathbf{R} = (\mathbf{r}+\mathbf{r}')/2$ and $\mathbf{S} = \mathbf{r}-\mathbf{r}'$ are the center-of-mass and relative coordinates respectively.

When a magnetic field $\mathbf{B} = B\mathbf{e_z}$ is applied, a diamagnetic current emerges in response. This current is proportional to the vector potential **A** and is expressed as:

$$\frac{e}{m^*}\rho(\mathbf{r})\,\mathbf{A} \tag{2.64}$$

This diamagnetic contribution must be added to the paramagnetic component of the current to ensure the gauge invariance of the total physical current density $\mathbf{J}(\mathbf{r})$, which must satisfy the continuity equation $\boldsymbol{\nabla}\cdot\mathbf{J}(\mathbf{r}) = 0$. In the symmetric gauge, the vector potential **A** is given by Eq. (2.3) and can also be expressed in polar coordinates:

$$\mathbf{A} = \frac{1}{2}Br\mathbf{e}_\varphi \tag{2.65}$$

Then, according to (2.63), (2.64) and (2.65), the expression of the physical orbital current as reads

$$\mathbf{J}(\mathbf{r}) = \frac{\hbar}{im^*}\mathcal{L}_\mu^{-1}\left\{\frac{1}{\xi}[\boldsymbol{\nabla}_\mathbf{S} C(\mathbf{R},\mathbf{S};\xi)]_{\mathbf{S}=\mathbf{0}}\right\} + \omega_L r\rho(\mathbf{r})\mathbf{e}_\varphi \tag{2.66}$$

where ω_L is given by (2.8). It can be seen from this expression that in the absence of the magnetic field ($\omega_L = 0$) the second term in the second member of (2.66) cancels out.

Using Eq (2.60) into (2.66) we get for $\mathbf{J}(\mathbf{r})$, the following expression of the current density allowing direct derivation from the Bloch density matrix

$$\mathbf{J}(\mathbf{r}) = \frac{\hbar}{m^*}\mathcal{L}_\mu^{-1}\left\{\frac{1}{\xi}\left[-i[\boldsymbol{\nabla}_\mathbf{S} C(\mathbf{R},\mathbf{S};\xi)]_{\mathbf{S}=\mathbf{0}} + \alpha\frac{r}{\ell^2}C(\mathbf{r};\xi)\mathbf{e}_\varphi\right]\right\} \tag{2.67}$$

6. Analytical expression of $\boldsymbol{C}(\mathbf{r},\mathbf{r}';\boldsymbol{\xi})$ for the system under study

The system's various densities of interest namely $\boldsymbol{\rho}(\mathbf{r},\mathbf{r}')$, $\boldsymbol{\rho}(\mathbf{r})$ and $\mathbf{J}(\mathbf{r})$ can be expressed in terms of the Bloch density matrix $\boldsymbol{C}(\mathbf{r},\mathbf{r}';\boldsymbol{\xi})$ (refer to Eqs. (2.56), (2.60), and (2.67)). Thus, once an explicit analytical expression for $\boldsymbol{C}(\mathbf{r},\mathbf{r}';\boldsymbol{\xi})$ is available, these physical properties can be determined directly, without resorting to the single-particle wave functions.

It is important to emphasize that such an analytical expression for $\boldsymbol{C}(\mathbf{r},\mathbf{r}';\boldsymbol{\xi})$, associated with the Hamiltonian in Eq. (2.10), has already been derived by March and Tosi. They achieved this by extending the method originally developed by Sondheimer and Wilson for solving the Bloch

equation, $\boldsymbol{HC}(\mathbf{r},\mathbf{r}';\boldsymbol{\xi}) = -\boldsymbol{\partial C}(\mathbf{r},\mathbf{r}';\boldsymbol{\xi}) \;/\; \boldsymbol{\partial \xi}$ which was initially applied to a free charged particle [62,63]. By employing the center-of-mass and relative coordinates, the corresponding Bloch density matrix can be written down explicitly as

$$C(\mathbf{R},\mathbf{S};\xi) = \frac{1}{2\pi\ell^2\sinh(\xi\hbar\Omega)}\exp\left\{\frac{1}{\ell^2}\left[i\frac{\sinh(\xi\hbar\omega_L)}{\sinh(\xi\hbar\Omega)}(\mathbf{R}\times\mathbf{e}_z).\mathbf{S}\right.\right. \\ \left.\left. -\left(\coth(\xi\hbar\Omega)-\frac{\cosh(\xi\hbar\omega_L)}{\sinh(\xi\hbar\Omega)}\right)\mathbf{R}^2-\frac{1}{4}\left(\coth(\xi\hbar\Omega)+\frac{\cosh(\xi\hbar\omega_L)}{\sinh(\xi\hbar\Omega)}\right)\mathbf{S}^2\right]\right\} \tag{2.68}$$

Its diagonal element $C(\mathbf{r};\xi)$ is obtained by setting $\mathbf{S}=\mathbf{0}$ in Eq (2.68), yielding

$$C(\mathbf{r};\xi) = \frac{1}{2\pi\ell^2\sinh(\xi\hbar\Omega)}\exp\left(-\frac{r^2}{\ell^2}g(\xi)\right) \tag{2.69}$$

where the function $g(\xi)$ is given by

$$g(\xi) = \coth(\xi\hbar\Omega) - \frac{\cosh(\xi\hbar\omega_L)}{\sinh(\xi\hbar\Omega)} \tag{2.70}$$

7. Derivation of the energy spectrum from the Bloch density matrix

One of the advantages of knowing the analytical form of the Bloch density matrix is that we can obtain the energy spectrum E_{nm} of the system without resorting to solving the eigenvalue equation (2.41). This is made possible thanks to the relation (2.48) which links the energies E_{nm} to the diagonal elements of the Bloch matrix. Knowing that the expression of these elements $C(\mathbf{r};\xi)$ is given by (2.69), let's then do the integral that appears in the left-hand side of (2.48), which is of Gaussian form. Using

$$\int_{-\infty}^{+\infty}\exp(-\alpha t^2)dt = \sqrt{\pi/\alpha} \tag{2.71}$$

We find that

$$\int C(\mathbf{r};\xi)d\mathbf{r} = \frac{1}{4}\sinh^{-1}(\xi\hbar\,\Omega_+/2)\sinh^{-1}(\xi\hbar\,\Omega_-/2) \tag{2.72}$$

Where the new frequencies $\Omega_+$and Ω_- are given by

$$\Omega_\pm = \Omega \pm \omega_L \tag{2.73}$$

In (2.72), we can use the following development

$$\sinh^{-1}(x) = 2\sum_{n=0}^{\infty}\exp[-(2n+1)x] \tag{2.74}$$

We then write

$$\int C(\mathbf{r};\xi)d\mathbf{r} = \sum_{n=0}^{\infty}\sum_{m=0}^{\infty} \exp\{-\xi[(n+1/2)\hbar\Omega_{+} + (m+1/2)\Omega_{-}]\} \tag{2.75}$$

Comparing (2.48) and (2.75) we find that

$$\begin{aligned} E_{nm} &= (n+1/2)\hbar\Omega_{+} + (m+1/2)\hbar\Omega_{-} \\ &= (n+m+1)\hbar\Omega + (n-m)\hbar\omega_{L} \end{aligned} \tag{2.76}$$

This alternative method provides a reliable means of deriving the energy spectrum E_{nm}, along side the techniques of creation and annihilation operators and the canonical transformations.

Chapter 3

Exact Analytical Expressions for Key Equilibrium Orbital Properties

Chapter 3

Exact Analytical Expressions for Key Equilibrium Orbital Properties

1. Introduction

In the field of 2DEGs gases, one of the issues that is still receiving a lot of attention is the study of particle and current densities. These are two fundamental quantities that are required for comprehending the physical properties of such systems, particularly in the context of current density functional theory (CDFT) which is a rigorous extension of DFT to inhomogeneous systems immersed in an external magnetic field [64-65].

In this chapter, we derive exact closed-form analytical expressions for key equilibrium orbital properties using the two approaches outlined in the preceding chapter: one based on the explicit use of single-particle wave functions, and the other employing the Bloch density matrix formalism.

The properties under consideration include the first-order density matrix, spatial matter distribution, electric current flow, microscopic magnetization, total magnetic moment, and integrated persistent current. While these two approaches may initially produce expressions that appear distinct, rigorous mathematical analysis or numerical computations demonstrate their equivalence. This equivalence not only confirms the reliability and consistency of the derived results but also enhances our understanding of the system's quantum behavior.

Additionally, some previously derived analytical results are revisited and refined here to produce more concise, simpler, and computationally efficient expressions. These improved formulations are particularly suited for numerical investigations, enabling a deeper exploration of the physical properties of interest.

A notable finding of this chapter is the relationship between the microscopic magnetization $\boldsymbol{\mathcal{M}}(\mathbf{r})$ and the system's total persistent electric current I. We demonstrate that I can be directly deduced from the value of $\boldsymbol{\mathcal{M}}(\mathbf{r})$ at the center of the electron system, eliminating the need for a full derivation of the current.

2. Exact quantum mechanical expressions for particle and current densities

In this section, we derive exact closed-form analytical expressions for the first-order density matrix $\rho(\mathbf{r},\mathbf{r}')$, particle density $\rho(\mathbf{r})$, and physical current density $\mathbf{J}(\mathbf{r})$of the system. Using the two approaches outlined earlier, we obtain expressions that, despite initial differences, are shown to be equivalent through rigorous numerical analysis.

2.1. The first-order density matrix $\rho(\mathbf{r},\mathbf{r}';\mu)$

2.1.1. Within single-particle wave functions

By substituting the explicit form of the wave functions $\psi_{n_r m}(\mathbf{r})$, given by (2.26), directly into Eq. (2.35), which describes the first-order density matrix $\rho(\mathbf{r},\mathbf{r}')$, we immediately arrive at the desired result

$$\rho(\mathbf{r},\mathbf{r}') = \frac{1}{\pi\ell^2}\exp\left(-\frac{r^2+r'^2}{2\ell^2}\right)\sum_{n_r=0}^{\infty}\sum_{m=-\infty}^{\infty}\left\{\frac{n_r!}{(n_r+|m|)!}\left(\frac{rr'}{\ell^2}\right)^{|m|}L_{n_r}^{|m|}\left(\frac{r^2}{\ell^2}\right)L_{n_r}^{|m|}\left(\frac{r'^2}{\ell^2}\right)\exp[im(\varphi-\varphi')]\Theta(\mu-E_{n_r m})\right\} \tag{3.1}$$

2.1.2. Within the Bloch density matrix formalism

Knowing the analytical expression (2.68) for the elements $C(\mathbf{r},\mathbf{r}';\xi)$ of the Bloch density matrix, we can find the expression for the elements $\rho(\mathbf{r},\mathbf{r}';\mu)$ of the particle density matrix using (2.56). Substituting (2.68) into (2.56), we obtain

$$\begin{aligned}\rho(\mathbf{r},\mathbf{r}';\mu) = \frac{1}{2\pi\ell^2}\mathcal{L}_{\mu}^{-1}\Bigg[\frac{1}{\xi\sinh(\xi\hbar\Omega)}\exp\Bigg\{\frac{1}{\ell^2}\Bigg[i\frac{\sinh(\xi\hbar\omega_L)}{\sinh(\xi\hbar\Omega)}(\mathbf{R}\times\mathbf{e}_z)\times\mathbf{S} \\ -\left(\coth(\xi\hbar\Omega)-\frac{\cosh(\xi\hbar\omega_L)}{\sinh(\xi\hbar\Omega)}\right)\mathbf{R}^2 \\ -\frac{1}{4}\left(\coth(\xi\hbar\Omega)+\frac{\cosh(\xi\hbar\omega_L)}{\sinh(\xi\hbar\Omega)}\right)\mathbf{s}^2\Bigg]\Bigg\}\Bigg]\end{aligned} \tag{3.2}$$

This expression can be written in the following condensed form

$$\begin{aligned}\rho(\mathbf{r},\mathbf{r}';\mu) = \frac{1}{2\pi\ell^2}\mathcal{L}_{\mu}^{-1}\Bigg\{\frac{1}{\xi\sinh(\xi\hbar\Omega)}\exp\big(-A\coth(\xi\hbar\Omega)\big)\exp\Bigg(\frac{\exp(\xi\hbar\omega_L)}{2\sinh(\xi\hbar\Omega)}B_+ \\ +\frac{\exp(-\xi\hbar\omega_L)}{2\sinh(\xi\hbar\Omega)}B_-\Bigg)\Bigg\}\end{aligned} \tag{3.3}$$

Where

$$\begin{cases} A = \frac{1}{\ell^2}\left(\mathbf{R}^2 + \frac{\mathbf{s}^2}{4}\right) = \frac{1}{\ell^2}(\mathbf{r}^2 + \mathbf{r}'^2) \\ B_{\pm} = \frac{1}{\ell^2}\left[\left(\mathbf{R}^2 - \frac{\mathbf{s}^2}{4}\right) \pm i(\mathbf{R} \times \mathbf{e}_z).\mathbf{s}\right] = \frac{1}{\ell^2}[\mathbf{r} \times \mathbf{r}' \pm i(\mathbf{r} \times \mathbf{r}')\mathbf{e}_z] \end{cases} \tag{3.4}$$

To evaluate the inverse Laplace transform in (3.3), we use the following developments

$$\exp\left(\frac{\exp(\xi\hbar\omega_L)}{2\sinh(\xi\hbar\Omega)}B_+\right) = \sum_{m=0}^{\infty}\frac{1}{m!}\left(\frac{\exp(m\xi\hbar\omega_L)}{(\exp(\xi\hbar\Omega) - \exp(-\xi\hbar\Omega))^{\boldsymbol{m}}}\right){B_+}^m \tag{3.5}$$

$$\exp\left(\frac{\exp(-\xi\hbar\omega_L)}{2\sinh(\xi\hbar\Omega)}B_-\right) = \sum_{n=0}^{\infty}\frac{1}{n!}\left(\frac{\exp(-n\xi\hbar\omega_L)}{(\exp(\xi\hbar\Omega) - \exp(-\xi\hbar\Omega))^{\boldsymbol{n}}}\right){B_-}^n \tag{3.6}$$

injected into (3.3) we get

$$\rho(\mathbf{r}, \mathbf{r}'; \mu) = \frac{1}{\pi\ell^2}\sum_{n=0}^{\infty}\sum_{m=0}^{\infty}\frac{B_-^n B_+^m}{n!\,m!}\mathcal{L}_\mu^{-1}\left\{\frac{1}{\xi}\frac{\exp\left(-A\coth(\xi\hbar\Omega)\right)}{(\exp(\xi\hbar\Omega) - \exp(-\xi\hbar\Omega))^{\boldsymbol{n+m+1}}}\exp[(m - n)\xi\hbar\omega_L]\right\} \tag{3.7}$$

If we also use the development

$$\frac{\exp\left(-A\coth(\xi\hbar\Omega)\right)}{(\exp(\xi\hbar\Omega) - \exp(-\xi\hbar\Omega))^{\boldsymbol{n+m+1}}} = \exp(-A)\sum_{k=0}^{\infty}L_k^{n+m}(2A)\exp(-(2k + m + n + 1)\xi\hbar\Omega) \tag{3.8}$$

we find that

$$\rho(\mathbf{r}, \mathbf{r}'; \mu) = \frac{\exp(-A)}{\pi\ell^2}\sum_{k=0}^{\infty}\sum_{n=0}^{\infty}\sum_{m=0}^{\infty}\left\{\frac{B_-^n B_+^m}{n!\,m!}\mathcal{L}_\mu^{-1}\left\{\frac{1}{\xi}\exp[-\xi(2k\hbar\Omega + E_{nm})]\right\}\right\} \tag{3.9}$$

Finally, if we use the identity (2.53), the one-body reduced density matrix then reads

$$\rho(\mathbf{r}, \mathbf{r}'; \mu) = \frac{1}{\pi\ell^2}\exp(-A)\sum_{k=0}^{\infty}\sum_{n=0}^{\infty}\sum_{m=0}^{\infty}\left\{\frac{B_-^n B_+^m}{n!\,m!}L_k^{n+m}(2A)\Theta(\mu - E_{knm})\right\} \tag{3.10}$$

Where

$$E_{knm} = E_{nm} + 2k\hbar\Omega \tag{3.11}$$

With E_{nm} given by Eq. (2.76)

The presence of the Heaviside function imposes constraints on the possible values of the integers k, n, and m in Eq. (3.10), effectively truncating the summation ranges in the expression.

2.2. The particle density $\rho(r)$

2.2.1. Within single-particle wave functions

Using the definition in Eq. (2.36), or setting $\mathbf{r} = \mathbf{r}'$ in Eq. (3.1), both straightforwardly give the following explicit form for the particle density

$$\rho(r) = \frac{1}{\pi\ell^2}\exp\left(-\frac{r^2}{\ell^2}\right)\sum_{n_r=0}^{\infty}\sum_{m=-\infty}^{\infty}\left\{\frac{n_r!}{(n_r+|m|)!}\left(\frac{r^2}{\ell^2}\right)^{|m|}\left[L_{n_r}^{|m|}\left(\frac{r^2}{\ell^2}\right)\right]^2\Theta(\mu - E_{n_r m})\right\} \tag{3.12}$$

2.2.2. Within the Bloch density matrix formalism

The particle density $\rho(\boldsymbol{r})$is just the diagonal part of the density matrix $\rho(\mathbf{r},\mathbf{r}';\mu)$. According to (3.10), for $\mathbf{r} = \mathbf{r}'$, ($\mathbf{R} = \mathbf{r}$ and $\mathbf{s} = \mathbf{0}$), we have $A = B_+ = B_- = \frac{\boldsymbol{r}^2}{\ell^2}$

We find

$$\rho(r) = \frac{1}{\pi\ell^2}\exp\left(-\frac{r^2}{\ell^2}\right)\sum_{k=0}^{\infty}\sum_{n=0}^{\infty}\sum_{m=0}^{\infty}\frac{1}{n!\,m!}\left(\frac{r^2}{\ell^2}\right)^{n+m}L_k^{n+m}\left(2\frac{r^2}{\ell^2}\right)\Theta(\mu - E_{knm}) \tag{3.13}$$

The explicit formulas in Eqs. (3.12) and (3.13) precisely describe the local particle density in the system. They are numerically evaluable, enabling accurate computations under various conditions. Their equivalence is confirmed numerically, validating the consistency of the analytical framework. In the discussion section, we will further explore the particle density's behavior and its implications.

2.3.The orbital electric current density $\mathbf{J}(\mathbf{r})$

2.3.1. Within single-particle wave functions

In the presence of a magnetic field, a nonuniform electron gas exhibits a finite orbital current, even in thermal equilibrium. Henceforth, we will refer to the electric current density while keeping the same notation, i.e., tacitly taking $\mathbf{J}(\mathbf{r}) \equiv (-e)\mathbf{J}(\mathbf{r})$.

To derive the expression for the physical current density $\mathbf{J}(\mathbf{r})$ within the first approach, we substitute Eq (2.26) into Eq(2.39). Recalling that $\boldsymbol{\nabla}_{\mathbf{r}} = (\partial/\partial r)\mathbf{e}_r + r^{-1}(\partial/\partial\varphi)\mathbf{e}_\varphi$, we find that the electric orbital current density is purely azimuthal

$$\mathbf{J}(\mathbf{r}) = j_\varphi(r)\mathbf{e}_\varphi \tag{3.14}$$

where $j_\varphi(r)$ is given by the explicit formula

$$j_\varphi(r) = -j_0 \exp\left(-\frac{r^2}{\ell^2}\right) \sum_{n_r=0}^{\infty} \sum_{m=-\infty}^{\infty} \left\{ \frac{n_r!}{(n_r+|m|)!} \left(\frac{r^2}{\ell^2}\right)^{|m|-\frac{1}{2}} \left[L_{n_r}^{|m|}\left(\frac{r^2}{\ell^2}\right)\right]^2 \left(m + \alpha \frac{r^2}{\ell^2}\right) \Theta(\mu - E_{n_r m}) \right\} \tag{3.15}$$

Here, we take $j_0 = e\Omega/\pi\ell$ as the unit for the electric current density j_φ and the minus sign comes from multiplying by $(-e)$. With this expression, it's evident that the current density $\mathbf{J}(\mathbf{r})$ depends solely on the radial variable r, resulting in a circular motion around the z axis along the equipotential lines of the oscillator confining potential.

2.3.2. Within the Bloch density matrix formalism

By substituting the explicit expressions of $C(\mathbf{R}, \mathbf{S}; \xi)$ and its diagonal element $C(\mathbf{r}; \xi)$ from Eqs. (2.68) and (2.69) into Eq. (2.67) , we get the following formula for the azimuthal current $j_\varphi(r)$

$$j_\varphi(r) = j_0 \mathcal{L}_\mu^{-1} \left\{ \frac{h(\xi)}{\xi} \frac{r}{\ell} \exp\left(-\frac{r^2}{\ell^2} g(\xi)\right) \right\} \tag{3.16}$$

where the function $h(\xi)$ is given by

$$h(\xi) = \frac{1}{2\sinh(\xi\hbar\Omega)} \left(\frac{\sinh(\xi\hbar\omega_L)}{\sinh(\xi\hbar\Omega)} - \alpha \right) \tag{3.17}$$

The exponential factor in Eq. (3.16) can be expanded in a power series in r^2 as follows

$$\exp\left(-\frac{r^2}{\ell^2} g(\xi)\right) = \sum_{n=0}^{\infty} \sum_{m=0}^{\infty} \frac{1}{n!\,m!} \left(\frac{r^2}{\ell^2}\right)^{n+m} \exp[\xi(m-n)\hbar\omega_L] \frac{\exp\left(-\frac{r^2}{\ell^2}\coth(\xi\hbar\Omega)\right)}{[\exp(\xi\hbar\Omega) - \exp(-\xi\hbar\Omega)]^{n+m}} \tag{3.18}$$

we obtain

$$h(\xi)\exp\left(-\frac{r^2}{\ell^2} g(\xi)\right) = \exp\left(-\frac{r^2}{\ell^2}\right) \sum_{k=0}^{\infty} \sum_{n=0}^{\infty} \sum_{m=0}^{\infty} \frac{1}{n!\,m!} \left(\frac{r^2}{\ell^2}\right)^{n+m} \left\{ L_k^{n+m+1}\left(2\frac{r^2}{\ell^2}\right) [\exp\{-\xi(E_{knm} + \hbar\Omega_-)\} - \exp\{-\xi(E_{knm} + \hbar\Omega_+)\}] - \alpha L_k^{n+m}\left(2\frac{r^2}{\ell^2}\right) \exp(-\xi E_{knm}) \right\} \tag{3.19}$$

The third summation over the integer k comes from the following identity

$$\frac{\exp\{-x\coth(\gamma)\}}{[\exp(\gamma) - \exp(-\gamma)]^{\nu+1}} = \exp(-x) \sum_{k=0}^{\infty} L_k^\nu(2x) \exp\{-(2k+\nu+1)\gamma\} \tag{3.20}$$

which follows directly from the generating function for the associated Laguerre polynomials

$$\frac{\exp\left(-2x\frac{t}{1-t}\right)}{(1-t)^{\nu+1}} = \sum_{k=0}^{\infty} L_k^{\nu}(2x)t^k \tag{3.21}$$

if one replaces t by $\exp(-2\gamma)$. Substituting Eq. (3.19) into Eq. (3.16) and then using Eq (2.53) we find the ultimate expression for $j_\varphi(r)$ as

$$\begin{aligned} j_\varphi(r) = j_0 \exp\left(-\frac{r^2}{\ell^2}\right) \sum_{k=0}^{\infty}\sum_{n=0}^{\infty}\sum_{m=0}^{\infty} \Bigg\{ \frac{1}{n!\,m!}\left(\frac{r^2}{\ell^2}\right)^{n+m+\frac{1}{2}} \Bigg[L_k^{n+m+1}\left(2\frac{r^2}{\ell^2}\right)\{\Theta(\mu \\ - E_{knm} - \hbar\Omega_-) - \Theta(\mu - E_{knm} - \hbar\Omega_+)\} \\ - \alpha L_k^{n+m}\left(2\frac{r^2}{\ell^2}\right)\Theta(\mu - E_{knm})\Bigg]\Bigg\} \end{aligned} \tag{3.22}$$

The two explicit formulas for the current density in Eqs (3.15)) and (3.22), derived through each approach, can also be evaluated numerically with high precision, thus verifying their mathematical equivalence. It is worth mentioning that when the confining potential is turned off ($\omega_0 = 0$), the current density becomes zero everywhere, as anticipated, since the system becomes homogeneous under these conditions.

3. The total orbital magnetic moment *M*

In stationary systems characterized by a time-independent charge density$\rho(\mathbf{r})$, the orbital current density $\mathbf{J}(\mathbf{r})$ and the microscopic magnetization $\boldsymbol{\mathcal{M}}(\mathbf{r})$ are related through the conventional definition

$$\mathbf{J}(\mathbf{r}) = \boldsymbol{\nabla} \times \boldsymbol{\mathcal{M}}(\mathbf{r}) \tag{3.23}$$

The possibility of such a representation stems immediately from the fact that the current density $\mathbf{J}(\mathbf{r})$ should satisfy the continuity equation $\boldsymbol{\nabla} \cdot \mathbf{J}(\mathbf{r}) = 0$ (The charge density $\rho(\mathbf{r})$ is independent of time, so $\frac{\partial \rho(\mathbf{r})}{\partial t} = 0$) .

At equilibrium, the microscopic magnetization $\boldsymbol{\mathcal{M}}(\mathbf{r})$ integrates to the total orbital magnetic moment **M** as follows

$$\mathbf{M} = \int \boldsymbol{\mathcal{M}}(\mathbf{r}) d\mathbf{r} = \frac{1}{2}\int \mathbf{r} \times \mathbf{J}(\mathbf{r}) d\mathbf{r} \tag{3.24}$$

Therefore, using the analytical expression for the current density $\mathbf{J}(\mathbf{r})$ of our system, we can proceed to determine the magnetic moment **M**. However, it is important to note that locally, the expression $\boldsymbol{\mathcal{M}}(\mathbf{r}) = \big(\mathbf{r} \times \mathbf{J}(\mathbf{r})\big)/2$, as might be at first glance inferred from Eq. (3.24),

cannot be readily applied. Instead, to derive the final integral expression in the right-hand side of Eq. (3.24), partial integration is required, as emphasized in Ref. [66]. Furthermore, for a uniform 2DEG ($\omega_0 = 0$), the current density $\mathbf{J}(\mathbf{r})$ vanishes everywhere, as previously mentioned. Consequently, according to this relation, $\boldsymbol{\mathcal{M}}(\mathbf{r})$ should also be null, which contradicts the expectation. It is worth highlighting that this discrepancy was identified in Ref [37].

The expression of **M** which may be obtained using Eq. (3.24) matches the one directly derived from the single-particle energy spectrum E_{nm} (or $E_{n_r m}$). At zero temperature, the total magnetic moment **M** can be calculated as

$$\mathbf{M} = -\sum_{n=0}^{\infty}\sum_{m=0}^{\infty}\left(\frac{\partial E_{nm}}{\partial B}\right)\Theta(\mu - E_{nm})\,\mathbf{e}_z \tag{3.25}$$

Which, according to Eq. (2.30), leads to

$$\mathbf{M} = \mu_B \sum_{n=0}^{\infty}\sum_{m=0}^{\infty}\{m - n - \alpha(n+m+1)\}\Theta(\mu - E_{nm})\,\mathbf{e}_z \tag{3.26}$$

Where $\mu_B = e\hbar/2m^*$ is the effective Bohr magneton. This result illustrates that the total orbital magnetic moment **M** is the sum, over all occupied quantum states, of individual magnetic moments carried by electrons in those states. In fact, the individual magnetic moment, denoted as $\mathbf{m}_{nm}$, for each occupied state ψ_{nm} is given by

$$\mathbf{m}_{nm} = \left(-\frac{e}{2m^*}\langle L_z\rangle_{nm} - \frac{e\omega_L}{2}\langle r^2\rangle_{nm}\right)\mathbf{e}_z \tag{3.27}$$

Here, $\langle L_z\rangle_{nm} = (n-m)\hbar$ represents the mean value of the z component of the orbital angular momentum, and $\langle r^2\rangle_{nm}$ is given by

$$r_{nm} = \sqrt{\langle r^2\rangle_{nm}} = \sqrt{(n+m+1)}\ell \tag{3.28}$$

One recognizes that the second term in (3.27) corresponds to an induced magnetic moment, disappearing as soon as the external magnetic field is turned off. Conversely, the first term represents a permanent moment persisting as long as $\langle L_z\rangle_{nm}$ does not vanish. Thus, a partially filled electron shell is necessary to maintain the total magnetic moment.

4. The microscopic magnetization $\boldsymbol{\mathcal{M}}(\mathbf{r})$

The expression in Eq. (3.23) indicates that the local magnetization $\boldsymbol{\mathcal{M}}(\mathbf{r})$ is defined only up to an arbitrary curl-free field. Fortunately, in two-dimensional media, this gauge freedom can be eliminated, leading to a uniquely defined out- of- plane microscopic magnetization as expressed in Ref. [66]

$$\boldsymbol{\mathcal{M}}(\mathbf{r}) = \int_{\mathbf{r}}^{\infty} d\mathbf{r}' \times \mathbf{J}(\mathbf{r}') \tag{3.29}$$

Here, the line integral extends along any chosen path from the point **r** within the medium to infinity, where $\boldsymbol{\mathcal{M}}$ vanishes. With the current density been entirely azimuthal (as indicated in Eq. (3.14)), the resulting microscopic magnetization naturally aligns perpendicular to the system's plane. Furthermore, it exclusively relies on the radial coordinate r, expressed as $\boldsymbol{\mathcal{M}}(\mathbf{r}) = \mathcal{M}(r)\mathbf{e}_z$. To evaluate the integral in Eq (3.29), it is better not to use for $j_\varphi(r)$ the forms provided in Eqs. (3.15) and (3.22), but rather the expression of Eq. (3.16), which, after insertion into Eq. (3.29), gives

$$\mathcal{M}(r) = \frac{e\Omega}{\pi\ell^2}\mathcal{L}_\mu^{-1}\left\{\frac{h(\xi)}{\xi}\int_r^\infty r'\exp\left(-\frac{r'^2}{\ell^2}g(\xi)\right)dr'\right\} \tag{3.30}$$

the integral within the inverse Laplace transform can easily be computed, yielding the following expression for $\mathcal{M}(r)$

$$\mathcal{M}(r) = \frac{e\Omega}{2\pi}\mathcal{L}_\mu^{-1}\left\{\frac{1}{\xi}\frac{h(\xi)}{g(\xi)}\exp\left(-\frac{r^2}{\ell^2}g(\xi)\right)\right\} \tag{3.31}$$

To perform the above inverse Laplace transform, it is convenient to express the ratio $h(\xi)/g(\xi)$ as follows

$$\frac{h(\xi)}{g(\xi)} = \frac{1}{4\sinh(\xi\hbar\Omega)}\left(\frac{\sinh(\xi\hbar\omega_L) - \alpha\sinh(\xi\hbar\Omega)}{\sinh(\xi\hbar\Omega_+/2)\sinh(\xi\hbar\Omega_-/2)}\right) \tag{3.32}$$

Which, upon using Eq. (2.74) for $x = \xi\hbar\Omega_\pm/2$, can be written as

$$\frac{h(\xi)}{g(\xi)} = \sum_{p=0}^{\infty}\sum_{q=0}^{\infty}\exp\left(-\xi E_{pq}\right)\left\{\frac{\exp(\xi\hbar\omega_L) - \exp(-\xi\hbar\omega_L)}{\exp(\xi\hbar\Omega) - \exp(-\xi\hbar\Omega)} - \alpha\right\} \tag{3.33}$$

Where E_{pq} is given by Eq. (2.76) with n and m replaced by p and q, respectively. Inserting Eq. (3.32) into Eq. (3.30), with employing Eq. (3.18) together with Eq (3.20), the magnetization $\mathcal{M}(r)$ takes the following expanded form

$$\mathcal{M}(r) = \frac{e\Omega}{2\pi}\exp\left(-\frac{r^2}{\ell^2}\right)\sum_{k=0}^{\infty}\sum_{n=0}^{\infty}\sum_{m=0}^{\infty}\sum_{p=0}^{\infty}\sum_{q=0}^{\infty}\frac{1}{n!\,m!}\left(\frac{r^2}{\ell^2}\right)^{n+m}\mathcal{L}_{\mu}^{-1}\left\{\frac{1}{\xi}\left[L_k^{n+m}\left(2\frac{r^2}{\ell^2}\right)\left[\exp\{-\xi(\mathcal{E}_{knmpq} - \hbar\omega_L)\} - \exp\{-\xi(\mathcal{E}_{knmpq} + \hbar\omega_L)\}\right] - \alpha L_k^{n+m-1}\left(2\frac{r^2}{\ell^2}\right)\exp\{-\xi(\mathcal{E}_{knmpq} - \hbar\Omega)\}\right]\right\} \tag{3.34}$$

Where $\mathcal{E}_{knmpq} = E_{knm} + E_{pq}$. Finally, upon using the identity in Eq. (2.53), the expression of the magnetization $\mathcal{M}(r)$ is given by

$$\mathcal{M}(r) = \frac{\mu_B}{\pi\ell^2}\exp\left(-\frac{r^2}{\ell^2}\right)\sum_{k=0}^{\infty}\sum_{n=0}^{\infty}\sum_{m=0}^{\infty}\sum_{p=0}^{\infty}\sum_{q=0}^{\infty}\frac{1}{n!\,m!}\left(\frac{r^2}{\ell^2}\right)^{n+m}\left\{L_k^{n+m}\left(2\frac{r^2}{\ell^2}\right)\left[\Theta(\mu - \mathcal{E}_{knmpq} + \hbar\omega_L) - \Theta(\mu - \mathcal{E}_{knmpq} - \hbar\omega_L)\right] - \alpha L_k^{n+m-1}\left(2\frac{r^2}{\ell^2}\right)\Theta(\mu - \mathcal{E}_{knmpq} + \hbar\Omega)\right\} \tag{3.35}$$

We believe that this is the first time that an exact analytical closed form for the orbital microscopic magnetization, in real physical space, is given for the system under study. Note that the established microscopic magnetization $\mathcal{M}(r)$ behaves well at limiting cases. Indeed, in the absence of magnetic field ($\omega_L = 0$), $\mathcal{M}(r) = 0$, and $\lim_{\alpha\to 1}\mathcal{M}(r) = -\mu_B/\pi\ell^2$, as it should since the system becomes uniform.

As a first direct application of our expression, we will use it to deduce the exact expression of the so-called integrated persistent current in the ensuing section.

5. The total azimuthal persistent current

The definition of the persistent current density itself (as delineated in Eqs (3.14) and(2.38) reveals its origin from two competing types of azimuthal currents - para and diamagnetic types - permeating the entire system. Furthermore, in next chapter, we will demonstrate that the current $\mathbf{J}(\mathbf{r})$ may also be understood as a combination of two other types of counter-propagating azimuthal currents. These currents exhibit notable characteristics under strong magnetic fields, corresponding to the emergence of well-defined compressible and incompressible structures within the particle density. To investigate the net effect of these pairs of opposing currents, it is necessary to calculate the total azimuthal current along a radial cross-section from the center to the physical edge of the sample. As defined in [22-24],

the so-called integrated azimuthal persistent current is expressed as follows

$$I = \int_0^\infty j_\varphi(r)dr \tag{3.36}$$

An exact analytical formula for this integrated current, valid for an arbitrary magnetic field strength, has been given earlier [41]. Given the exact expression of the microscopic magnetization $\mathcal{M}(r)$ provided herein, such a precise formula for I can be directly deduced from Eq (3.35), without going through its full derivation. Indeed, upon comparing Eqs (3.29). and (3.36), it follows that the integrated current I is simply the magnetization at the center of the electron system, $I = \mathcal{M}(0)$. Thus, putting $r = 0$ in Eq (3.34), one is left with

$$I = \frac{\mu_B}{\pi\ell^2}\left\{\sum_{k=0}^{\infty}\sum_{n=0}^{\infty}\sum_{m=0}^{\infty}[\Theta(\mu - E_{knm} - \hbar\Omega_-) - \Theta(\mu - E_{knm} - \hbar\Omega_+)] - \alpha\sum_{n=0}^{\infty}\sum_{m=0}^{\infty}\Theta(\mu - E_{nm})\right\} \tag{3.37}$$

In above, the last double sum is nothing but the number of particles, $N = \sum_{n=0}^{\infty}\sum_{m=0}^{\infty}\Theta(\mu - E_{nm})$. Moreover, the triple summation can be reduced to double one as done in [41]. Consequently, we get for the total integrated current

$$I = \frac{e\Omega}{2\pi}\sum_{n=0}^{\infty}\sum_{m=0}^{\infty}\{\Theta[\mu - (2n+1)\hbar\Omega - m\hbar\Omega_-] - \Theta[\mu - (2n+1)\hbar\Omega - m\hbar\Omega_+]\} - \frac{e\omega_L}{2\pi}N \tag{3.38}$$

which is identical to the expression found in [41], if one multiplies there result by the electron charge $(-e)$.

In order to further simplify the precedent expression of I, the double sum appearing in Eq(3.38). can be reduced to just one over n through the use of the following identity

$$\sum_{m=0}^{\infty}\Theta(x - m) = \Theta(x)(\lfloor x\rfloor + 1) \tag{3.39}$$

Where $\lfloor x\rfloor$ denotes the integer part of x. Recalling that $\Omega_\pm > 0$, Eq (3.38) then becomes

$$I = \frac{e\Omega}{2\pi}\sum_{n=0}^{\infty}\left(\left\lfloor\frac{\mu-(2n+1)\hbar\Omega}{\hbar\Omega_{-}}\right\rfloor-\left\lfloor\frac{\mu-(2n+1)\hbar\Omega}{\hbar\Omega_{+}}\right\rfloor\right)\Theta[\mu - (2n+1)\hbar\Omega] - \frac{e\omega_L}{2\pi}N \tag{3.40}$$

Once again, we have provided in Eq(3.40) another expression for the integrated current I which turns out to be rather concise and suitable for numerical calculations, compared to that displayed in Eq (3.38).

In this chapter, we have provided all the necessary analytical expressions to thoroughly analyze the behavior of the physical quantities under investigation. The upcoming section will delve into the numerical results and subsequent discussions.

Chapter 4

Results and Discussion

Chapter 4

Results and Discussion

1. Introduction

In the preceding chapter, we derived and presented all the necessary analytical expressions required to thoroughly analyze and discuss the behavior of the physical properties under investigation. These expressions serve as the foundation for understanding the system's quantum mechanical and thermodynamic characteristics. Building on this theoretical groundwork, we now turn our attention to the numerical results and their interpretation, aiming to provide a deeper insight into the system's behavior under varying conditions.

At high magnetic field regimes, quantum effects become particularly pronounced, playing a pivotal role in shaping the behavior of various thermodynamic quantities. To explore these effects numerically, we focus on a system composed of $N = 2000$ independent spinless electrons. For our analysis, we restrict the magnetic field intensity to the range $0.9 \leq \alpha \leq 1$, as this interval captures the most significant quantum phenomena. As will be demonstrated, distinct and regular patterns in the behavior of the studied physical properties become strikingly evident as α approaches 0.99 and beyond. This behavior is a direct consequence of the magnetic field's influence on the energy spectrum, which clusters into highly degenerate Landau levels. These levels, in turn, govern the equilibrium properties of the system in unique and specific ways, revealing the intricate relationship between quantum mechanical phenomena and macroscopic observables.

To facilitate clarity and consistency in our analysis, all energies and lengths in the presented plots are scaled by $\hbar\Omega$ and ℓ, respectively. This normalization allows for a more intuitive comparison of results and highlights the universal features of the system's behavior. In the following discussion, we will explore these numerical findings in greater detail, shedding light on the underlying physics and its broader implications.

2. Evolution of the energy spectrum

2.1. Evolution of the energy spectrum with magnetic field

To understand the critical role of the energy spectrum in shaping the behavior of equilibrium properties, we analyze its evolution as the magnetic field strength increases. In our discussion, we alternate between Eqs. (2.29) and (2.30) to describe the energy spectrum, selecting the most appropriate form based on the context.

When $\alpha = 0$, corresponding to the absence of a magnetic field, the energy levels $E_{n_r,m}$ in Eq. (2.29) simplify to those of a two-dimensional isotropic harmonic oscillator, expressed as $E_N = (N+1)\hbar\omega_0$. Each level exhibits a $(N+1)$-fold degeneracy. As a weak magnetic field is introduced $(\omega_L \ll \omega_0)$, the degeneracy is lifted due to orbital Zeeman splitting, creating an energy gap of $2\hbar\omega_L$ between consecutive levels within the same shell N. As the magnetic field strengthens, accidental degeneracies arise, where Zeeman sublevels intersect with neighboring sets.

In the case of $\alpha = 1$, which represents free electrons in a magnetic field, the spectrum in Eq. (2.30) displays an infinitely degenerate structure of equally spaced Landau levels, given by $E_n = (2n+1)\hbar\omega_L$. However, when the confining harmonic potential is present $(\alpha \neq 0)$, Eq. (2.30) shows that the degeneracy of these Landau levels is lifted.

Thus, the energy spectrum of the system transitions smoothly from the bound states of a 2D isotropic harmonic oscillator to the Landau levels characteristic of a free charged particle in a perpendicular magnetic field. In the general case, where neither ω_L nor ω_0 is zero, the energy spectrum becomes nondegenerate, except for accidental degeneracies. Under these conditions, the eigenstates are identified as edge states [35], which are susceptible to carrying currents throughout the entire system. This behavior contrasts sharply with systems involving sharp boundary potentials, where degeneracy is lifted only for a small number of states at the physical edges, leaving the bulk levels largely degenerate.

Under strong magnetic fields $(\alpha \to 1)$, the energy spectrum E_{nm} in Eq. (2.30) closely mirrors the structure of Landau levels. Although these levels are not strictly degenerate due to the confining potential, they are conventionally referred to as Landau levels in this regime. Here, the quantum number n designates each Landau level, while m labels its sublevels. The confining potential introduces a unique feature: each Landau level exhibits a distinct degeneracy. Specifically, for a given n, the maximum allowed value of m is determined by:

$$m_{max}(n,\alpha) = \left\lfloor \frac{\mu - n\hbar\Omega_+ - \hbar\Omega_-}{\hbar\Omega_-} \right\rfloor \quad (4.\ 1)$$

As illustrated in Fig. 1, the degeneracy of Landau levels displays contrasting trends as the magnetic field increases. Lower Landau levels show an increase in degeneracy, while higher levels experience a decrease. Consequently, more sublevels from lower Landau levels intersect the Fermi level from above, contributing to the filling of states. Simultaneously, more quantum states from higher levels cross the Fermi level in an upward direction, gradually depleting these levels.

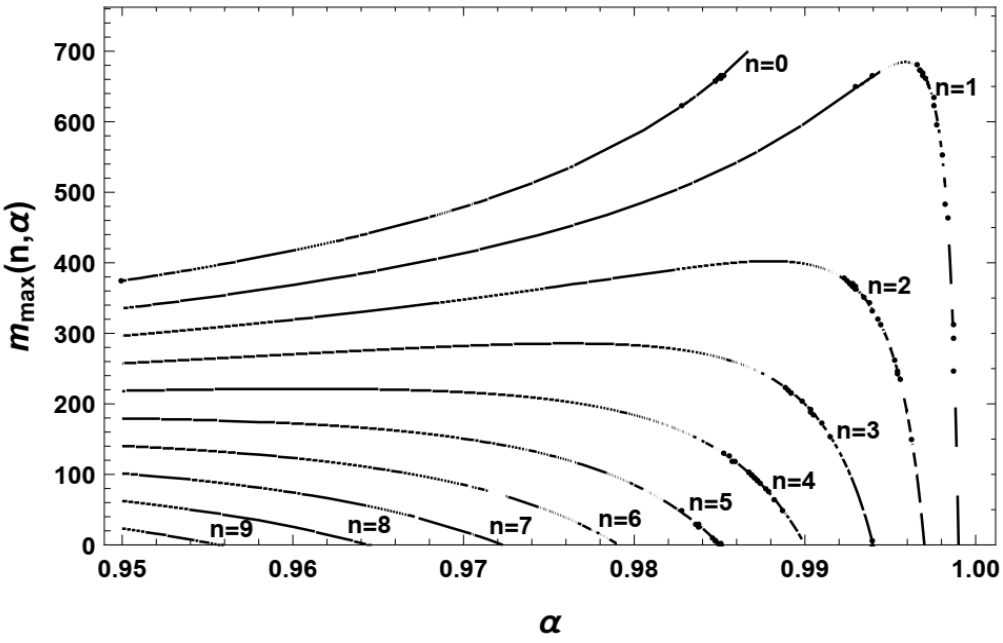

Fig 1 : Evolution of Landau level degeneracies with increasing magnetic field. Initially, ten levels are present within the selected range. However, as the magnetic field strengthens, the number of levels steadily diminishes. At extremely high magnetic fields, only the lowest Landau level (LLL) remains populated.

Figure 2 demonstrates the described behavior for a selected range of magnetic field strengths within the strong-field regime, specifically $0.95 \leq \alpha \leq 0.956$. To ensure clarity, only sublevels from the lowest ($n = 0$) and highest ($n = 9$) Landau levels are displayed. The figure highlights the intensity α at which the Fermi level E_F (represented by a thick red line) intersects the lowest available sublevel E_{90} (thick black line). This intersection marks the point at which the highest Landau level ($n = 9$) becomes completely depleted.

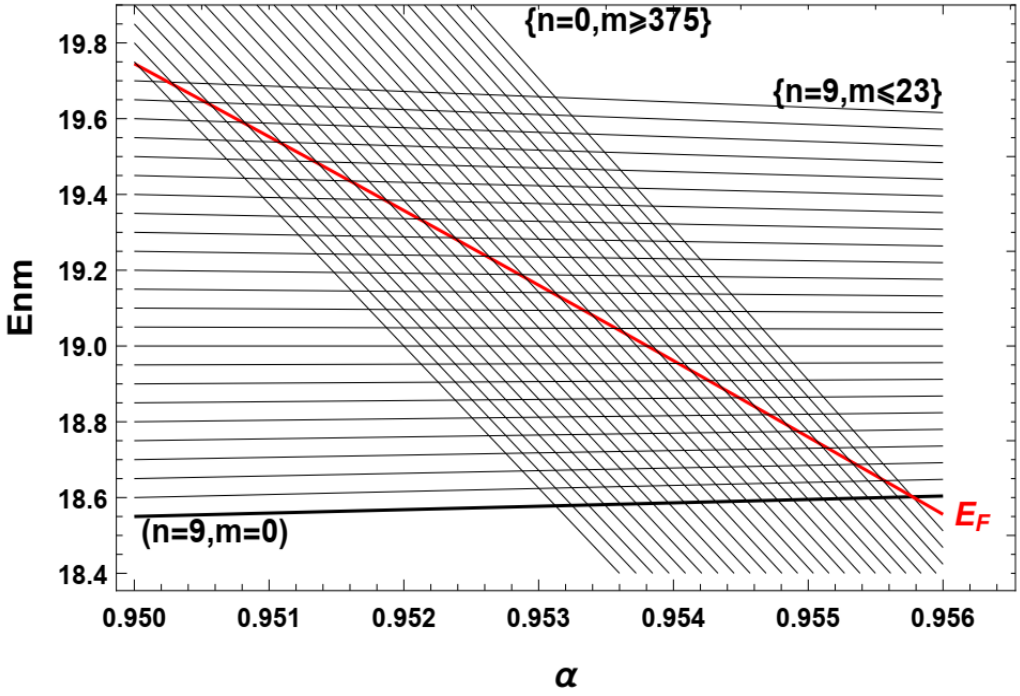

Fig 2: Evolution of quantum states belonging to the highest and lowest Landau levels with magnetic fields. As the intensity increases, new sublevels cross the Fermi level E_F (thick red line) from above and join the lowest level $n = 0$, increasing its degeneracy. Meanwhile, sublevels belonging to the highest level $n = 9$ pass above the Fermi level, reducing its degeneracy, thus maintaining a fixed number of quantum states below the Fermi level. The point where the Fermi level E_F intersects the last sublevel E_{90} (thick black line) corresponds to the complete depletion of the Landau level $n = 9$.

In Fig. 3, we illustrate the evolution of the lowest sublevel from each of the ten available Landau levels as a function of the magnetic field strength within the range $0.95 \leq \alpha < 1$. The black filled circles indicate the magnetic field strengths at which each Landau level becomes completely depleted. When a Landau level crosses the Fermi energy, it triggers an abrupt change in the behavior of magnetic field-dependent properties—a phenomenon known as de Haas-van Alphen oscillations. Furthermore, the intersections of sublevels from a specific Landau level with the Fermi level, as partially shown in Fig. 2, give rise to the Aharonov-Bohm effect [35]. In subsequent sections, we will explore these phenomena, examining their influence on important physical quantities, such as quantum oscillations in the total magnetic moment and the integrated persistent electric current.

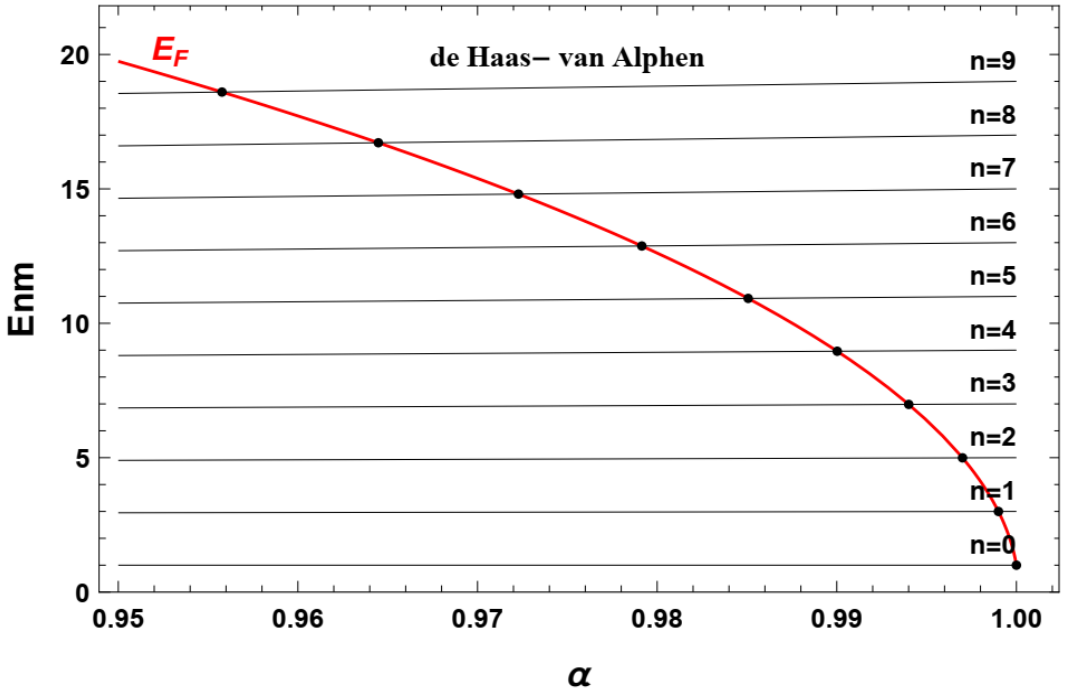

Fig 3: Evolution of the lowest sublevel (bottom) from each of the ten available Landau levels as a function of magnetic field strength. Black filled circles indicate magnetic field strengths where complete level depletion occurs.

2.2. Evolution of the Energy Spectrum with root-mean-square radial distance

The root-mean-square (rms) distance r_{nm} of an orbital, characterized by quantum numbers n and m, from the center of the system can be calculated using the analytical form of the wave function ψ_{nm} provided in Eq. (2.27). This calculation leads to the following expression:

$$r_{nm} = \sqrt{\langle r^2 \rangle_{nm}} = \sqrt{(n + m + 1)}\ell \qquad (4.\ 2)$$

The wave function ψ_{nm} attains its maximum value at r_{nm} and exhibits a Gaussian-like decay over a characteristic length scale ℓ. As a result, the probability density maintains rotational symmetry about the z-axis, with its peak lying on a circle of radius r_{nm} . Additionally, the magnetic flux enclosed between consecutive radius for states sharing the same quantum number n is given by $\pi B\left(r_{n,m+1}^2 - r_{n,m}^2\right) = \alpha\phi_0$, where $\phi_0 = h/e$ represents the magnetic flux quantum.

An alternative approach to computing r_{nm} involves the Hellmann-Feynman theorem. According to this theorem, we can express r_{nm} as:

$$\langle r^2 \rangle_{nm} = \frac{2}{m^*} \left\langle \psi_{nm} \left| \frac{\partial H}{\partial \Omega^2} \right| \psi_{nm} \right\rangle = \frac{2}{m^*} \frac{\partial E_{nm}}{\partial \Omega^2} \quad (4.\ 3)$$

where the Hamiltonian from Eq. (2.10) and the energy spectrum from Eq. (2.30) are utilized, with Ω^2 treated as a real parameter.

Figures 4(a) and 4(b) depict the quadratic relationship between the system's energy spectrum E_{nm} and the radial distance r_{nm} under varying magnetic field strengths. In Fig. 4(a), which corresponds to a relatively weak magnetic field ($\alpha = 0.9$), the energy levels E_{nm} display steep slopes, resulting in numerous closely spaced intersections with the Fermi energy E_{F} . These intersections give rise to compressible regions within the particle density profile, which are densely packed. Consequently, the formation of wide incompressible strips is inhibited, particularly as one moves away from the system's center. This behavior is further elaborated in the discussion of the particle density profile.

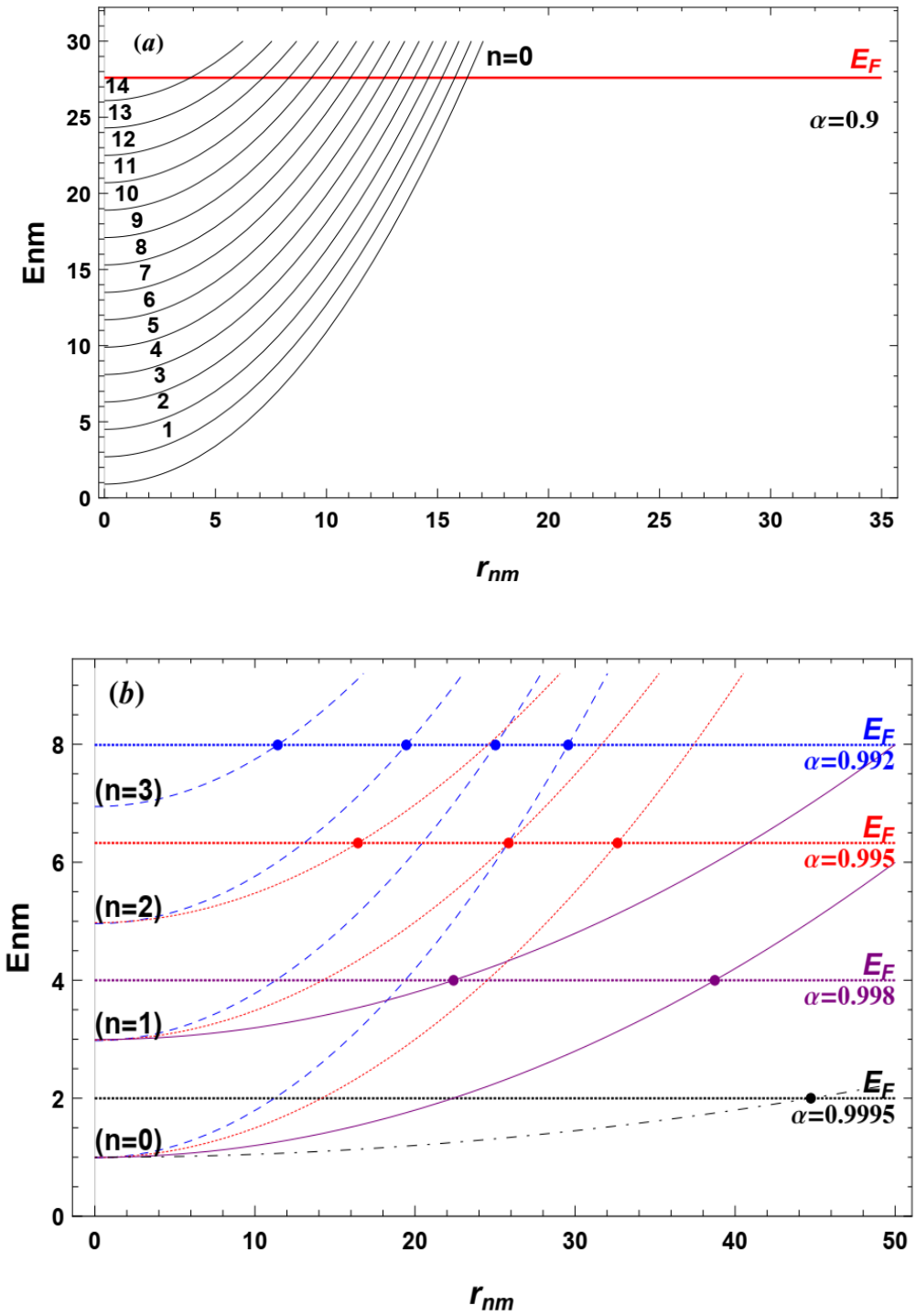

Fig 4: (a) Under a relatively weak magnetic field ($\alpha = 0.9$), closely spaced intersections between E_{nm} and the Fermi energy E_F occur, resulting in the formation of compressible regions within the particle density structure. This prevents wide incompressible strips, particularly towards the system's center. (b) Increasing the magnetic field preferentially populates lower energy levels while depleting higher ones. This is evident for selected α values, where only a few lowest parabolic Landau levels are fully occupied. The particle density thus locks into specific quantized values, inducing incompressibility. The distant positions where the energy spectrum intersects the Fermi level exactly correspond to transitions between different incompressible regions.

As the magnetic field strength increases, lower energy levels become preferentially populated, leading to the gradual depletion of higher levels. This phenomenon is clearly illustrated for selected values of α $(0.992, 0.995, 0.998, and\ 0.9995)$, where only the lowest parabolic Landau levels remain fully occupied ($n_{max}(\alpha) = 3,2,1,$ and 0, respectively). This results in the particle density locking into quantized values in specific regions, inducing incompressibility. In Fig. 4(b), the evolution of the energy levels E_{nm} under these conditions is shown, with distant intersection points (marked by filled colored circles) where the energy spectrum crosses the Fermi level. These intersection points correspond precisely to the centers of transitions between different incompressible regions, as illustrated in Fig. 5(b).

3. Spatial distribution of particle, current and magnetization densities

3.1. The particle density profile

As observed in Fig. 4(a), for a relatively weak magnetic field, the energy levels E_{nm}, characterized by steep slopes and small degeneracies, closely intersect with the Fermi level E_F, leading to fast changes in the particle density distribution as a function of radial position. This behavior is further illustrated in Fig 5(a), which depicts closely spaced compressible regions, where the density $\rho(r)$ decreases with position, interspersed by extremely narrow incompressible regions where $\rho(r)$ remains constant. Moving outward from the center, the compressible regions spread, causing the narrow incompressible regions to shrink. Eventually, these regions with constant density entirely disappear as we approach the system's boundary.

As the magnetic field strengthens, the particle density $\rho(r)$ progressively develops a sequence of incompressible regions, characterized by plateau structures, which widen with increasing magnetic field, as demonstrated in Figs. 5(a) and 5(b). Notably, these plateaus occur precisely for quantized values of the density $\rho(r) = \nu/\pi\ell^2$, where ν is an integer. At the end of each plateau, the particle density undergoes gradual changes, giving rise to compressible regions between these plateaus. This phenomenon reflects the underlying structure of slowly evolving parabolic Landau levels having distinct degeneracies $m_{max}(n, \alpha)$. Each density plateau corresponds to the occupation of a new Landau level. Furthermore, we note that crossings between these Landau levels and the Fermi energy, as shown in Fig 4(b), align exactly to the centers of the compressible regions shown in Fig. 5 (b).

The key difference between the two aforementioned scenarios lies in the considerable width of incompressible strips, compared to the compressible ones, exhibited by the particle density under strong magnetic fields. This fact leads to notable features in the behavior of the persistent current density and the microscopic magnetization, as will be discussed subsequently.

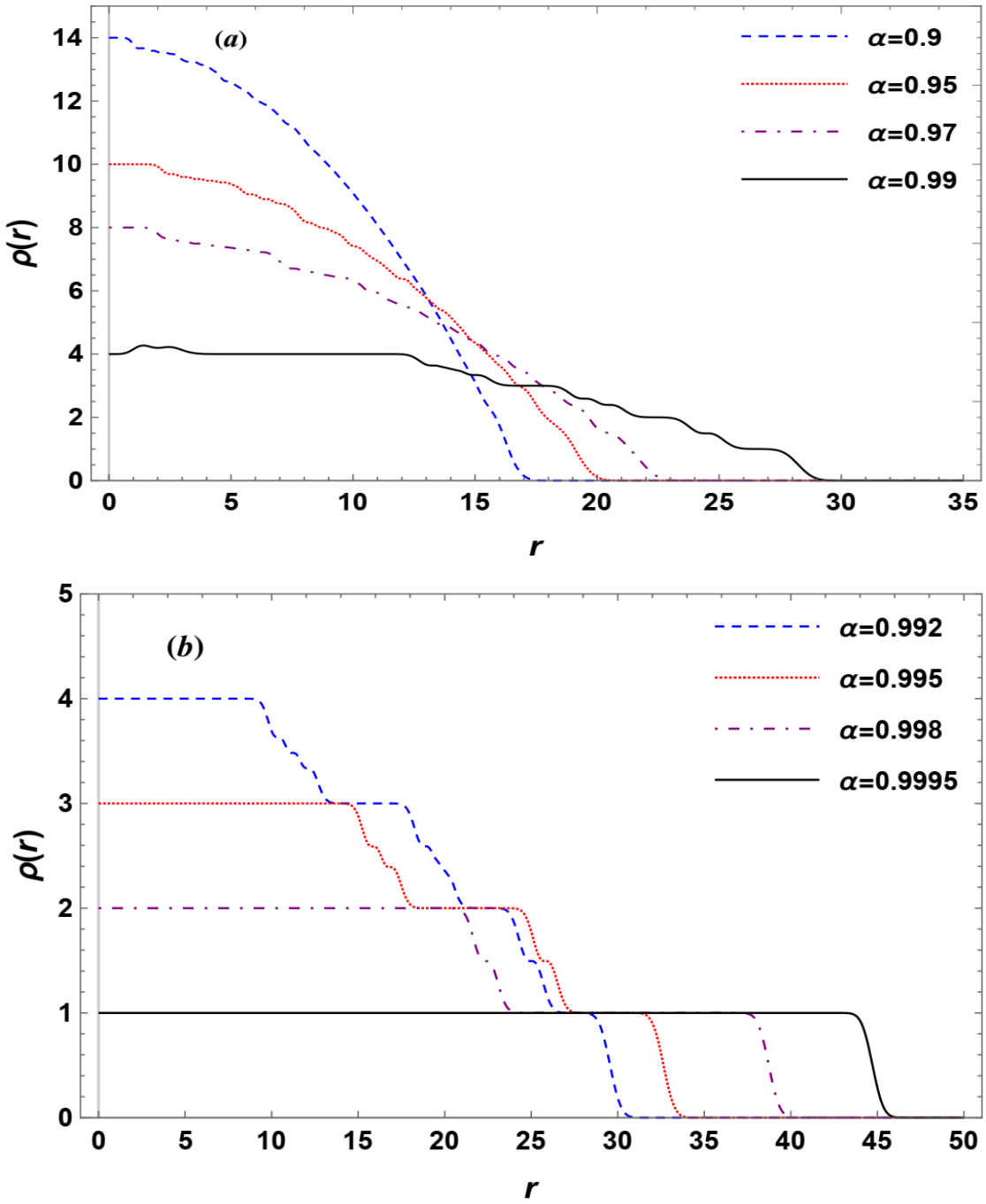

Fig 5: Under a weak magnetic field, the Fermi level closely intersects with energy levels E_{nm} (see Fig. 4(a)), causing rapid changes in particle density. This is illustrated (a), showing closely spaced compressible regions with decreasing density and narrow incompressible regions with constant density, which shrink towards the system's boundary. As the magnetic field strengthens, (a) and (b) reveal the progressive development of wider incompressible regions in particle density, occurring at quantized density values. These plateaus correspond to the occupation of new Landau levels, with crossings between Landau levels and the Fermi energy aligning precisely with compressible region centers. The density $\rho(r)$ is plotted in units of $(1/\pi\ell^2)$.

3.2. The equilibrium orbital current distribution

To demonstrate the irregular behavior of the equilibrium current density at weak magnetic fields, we present in Fig. 6 its distributions throughout the system for select small values of α. However, the current density proves highly responsive to changes in the applied magnetic field, as expected for all equilibrium properties considered herein. Notably, with increasing magnetic field, a discernible regularity in the current distribution progressively emerges. This evolution is clearly depicted in Figs 7(a) and 7(b), showcasing the current distribution as a function of position under varying magnetic field strengths. As previously emphasized, this regularity becomes markedly apparent at values $\alpha \geq 0.99$, coinciding with distinctly structured patterns in the particle density, featuring well-defined compressible and incompressible regions. Consequently, the spatial distribution of the current exhibits a notable alternating pattern, characterized by a series of strips (or channels) with currents flowing in opposite directions within these two types of regions.

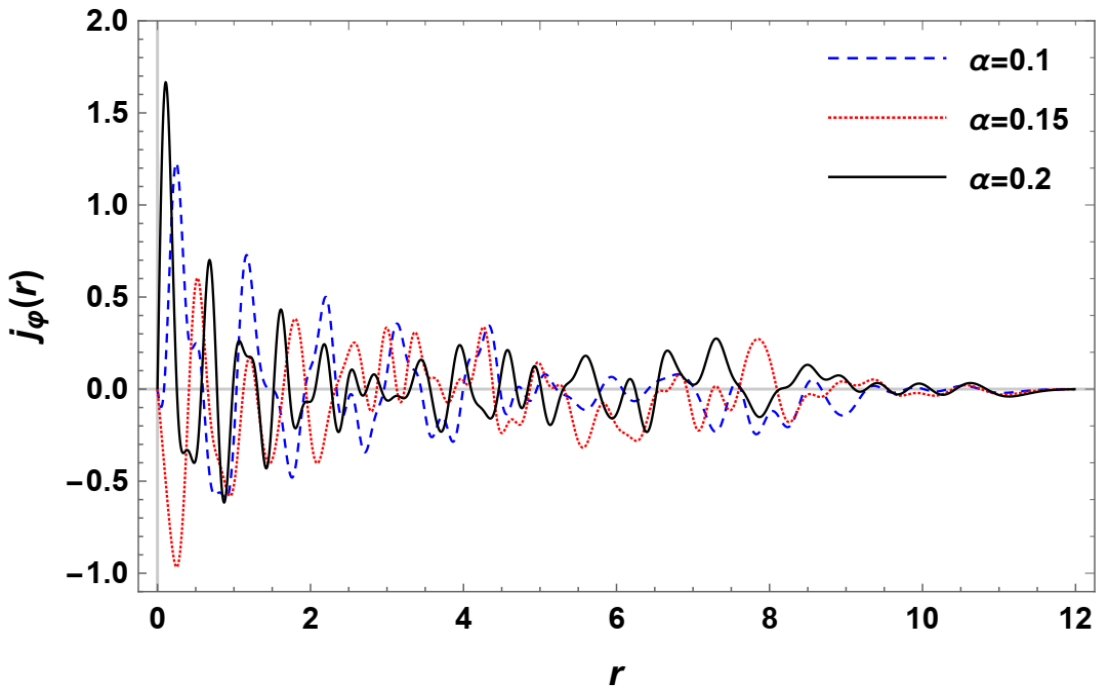

Fig 6: The irregular behavior of equilibrium current density at weak magnetic fields. The current $j_\varphi(r)$ is plotted in units of j_0.

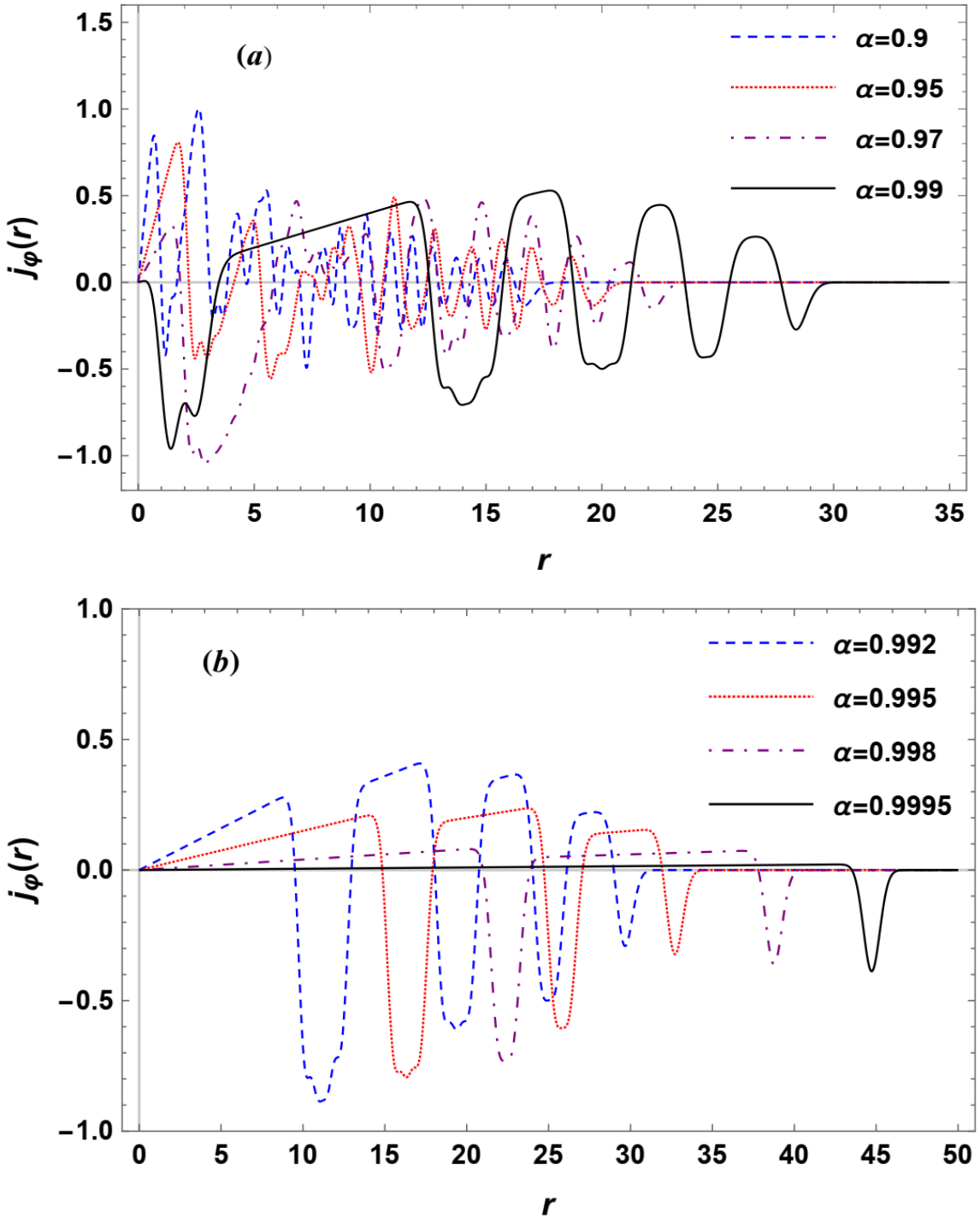

Fig 7: With increasing magnetic field, a noticeable regularity emerges in the current distribution, evident in (a) and (b). This becomes particularly pronounced at $\alpha \geq 0.99$, coinciding with structured patterns in particle density, delineating distinct compressible and incompressible regions. Consequently, the current spatial distribution displays a distinct alternating pattern, with currents flowing oppositely within these regions.

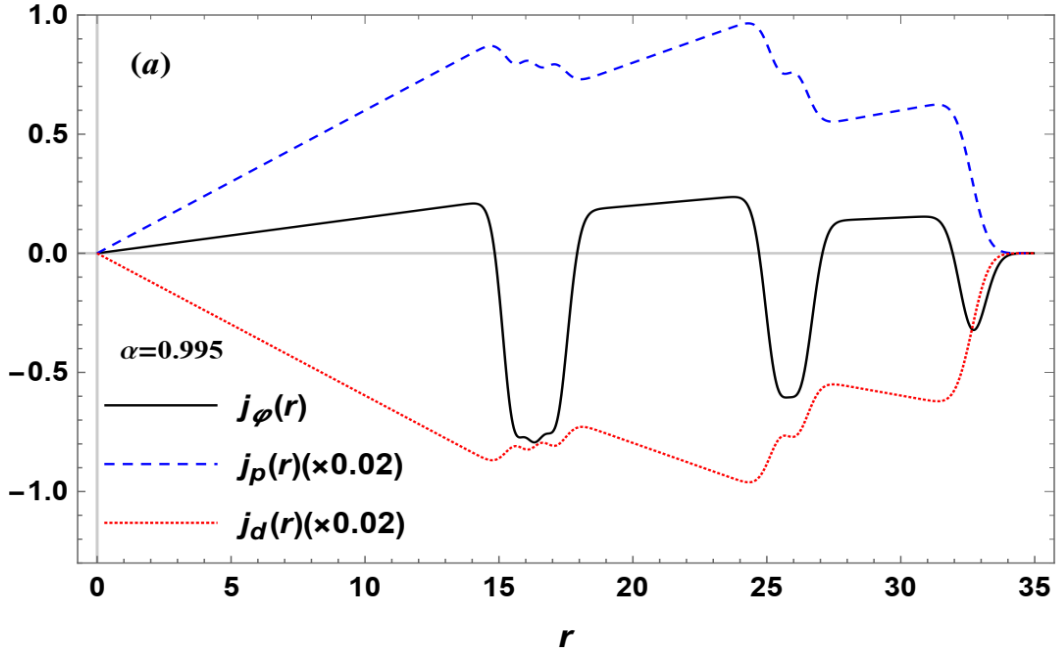

Fig 8: The interplay between its significant para and diamagnetic components, permeating the entire system, primarily generates the induced current $j_\varphi(r)$. This is showcased for a specific value $\alpha = 0.995$.

Let us now focus on investigating the structure of the current density in cases of high magnetic field regimes. It is evident that, within the scope of our study, the induced current $\mathbf{J}(\mathbf{r})$ primarily arises from the interplay between its huge para and diamagnetic components, *both concurrently present within the entire system*. This is depicted in Fig. 8 for a specific value $\alpha = 0.995$. However, the pattern of current reversals observed when going from an incompressible region to a neighboring compressible one suggests a deeper underlying structure. Indeed, the current density $\mathbf{J}(\mathbf{r})$ can be straightforwardly decomposed into two other types of counters propagating azimuthal currents, which exhibit notable properties at strong fields. As per Eq (3.15), the physical current $\mathbf{J}(\mathbf{r})$ can also be expressed as

$$j_\varphi(r) = j_{inc}(r) + j_c(r) \tag{4. 4}$$

Where

$$j_{inc}(r) = e\Omega_- r\rho(r) \tag{4. 5}$$

And

$$j_c(r) = -e\Omega r^{-1} \sum_{n_r=0}^{\infty} \sum_{m=-\infty}^{\infty} (m\ell^2 + r^2)\mathcal{R}^2_{n_r m}(r)\Theta\left(\mu - E_{n_r m}\right) \tag{4. 6}$$

As will be commented below, the subscripts "*c*" and "*inc*" in j_c and j_{inc}, stand for *the currents flowing in compressible and incompressible regions*, respectively.

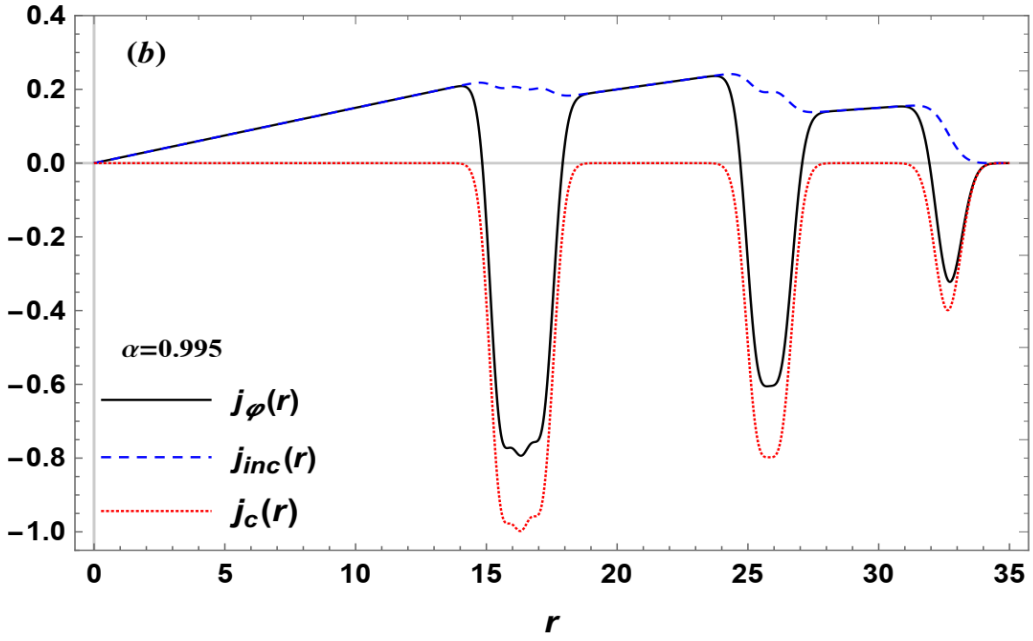

Fig 9: Using the same parameter $\alpha = 0.995$ as in Fig. 8 for comparison, we observe that the component j_{inc} precisely matches the total current density j_φ in incompressible regions where the second component j_c is absent. However, in compressible regions, the persistence of j_{inc} slightly alters the agreement between the component j_c and the actual current j_φ.

It is important to note that the decomposition outlined in Eq (4.4). holds true across all magnetic field strengths. However, it does not reveal any noteworthy features under weak field conditions. At low field strengths, the newly introduced components j_{inc} and j_c exhibit behaviors resembling competing para and diamagnetic currents spreading throughout the whole system.

Quite the contrary, in high-regime scenarios, the behavior of j_{inc} and j_c significantly diverges from the previous case. Figure 9, displayed below using the same parameter $\alpha = 0.995$ as shown in Fig. 8 for comparison, shows that the component j_{inc} precisely matches the total current density j_φ in incompressible regions where the second component j_c is entirely absent. However, the persistence of j_{inc} in the compressible regions slightly alters the agreement between the component j_c and the actual current j_φ therein. The continued presence of the component j_{inc} in the compressible regions can be understood from its direct proportionality to the gradient of the confining potential $V(r) = m^*\omega_0^2 r^2/2$, which does not vanish at these compressible regions. In fact, at strong fields ($\omega_L \gg \omega_0$), the frequency Ω_- can be expressed at first order as

$$\Omega_- \approx \frac{\omega_0^2}{2\omega_L} \qquad (4.7)$$

Which, after inserting it in Eq (4.5), yields

$$j_{inc}(r) = \left(\frac{e}{2\omega_L}\right)\omega_0^2 r\rho(r) \tag{4. 8}$$

Consequently, we can write down the component $\mathbf{J}_{inc}$ as

$$\mathbf{J}_{inc}(r) = -\frac{e}{2m^*\omega_L}\rho(r)\boldsymbol{\nabla}V(r)\times\mathbf{e}_z \tag{4. 9}$$

Consistent with the general theory presented in Refs. [24-25]. Further insight is gained at super-strong magnetic fields, where only the lowest Landau level is occupied $(n = n_r = 0)$. In this regime, the incompressible current $\mathbf{J}_{inc}$ can be directly related to the gradient of the particle density $\rho(r)$, through Eqs (3.15) and (4.6) by

$$\mathbf{J}_c(r) = -\frac{e\hbar}{2m^*}\boldsymbol{\nabla}\rho(r)\times\mathbf{e}_z \tag{4. 10}$$

Under such a super-strong field regime, the current $\mathbf{J}_{inc}$ in the wide incompressible region is significantly reduced due to flatness of the confining potential, leaving predominantly diamagnetic current $\mathbf{J}_c$ flowing along the physical edge of the system. This corresponds to the typical Landau diamagnetism, as evidenced, for example, by the value $\alpha = 0.9995$ in Fig. 7(b).

It should be noted that, according to the perfect screening theorem, the self-consistent confining potential should be uniform in compressible regions, leading to vanishing "incompressible" currents j_{inc} there. Therefore, the j_c component contribute exclusively to these compressible regions, while the j_{inc} current exists only in incompressible ones [25].

Before closing this discussion, we wish to emphasize that in the literature, the terms 'bulk current' and 'edge current' have been used to describe the currents j_{inc} and j_c in Ref. [24], respectively. However, given that all the eigenstates in our model are edge states, this classification may not be sufficiently relevant. Furthermore, the terms "bulk" and "edge" can be misleading concerning the actual distribution of these two currents, suggesting that the first flows throughout the entire system, whereas the second is confined to circulating at its physical boundaries. This implication is evidently not meaningful in our case. On the other hand, in the recent experimental study of equilibrium currents in a graphene quantum Hall electron system [50], these two types of currents were instead referred to as topological and non-topological currents, respectively. In the context of their study, the non-topological current is noticeably absent in the $n = 0$ Landau level which carries only a topological component, an exception observed in graphene. This is not the case for 2DEGs where all the LLs carry pairs of counter

propagating currents distinguishing it from the singular behavior observed in graphene. Moreover, in a more recent work (see ref. [31]), they are called "drift" and "circulating" currents, respectively. Given what has been mentioned and to prevent any confusion, we have opted for a notation where the subscript "c" in j_c signifies the current flowing in the compressible region, while "inc" in j_{inc} denotes that flowing in the incompressible region.

3.3. Oscillations of the orbital microscopic magnetization

The reversal in the flow direction of the induced current density observed when transitioning from an incompressible to a neighboring compressible region stems from the oscillatory nature of the microscopic magnetization $\mathcal{M}(r)$, as governed by the standard relation in Eq (3.23). Figures 10(a) and 10(b) show the evolution of the oscillation pattern of $\mathcal{M}(r)$, as a function of the radial distance r, for various values of magnetic field intensity.

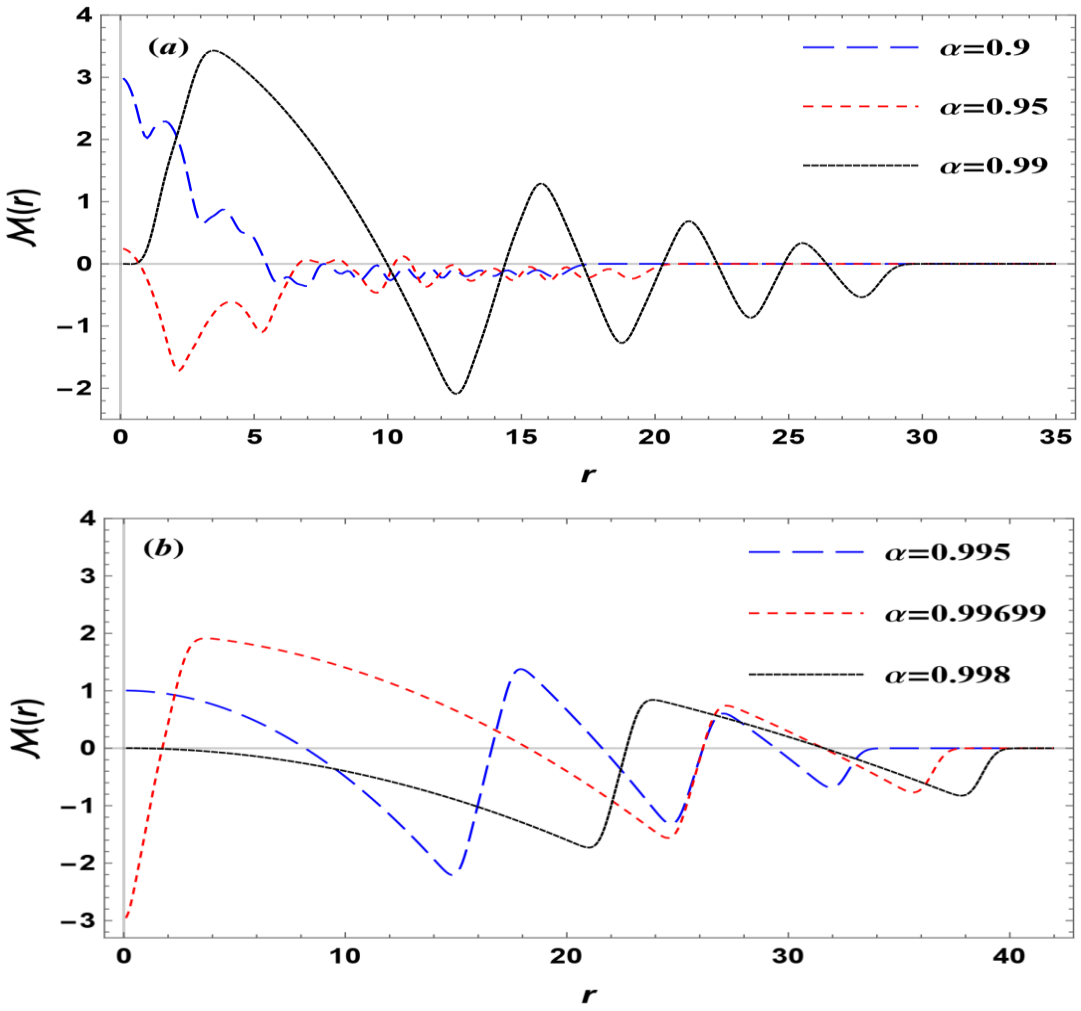

Fig 10: (a) and (b) Show the evolution of the oscillation pattern of the orbital microscopic magnetization $\mathcal{M}(r)$ as a function of the radial distance r, for various values of magnetic field intensity. The magnetization $\mathcal{M}(r)$ is plotted in units of $\mu_B/\pi\ell^2$.

In plotting the microscopic magnetization as a function of r, we intentionally excluded $\mathcal{M}(r)$ for the values $\alpha = 0.97$, 0.992 and 0.9995 in Figs. 10(a) and 10(b), unlike the particle and current densities previously shown. Instead, we displayed the magnetization $\mathcal{M}(r)$ for a specific intensity $\alpha = 0.99699$, chosen to highlight the negative starting value $\mathcal{M}(0)$ at the system's center. Recall that the total persistent current I is nothing but the microscopic magnetization at the center of the system, $I = \mathcal{M}(0)$. This negative value of the local magnetization $\mathcal{M}(r)$ at $r = 0$ corresponds to a Fermi energy lying just above the bottom of the $n = 2$ Landau level (See Fig. 3). A slight increase in the magnetic field causes the $n = 2$ level to cross the Fermi energy, resulting in a drastic change in $\mathcal{M}(0)$ (or equivalently, in the integrated current value), consistent with the general characteristic behavior observed in de Haas-van Alphen oscillations. We omitted plotting the magnetization for the second case, where the Fermi energy lies just below the $n = 2$ level, as we will address this point when discussing the total azimuthal current in the following section. However, according to Eq. (4.12) given below, we find the positive value $\mathcal{M}(0) \approx 2(\mu_B/\pi\ell^2)$ for an intensity $\alpha = 0.997$.

To provide a comprehensive visual depiction of how particle, current, and magnetization densities vary spatially, we have combined them in a single figure for the specific value $\alpha = 0.995$, as vividly shown in Fig. 11. It is evident from this figure that the magnetization $\mathcal{M}(r)$ decreases within the incompressible regions, leading to positive induced electric currents $j_\varphi(r)$, whereas in compressible regions, the magnetization increases, resulting in negative currents in these regions. This behavior aligns with Eq (3.23), where $\boldsymbol{\mathcal{M}}(\mathbf{r}) = \mathcal{M}(r)\mathbf{e}_z$, yielding $j_\varphi(r) = -\,d\mathcal{M}(r)/dr$.

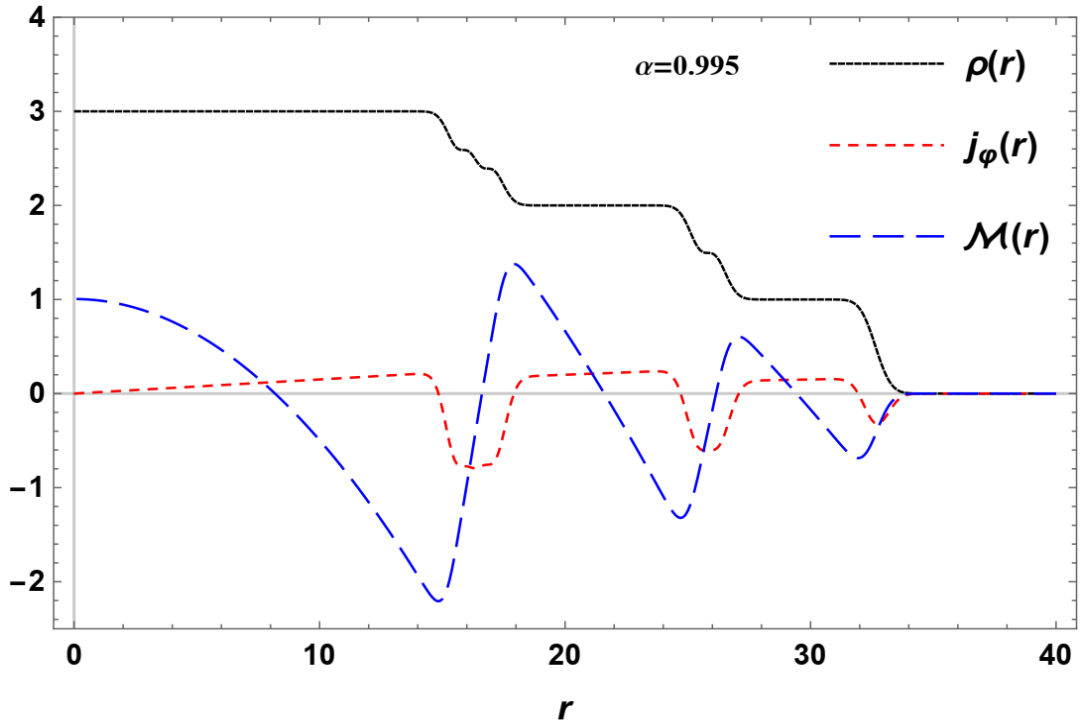

Fig 11: A clear visual representation of spatial variations in particle $\rho(r)$, current $j_\varphi(r)$, and magnetization $\mathcal{M}(r)$ densities is provided for the specific value $\alpha = 0.995$. The figure clearly shows that within incompressible regions, the magnetization $\mathcal{M}(r)$ decreases, resulting in positive induced electric currents $j_\varphi(r)$. Conversely, in compressible regions, the magnetization increases, leading to negative currents therin.

4. Quantum oscillations of total magnetic moment and integrated current

4.1. Oscillations of total magnetic moment

Although our primary focus is not on weak magnetic fields, it's worth mentioning that for $N = 2000$ electrons, strong paramagnetism is observed at very low fields due to the partial occupation of the last energy level (corresponding to oscillator shell $\mathcal{N}_{max} = 62$), as shown in Fig. 12(a). In fact, the Fermi level lies within the set of Zeeman levels of this shell, leaving some highest energy states unoccupied above it. This results in uncompensated individual magnetic moments $\mathbf{m}_{nm}$ of the corresponding lowest-energy states, contributing to the observed strong paramagnetism. Note that this behavior is basically due to the particular symmetric geometry of the harmonic oscillator confining potential.

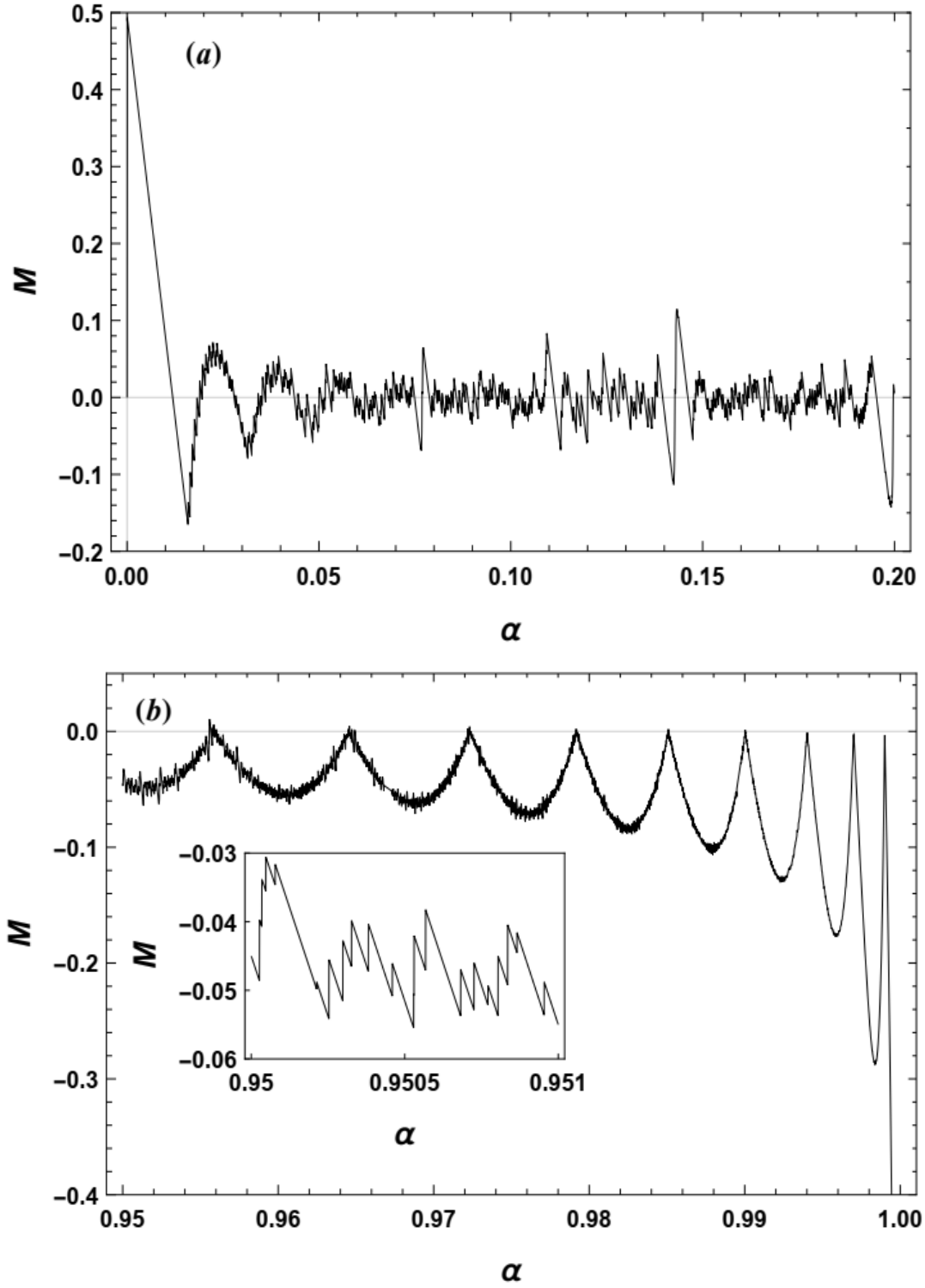

Fig 12: Evolution of the total magnetic moment (plotted in units $N\mu_B$) with magnetic fields (a) Total magnetic moment at weak magnetic fields. At these low field regimes, strong paramagnetism is evident, attributed to the partial occupation of the last energy level corresponding to oscillator shell $\mathcal{N}_{max} = 62$. (b) In high magnetic fields, the total orbital magnetic moment exhibits slow oscillations with large amplitudes, known as de Haas-van Alphen oscillations, occurring whenever a Landau level crosses the Fermi energy. Additionally, smaller and faster oscillations are superimposed on these de Haas-van Alphen oscillations, as shown in the inset of Fig. 12(b). These rapid oscillations, occurring within a single de Haas-van Alphen oscillation range, correspond to intersections between sublevels from different Landau levels.

In high magnetic fields, the total orbital magnetic moment $\mathbf{M} = M\mathbf{e}_z$ exhibits slow oscillations with large amplitudes, as depicted in Fig. 12(b). These oscillations, known as de Haas-van Alphen oscillations, occur whenever a Landau level crosses the Fermi energy, as seen previously in Fig. 3.

Superimposed on these de Haas-van Alphen oscillations are smaller and faster ones. The inset within Fig. 12(b) highlights these faster oscillations, occurring within a single de Haas-van Alphen oscillation, over a narrow range of intensities. These smaller oscillations correspond to intersections between sublevels from different Landau levels. Figure 13 provides further insight by displaying only the sublevels intersecting, downward and upward, with the Fermi energy, within the specified range. This allows for elucidating the intricate nature of these smaller oscillations, which are slightly obscured by the larger image.

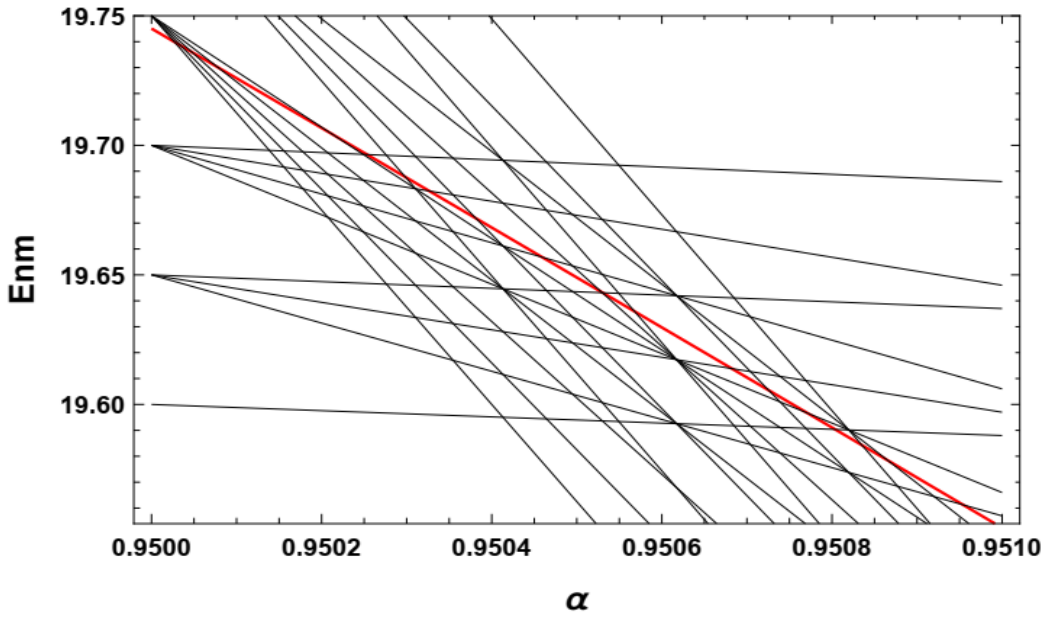

Fig 13 : Displaying only the sublevels intersecting, both downward and upward, with the Fermi energy within the specified range provides further insight. This focused view elucidates the intricate nature of the smaller oscillations, which may be slightly obscured in the larger image.

We will not delve deeper into the behavior of the total orbital magnetic moment, as it has been thoroughly investigated in literature. However, the brief discussion provided here serves to illustrate how the evolution of the system's energy spectrum with magnetic field intricately influences its properties down to their subtle details, as is exemplified by the oscillations of the total magnetic moment.

4.2. Oscillations of the integrated current

At low magnetic fields, the integrated persistent current I behaves similarly to the total magnetic moment M. It has been shown in Ref. [28] that in the weak-magnetic-field limit, the persistent current is proportional to the total magnetic moment, exhibiting Aharonov-Bohm type oscillations (see Fig. 12(a)).

However, as the magnetic field increases, the total persistent current begins to display de Haas-van Alphen oscillations but assumes a saw-tooth pattern, as depicted in Fig. 14(a). Each tooth is accompanied by small fluctuations that dampen as the magnetic field strengthens, until they are entirely suppressed at superstrong magnetic fields. This corresponds to the scenario where the lowest Landau level is fully occupied $(n = 0)$, and there are no more sublevels intersecting the Fermi level.

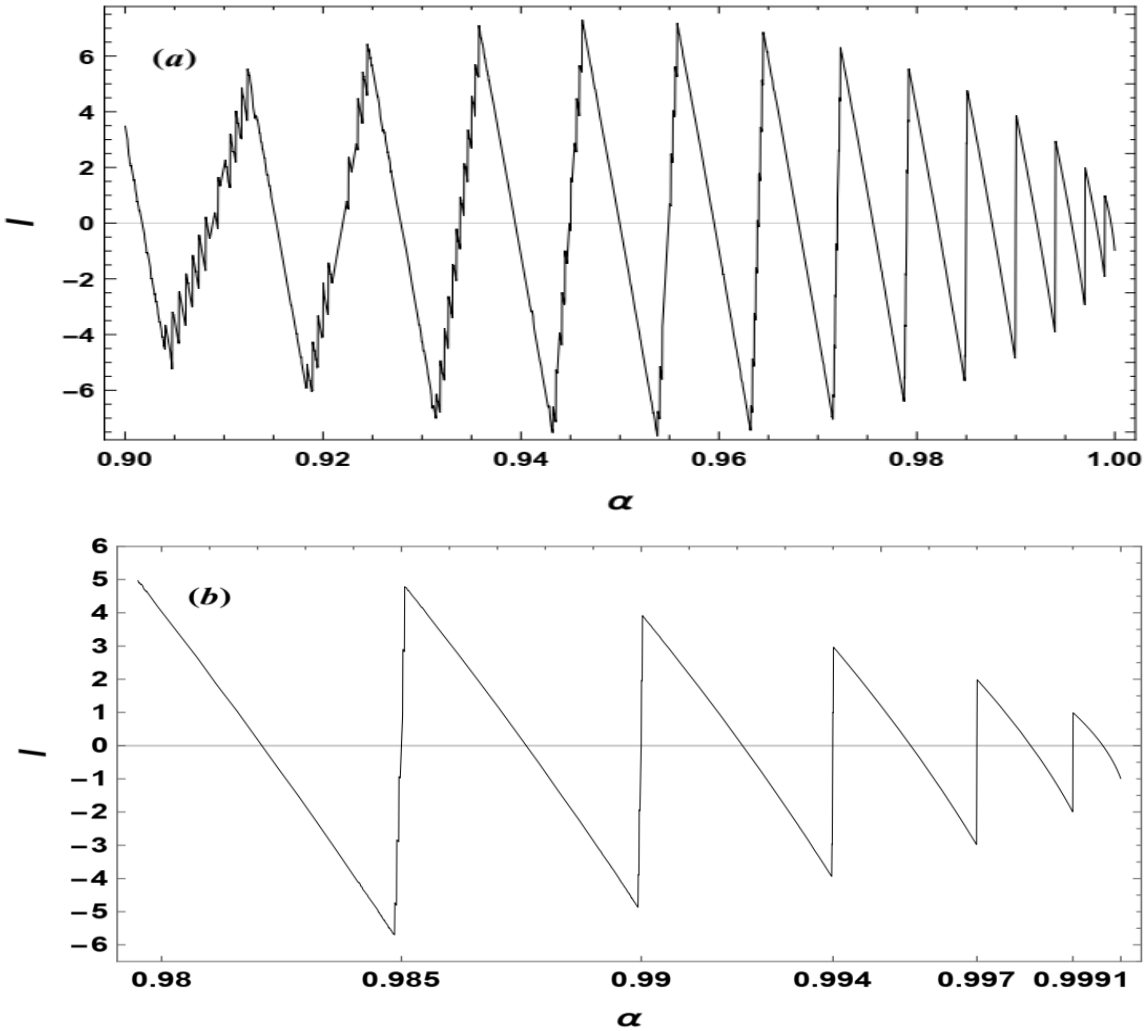

Fig 14 : (a) Evolution of the total persistent current I (in units $e\Omega/2\pi$) with high magnetic fields, displaying de Haas-van Alphen oscillations with a saw-tooth pattern. Small fluctuations accompany each tooth, dampening as the magnetic field strengthens until they are entirely suppressed at superstrong magnetic fields. (b) Abrupt changes of I at high magnetic fields whenever the Fermi level intersects a Landau level between values $-(n+1)\ e\Omega/2\pi$ and $n\ e\Omega/2\pi$, resulting in a jump $\Delta I = (2n+1)e\Omega/2\pi$, depending on the position of the Fermi level relative to the Landau level.

Furthermore, the persistent current exhibits abrupt changes at high magnetic fields whenever the Fermi level intersects a Landau level, as shown in Fig. 14(b) (also refer to Fig. 3). Two important cases arise depending on the relative positions of the Fermi energy and the Landau levels. When the Fermi level lies just above the bottom of a Landau level n, the integrated current closely approximates the following value

$$I = -(n+1)\frac{e\Omega}{2\pi} \tag{4. 11}$$

As the magnetic field slightly increases, causing the Fermi level to descend and cross the level n and then reside just below it, the integrated current undergoes a drastic change by taking the following positive value

$$I = n\frac{e\Omega}{2\pi} \tag{4. 12}$$

Leading to a jump $\Delta I = (2n+1)e\Omega/2\pi$. It is worth noting that in strong magnetic field regimes, one can approximate, at first order, $\Omega \approx \omega_L\left(1 + (\omega_0^2/2\omega_L^2)\right)$. The expressions in Eqs. (4.11) and (4.12) are reminiscent of those of the quantized integrated current as a function of the particle number N [24]. Nevertheless, in our context, we are discussing the evolution of the integrated current as a function of magnetic field strength with constant number of particles, where there is no quantization for I.

General conclusion

General conclusion

In summary, this study offers a thorough exploration of the equilibrium orbital properties of a completely degenerate, harmonically confined 2DEG under a perpendicular magnetic field. By employing both the single-particle wave function approach and the Bloch density matrix formalism, we derived exact analytical expressions for key properties, including the spatial matter distribution, electric current flow, microscopic magnetization, first-order density matrix, total magnetic moment, and integrated persistent current. Although the two approaches initially produced seemingly distinct results, numerical verification confirmed their equivalence, ensuring the reliability of our findings and providing a robust understanding of the system's quantum behavior. Notably, the exact expression for the microscopic magnetization allowed us to directly deduce the total persistent electric current, highlighting the deep connection between these quantities. Our analysis also revealed how subtle changes in the energy spectrum profoundly influence orbital properties, leading to striking quantum oscillations at high magnetic fields.

Focusing on strong magnetic field regimes, we uncovered intriguing phenomena such as the formation of compressible and incompressible regions in the particle density profile, driven by the emergence of Landau levels. We also explored the underlying structure of counter-propagating equilibrium currents, which arise from the oscillatory nature of the microscopic magnetization. These findings deepen our understanding of confined electron gases under magnetic fields and shed light on the complex interplay of quantum effects. The results not only advance fundamental knowledge but also have potential applications in the design of nanoscale electronic devices, such as quantum dots and high-mobility transistors, where precise control over electron behavior is crucial.

Recent advancements in scanning probe techniques, such as scanning SQUID-on-tip microscopy, have enabled the precise measurement of local magnetic fields at nanometer scales. For 2D systems—including thin films, semiconductor electron gases, and other low-dimensional materials—mapping a single component of the magnetic field can uniquely reconstruct the underlying source current or out-of-plane magnetization distribution. This capability offers a powerful tool for probing the quantum behaviors explored in this work, particularly for a harmonically confined 2DEG. The theoretical framework developed here aligns closely with these cutting-edge experimental methods, providing a critical link between theoretical predictions and

observable phenomena in real-world systems. Such synergy between theory and experiment not only validates our findings but also opens new avenues for exploring and manipulating quantum states in confined geometries.

While this study focused on zero-temperature conditions, future research could extend the analytical framework to include finite-temperature effects. Investigating the interplay between temperature, magnetic field strength, and carrier density promises to uncover new and interesting physics. Additionally, exploring the role of electron-electron interactions and many-body effects could provide further insights into the system's quantum coherence and transport properties, enriching our understanding of confined quantum systems.

References

[1] D. Shoenberg, *Magnetic Oscillations in Metals*, Cambridge University Press, 1984, **ISBN** 978-0-521-22480-2.

[2] A. A. Abrikosov, *Fundamentals of The Theory of Metals*, North-Holland, 1988, **ISBN** 0 444 87004 6.

[3] D. K. Ferry, S. M. Goodnick, J. Bird, *Transport in Nanostructures*, 2nd ed., Cambridge University Press, Cambridge, 2009, **ISBN:**9780511840463

[4] T. Ihn, *Semiconductor Nanostructures*, Oxford University Press, New York, 2010, **ISBN:**9780199534425

[5] M. P. Schwarz, M. A. Wilde, S. Groth, D. Grundler, C. Heyn, D. Heitmann, *Sawtoothlike de Haas–van Alphen oscillations of a two-dimensional electron system, Phys. Rev. B* **65**, 245315 (2002), **DOI**:10.1103/PhysRevB.65.245315.

[6] J. K. Wang, D. C. Tsui, M. Santos, M. Shayegan, *Heat-capacity study of two-dimensional electrons in GaAs/Al_x Ga $_{1-x}$As multiple-quantum-well structures in high magnetic fields: Spin-split Landau levels, Phys. Rev. B* **45,** 4384 (1992), **DOI**: 10.1103/PhysRevB.45.4384.

[7] E. Gornik, R. Lassnig, G. Strasser, H. L. Stormer, A. C. Gossard, W. Wiegmann, *Specific Heat of Two-Dimensional Electrons in GaAs-GaAlAs Multilayers*, *Phys. Rev. Lett.* **54**, 1820 (1985), **DOI**:10.1103/PhysRevLett.54.1820 .

[8] M. A. Hidalgo, *Equilibrium properties of 2D electron systems in quantum wells and graphene*, *Eur. Phys. J. Plus* 138, 983 (2023), **DOI**: 10.1140/epjp/s13360-023-04586-x.

[9] T. Ando, A. B. Fowler, F. Stern, *Rev. Mod, Electronic properties of two-dimensional systems*, *Phys.* **54,** 437 (1982), **DOI**:10.1103/RevModPhys.54.437.

[10] Z. T. Wang, M. Hilke, N. Fong, D. G. Austing, S. A. Studenikin, K. W. West, L. N. Pfeiffer, *Nonlinear transport phenomena and current-induced hydrodynamics in ultrahigh mobility two-dimensional electron gas*, *Phys. Rev. B* **107**, 195406 (2023), **DOI**:10.1103/PhysRevB.107.195406.

[11] X. Huang, C. Liu, P. Zhou, *2D semiconductors for specific electronic applications: from device to system,* npj 2D Mater, *Appl.* **6**, 51 (2022), **DOI**:10.1038/s41699-022-00327-3

[12] P. Kaushal, G. Khanna, Mater*, The role of 2-Dimensional materials for electronic devices*, Sci. Semicond. Process. **143**, 106546 (2022), **DOI**:10.1103/PhysRevB.107.195406

[13] A. Thakur, B. Anasori, *Accelerating 2D materials discovery*, *Science* **383**, 1182 (2024), **DOI**: doi/10.1126/science.ado4113

[14] K. Dini, O. V. Kibis, I. A. Shelykh, *Magnetic properties of a two-dimensional electron gas strongly coupled to light*, *Phys. Rev. B* **93**, 235411 (2016), **DOI**:10.1103/PhysRevB.93.235411

[15] Y. Sawa, T. Yokoyama, Y. Tanaka, *Charge transport in 2DEG/s-wave superconductor junction with Dresselhaus-type spin–orbit coupling*, *J. Magn. Magn. Mater.* **310**, 2277 (2007), Proceedings of the 17th International Conference on Magnetism, **DOI**:10.1016/j.jmmm.2006.10.744

[16] I. D. Vagner, *Quantum mechanics of electrons in strong magnetic field*, *HIT J. Sci. Eng. A* **3**, 102 (2006), **PACS:** 73.20.Fz, 72.15.Rn

[17] L. Casparis, M. R. Connolly, M. Kjaergaard, N. J. Pearson, A. Kringhoj, T. W. Larsen, F. Kuemmeth, T. Wang, C. Thomas, S. Gronin, G. C. Gardner, M. J. Manfra, C. M. Marcus, K. D. Petersson, *Superconducting gatemon qubit based on a proximitized two-dimensional electron gas*, Nature Nanotech **13**, 915 (2018), **DOI:** 10.1038/s41565-018-0207-y

[18] L. T. Chang, I. A. Fischer, J. Tang, C.-Y. Wang, G. Yu, Y. Fan, K. Murata, T. Nie, M. Oehme, J. Schulze, K. L. Wang, *Electrical detection of spin transport in Si two-dimensional electron gas systems*, Nanotechnology **27**, 365701 (2016), **DOI:** 10.1088/0957-4484/27/36/365701

[19] V. Gudmundsson, R. R. Gerhardts, R. Johnston, L. Schweitzer, *Magnetic field effects in a confined two-dimensional electron gas: A comparison between continuum and lattice model*, *Z. Phys. B: Condens. Matter* **70**, 453 (1988), **DOI:**10.1007/BF01312119

[20] C. S. Lent, *Edge states in a circular quantum dot*, Phys. Rev. B **43**, 4179 (1991), **DOI:** 10.1103/physrevb.43.4179

[21] G. Vignale, *Rigorous upper bound for the persistent current in systems with toroidal geometry, Phys. Rev. B* **51**, 2612 (1995), **DOI:** 10.1103/physrevb.51.2612

[22] Y. Avishai and M. Kohmoto, *Quantized persistent currents in quantum dot at strong magnetic field*, *Phys. Rev. Lett.* **71**, 279 (1993), **DOI:**10.1103/PhysRevLett.71.279

[23] E. Anisimovas, A. Matulis, and F.M. Peeters, *Currents in a many-particle parabolic quantum dot under a strong magnetic field*, *Phys. Rev. B* **70**, 195334 (2004). DOI:10.1103/PhysRevB.70.195334

[24] M.R. Geller and G. Vignale, *Currents in the compressible and incompressible regions of the two-dimensional electron gas*, Phys. Rev. B **50**, 11714 (1994), **DOI**: 10.1103/physrevb.50.11714

[25] M.R. Geller and G. Vignale, *Universal equilibrium currents in the quantum Hall fluid*, *Phys. Rev. B* **52**, 14137 (1995), **DOI**:10.1103/PhysRevB.52.14137

[26] M.R. Geller and G. Vignale, *Equilibrium current and orbital magnetization in the quantum Hall fluid*, *Physica B* **212**, 283 (1995), **DOI**: 10.1016/0921-4526(95)00045-B

[27] K. Shizuya, *Current Distributions and the De Haas–Van Alphen Oscillation in a Planar System of Hall Electrons, Int. J. Mod. Phys. B* **11**, 1799 (1997), **DOI**:10.1142/s0217979297000927

[28] W.C. Tan and J.C. Inkson, *Magnetization, persistent currents, and their relation in quantum rings and dots*, *Phys. Rev. B* 60, 5626 (1999), **DOI**:10.1103/PhysRevB.60.5626

[29] H. Bluhm, N.C. Koshnick, J.A. Bert, M.E. Huber, and K.A. Moler, *Persistent Currents in Normal Metal Rings*, *Phys. Rev. Lett.* **102**, 136802 (2009), **DOI**:10.1103/PhysRevLett.102.136802

[30] Y. Yerin, V.P. Gusynin, S.G. Sharapov, and A.A. Varlamov, *Genesis and fading away of persistent currents in a Corbino disk geometry*, *Phys. Rev. B 104,* 075415 (2021), **DOI**:10.1103/PhysRevB.104.075415

[31] K. Shizuya, *Equilibrium current distributions and W_∞ gauge theory in quantum Hall systems of conventional electrons and Dirac electrons*, *Phys. Rev. B* **107**, 165410 (2023), **DOI**:10.1103/PhysRevB.107.165410

[32] L. Landau, *Diamagnetismus der Metalle*, *Z. Phys.* **64**, 629 (1930), **DOI**:10.1007/BF01397213

[33] V. Fock, *Bemerkung zur Quantelung des harmonischen Oszillators im Magnetfeld*, *Z. Physik* 47, 446 (1928), **DOI**:10.1007/BF01390750

[34] (a) R.V. Denton, *On size corrections to the diamagnetic susceptibility of a free electron gas*, *Z. Phys.* **265**, 119 (1973), **DOI**:10.1007/BF01394652.

(b) M.J. Harrison, *Diamagnetic spike modification of a two-dimensional electron gas confined within a parabolic quantum well, Phys. Rev. B* 45, 3815 (1992), **DOI**:10.1103/PhysRevB.45.3815

(c) J.-X. Zhu and Z.D. Wang, *Orbital magnetic susceptibility of a confined two-dimensional electron gas, Phys. Lett. A* **203**, 144 (1995), **DOI**:10.1016/0375-9601(95)00401-N

(d) K. Richter, D. Ullmo, and R.A. Jalabert, *Orbital magnetism in the ballistic regime: geometrical effects, Phys. Rep.* **276**, 1 (1996), **DOI**:10.1016/0370-1573(96)00010-5.

(e) V.A. Geyler and V.A. Margulis, Specific heat of quasi-two-dimensional systems in a magnetic field, *Phys. Rev. B* **55**, 2543 (1997), **DOI**:10.1103/PhysRevB.55.2543.

(f) L. Bremme, T. Ihn, and K. Ensslin, *Magnetization of a two-dimensional electron gas and the role of one-dimensional edge currents*, *Phys. Rev. B* **59**, 7305 (1999), **DOI**:10.1103/PhysRevB.59.7305

(g) I. Magnúsdóttir and V. Gudmundsson, *Magnetization of noncircular quantum dots*, *Phys. Rev. B* **61**, 10229 (2000), **DOI**: 10.1103/PhysRevB.61.10229

(h) M. Saito, T. Sasaki, and H. Fukuyama, *Orbital Magnetism in Two-Dimensional Mesoscopic Ring Systems*, *J. Phys. Soc. Jpn.* **72**, 2556 (2003), **DOI**:10.1143/JPSJ.72.2556.

(i) L.S. Georgiev and M.R. Geller, *Magnetic-moment oscillations in a quantum Hall ring, Phys. Rev. B* **70**, 155304 (2004), **DOI**:10.1103/PhysRevB.70.155304

(j) Z. Wang, W. Zhang, and P. Zhang, *Magnetization in two-dimensional electron gas in a perpendicular magnetic field: The roles of edge states and spin-orbit coupling*, *Phys. Rev. B* **79**, 235327 (2009), **DOI**:10.1103/PhysRevB.79.235327

(k) Y. Li and H. Liu, *Diamagnetism versus paramagnetism of charged ideal spin-1/2 fermions in a harmonic trap under a uniform magnetic field*, Int. J. Mod. Phys. B **33**, 1950026 (2019), **DOI**:10.1142/S0217979219500267

(l) V.V. Dodonov and A.V. Dodonov, *Magnetic-moment probability distribution of a quantum charged particle in thermodynamic equilibrium*, *Phys. Rev. A* **102**, 042216 (2020), **DOI**: https://doi.org/10.1103/PhysRevA.102.042216.

(m) V.V. Dodonov, *Magnetization dynamics of a harmonically confined quantum charged particle in time dependent magnetic fields inside a circular solenoid, J. Phys. A: Math. Theor.* **54**, 295304 (2021), **DOI**:10.1088/1751-8121/ac0962

(n) V.V. Dodonov and A.V. Dodonov, *Giant diamagnetism of a quantum charged particle after inversion of the magnetic field*, *Phys. Rev. A* **105**, 062201 (2022), **DOI**:10.1103/PhysRevA.105.062201

[35] Y. Meir, O. Entin-Wohlmann, and Y. Gefen, *Magnetic-field and spin-orbit interaction in restricted geometries: Solvable models*, Phys. Rev. B **42**, 8351 (1990), **DOI**: 10.1103/physrevb.42.8351

[36] C.G. Darwin, *The Diamagnetism of the Free Electron***,** Proc. Cambridge Philos. Soc. **27**, 86 (1931), **ISSN:** 0305-0041

[37] Y. Ishikawa and H. Fukuyama, *Orbital Magnetism and Current Distribution of Two-Dimensional Electrons under Confining Potential*, J. Phys. Soc. Jpn. **68**, 2405 (1999), **DOI**:10.1143/JPSJ.68.2405

[38] P. Shea and B.P. van Zyl, *Thermodynamic properties of a harmonically trapped, two-dimensional charged quantum gas in a magnetic field*, J. Phys. A: Math. Theor. **41**, 135305 (2008), **DOI** 10.1088/1751-8113/41/13/135305

[39] (a) P. Shea and B.P. van Zyl, *Exact results for a charged harmonically trapped quantum gas at arbitrary temperature and magnetic field strength*, Phys. Rev. B **74**, 205334 (2006), **DOI**:10.1103/PhysRevB.74.205334

(b) P. Shea and B.P. van Zyl, Simple analytical results for harmonically trapped quantum gases, J. Phys. A **40**, 10589 (2007), **DOI:** 10.1088/1751-8113/40/34/014

[40] B.U. Felderhof and S.P. Raval, *Diamagnetism of a confined electron gas*, Physica A **82**, 151 (1976), **DOI**:10.1016/0378-4371(76)90096-0

[41] H. Naïdja, K. Bencheikh, J. Bartel, and P. *Quentin, System of fermions confined in a harmonic potential and subject to a magnetic field or a rotational motion*, Phys. Rev. A **83**, 053631 (2011), **DOI**:10.1103/PhysRevA.83.053631

[42] B. Kramer, *Quantum Coherence in Mesoscopic Systems*, Springer US, May **31**, 1991, ISBN-13-978-0306438899

[43] R. Bogdanovic and M.S. Gopinathan, *A canonical transformation of the Hamiltonians quadratic in coordinate and momentum operators,* J. Phys. A **12**, 1457 (1979), **DOI** :10.1088/0305-4470/12/9/013

[44] S.M. Reimann and M. Manninen, *Electronic structure of quantum dots*, Rev. Mod. Phys. **74**, 1283 (2002), **DOI**:10.1103/RevModPhys.74.1283

[45] (a) J.P. Gazeau and P-Y. Hsiao, *Symmetry and Structural Properties of Condensed Matter*, World Scientific, Singapore, 2001, **DOI**:10.1142/4653

(b) I. Aremua, M.N. Hounkonnou, and E. Baloïtcha, *Coherent States for Landau Levels: Algebraic and Thermodynamical Properties*, Rep. Math. Phys. **76**, 247 (2015), **DOI**:10.1016/S0034-4877(15)30032-X

[46] J.P. Gazeau, P.Y. Hsiao, A. Jellal, *Exact trace formulas for two-dimensional electron magnetism*, Phys. Rev. B **65**, 094427 (2002), **DOI**:10.1103/PhysRevB.65.094427

[47] A. Jellal, *Orbital magnetism of a two-dimensional noncommutative confined system*, J. Phys. A **34**, 10159 (2001), **DOI**:10.1088/0305-4470/34/47/319

[48] K. Nouicer, *Effect of minimal lengths on electron magnetism*, J. Phys. A **40**, 2125 (2007), **DOI**:10.1088/1751-8113/40/9/017

[49] E. Marchiori, L. Ceccarelli, N. Rossi, L. Lorenzelli, C.L. Degen, and M. Poggio, *Nanoscale magnetic field imaging for 2D materials*, Nat. Rev. Phys. **4**, 49 (2022), **DOI:** 10.1038/s42254-021-00380-9

[50] A. Uri, Y. Kim, K. Bagani, C.K. Lewandowski, S. Grover, N. Auerbach, E.O. Lachman, Y. Myasoedov, T. Taniguchi, K. Watanabe, J. Smet, and E. Zeldov, *Nanoscale imaging of equilibrium quantum Hall edge currents and of the magnetic monopole response in graphene*, Nat. Phys. **16**, 164 (2020), **DOI**: 10.1038/s41567-019-0713-3

[51] S. Komatsu, H. Irie, T. Akiho, T. Nojima, T. Akazaki, and K. Muraki, *Gate tuning of fractional quantum Hall states in an InAs two-dimensional electron gas*, Phys. Rev. B **105**, 075305 (2022), **DOI**:10.1103/PhysRevB.105.075305

[52] H. Xiao-Guang, Z. De-Gang, and J. De-Sheng, *Formation of two-dimensional electron gas at AlGaN/GaN heterostructure and the derivation of its sheet density expression*, Chinese Phys. B **24**, 067301 (2015), **DOI**: 10.1088/1674-1056/24/6/067301

[53] https://en.wikipedia.org/wiki/Two-dimensional_electron_gas

[54] E.Borovitskaya, M.S.Shur, *Quantum dots*, World Scientific Publishing CO.Pte.Ltd (2002), ISBN 981-02-4918-7

[55] D. Tong, *Applications of Quantum Mechanics*, University of Cambridge, Part II Mathematical Tripos (2017), https://www.damtp.cam.ac.uk/user/tong/aqm.html

[56] T. Chakraborty and P. Pietiläinen, *The Quantum Hall Effects: Integral and Fractional*, Springer Series in Solid State Sciences, (1995), https://link.springer.com/book/10.1007/978-3-642-79319-6

[57] Zhuo Yang, B. Fauqué, T. Nomura, T. Shitaokoshi, S. Kim, D. Chowdhury, Z. Pribulová, J. Kačmarčík, A. Pourret, G. Knebel, D. Aoki, T. Klein, D.K. Maude, C. Marcenat, and Y. Kohama, *Unveiling the double-peak structure of quantum oscillations in the specific heat*, Nature Commun. **14**, 7006 (2023), **DOI**:10.1038/s41467-023-42730-4

[58] M. Saito, T. Sasaki, and H. Fukuyama, *A theoretical study on orbital magnetism of mesoscopic ring systems*, Physica E **18**, 362–363 (2003), **DOI**:10.1016/S1386-9477(02)01096-2

[59] M. Brack and R. K. Bhaduri, *Semiclassical physics*, Frontiers in Physics, 96 (2003), ISBN: 0-8133-4084-5

[60] S. Flügge, *Practical Quantum Mechanics*, Springer-Verlag Berlin Heidelberg, Germany (1999), ark:/13960/t3cz9hh4z

[61] I. S. Gradshteyn and I. M. Ryzhik, *Table of Integrals, Series*, *and Products*, Academic Press, New York, 5th edition, (1994), ISBN-13: 978-0-12-373637-6

[62] N. H. March, M P Tosi, *The Bloch density matrix for a localised oscillator in a magnetic field*, J. Phys. A: Math. Gen. **18**, L643-L645 (1985), **DOI**: 10.1088/0305-4470/18/11/002

[63] E.H. Sondheimer, A.H. Wilson, *The diamagnetism of free electrons*, Proc. R. Soc. A **210** (1951) 173, **DOI**:10.1098/rspa.1951.0239

[64] G. Vignale, M. Rasolt, *Density-functional theory in strong magnetic fields*, Phys. Rev. Lett. **59** (1987) 2360, **DOI:** 10.1103/PhysRevLett.59.2360

[65] G. Vignale, M. Rasolt, *Current- and spin-density-functional theory for inhomogeneous electronic systems in strong magnetic fields*, Phys. Rev. B **37** (1988) 10685, **DOI**:10.1103/PhysRevB.37.10685

[66] L. L. Hirst, *The microscopic magnetization: concept and application*, Rev. Mod. Phys. **69**, 607 (1997), **DOI**:10.1103/RevModPhys.69.607

ملخص

نقدم في هذا العمل دراسة شاملة لعدد من الخصائص المدارية الأساسية لغاز إلكتروني ثنائي الأبعاد في حالة توازن ومحصور بواسطة كمون هزاز توافقي وذلك تحت تأثير مجال مغناطيسي عمودي على النظام المدروس. باستخدام دوال الموجة أحادية الجسيم وتقنية مصفوفة الكثافة لبلوخ، نشتق عبارات تحليلية دقيقة للخصائص المحلية والتكاملية المدارية، بما في ذلك كثافة الجسيمات، كثافة التيار، المغنطة المجهرية، العزم المغناطيسي الكلي والتيار الكهربائي الدائم الكلي. نثبت هنا إمكانية استنتاج عبارة التيار المستدام الكلي مباشرة من عبارة المغنطة المجهرية، مما يؤكد الترابط الجوهري بينهما. من جهة أخرى، فإن التحليل العددي يركز على المجالات المغناطيسية القوية، حيث يتم الكشف عن مناطق انضغاطية وأخرى لا انضغاطية ضمن توزيع كثافة الجسيمات. على وجه التحديد، نكشف عن البنية الأساسية للتيارات المتعاكسة في الاتجاهات والتي نُلاحظ في هذه الرتب العالية للمجال المغناطيسي، والتي تنتج عن السلوك التذبذبي للمغنطة المجهرية. من خلال استكشاف التغيرات في طيف الطاقة، نكشف عن التحسس الشديد للخصائص المدروسة لهذه التغيرات، مما يؤدي إلى أنماط تذبذبات كمومية مثيرة للاهتمام في المجالات العالية للحقل المغناطيسي.

الكلمات المفتاحية: المغنطة المجهرية المدارية، التيار الكهربائي المستديم، المغناطيسية المدارية، كثافة الجسيمات، غاز إلكتروني ثنائي البعد، الاهتزازات الكمومية.

Abstract

This thesis conducts a comprehensive analysis of some important fundamental equilibrium properties of a harmonically confined two-dimensional electron gas subjected to a uniform perpendicular magnetic field. Using single-particle wave functions and Bloch density matrix method, we obtain exact analytical expressions for various local and integral properties, including particle density, current distribution, microscopic magnetization, total magnetic moment, and the integrated persistent current. We provide a direct deduction of the total persistent current from the orbital microscopic magnetization, emphasizing their inherent connection. Numerical investigation, concentrating on strong magnetic field regimes, uncovers well-defined compressible and incompressible regions within the particle density profile. We unravel the underlying structure of the counter-propagating equilibrium currents in high-field regimes, induced by the oscillatory behavior of microscopic magnetization, which we derive in exact analytical form in real physical space. Moreover, an examination of changes in the energy spectrum reveals intricate influences on these properties, resulting in quantum oscillation patterns at high magnetic fields.

Keywords: Orbital microscopic magnetization, Persistent electric current, Orbital magnetism , Particle density, Two-dimensional electron gas, Quantum oscillations.

Résumé

Nous proposons une étude approfondie d'une gamme de propriétés d'équilibre clés d'un gaz d'électrons bidimensionnel confiné harmoniquement sous un champ magnétique normal. En utilisant les fonctions d'onde à une particule et l'approche de la matrice de densité de Bloch, nous dérivons des expressions analytiques exactes pour les propriétés locales et intégrales, y compris la densité de pa rticules, la distribution de courant, l'aimantation microscopique, le moment magnétique total et le courant électrique persistant intégré. Nous démontrons une déduction directe du courant persistant total à partir de l'aimantation microscopique, soulignant leur connexion intrinsèque. L'analyse numérique se concentre sur les champs magnétiques intenses, révélant des régions compressibles et incompressibles bien définies dans le profil de densité de particules. Plus précisément, nous dévoilons la str ucture sous-jacente des courants d'équilibre contre-propageant observés dans ces régimes de haut champ magnétique, entraînés par le comportement oscillatoire de l'aimantation microscopique. L'exploration des changements dans le spectre énergétique révèle des influences complexes sur ces propriétés, entraînant des oscillations quantiques à haut champs.

Mots-clés : Aimantation microscopique orbitale, Courant électrique persistant, Magnétisme orbital, Densité de particules, Gaz d'électrons bidimensionnel, Oscillations quantiques.